2019 年 28 巻 2 号（通巻 85 号）
ISSN 1342-2634
日本バイオイメージング学会

バイオイメージング

- Program & Abstracts -

The 6th International Symposium on Bioimaging
The 28th Annual Meeting of Bioimaging Society

The 27th Annual Meeting of Bioimaging (2018)
Best Imaging Award (Nikon Award)

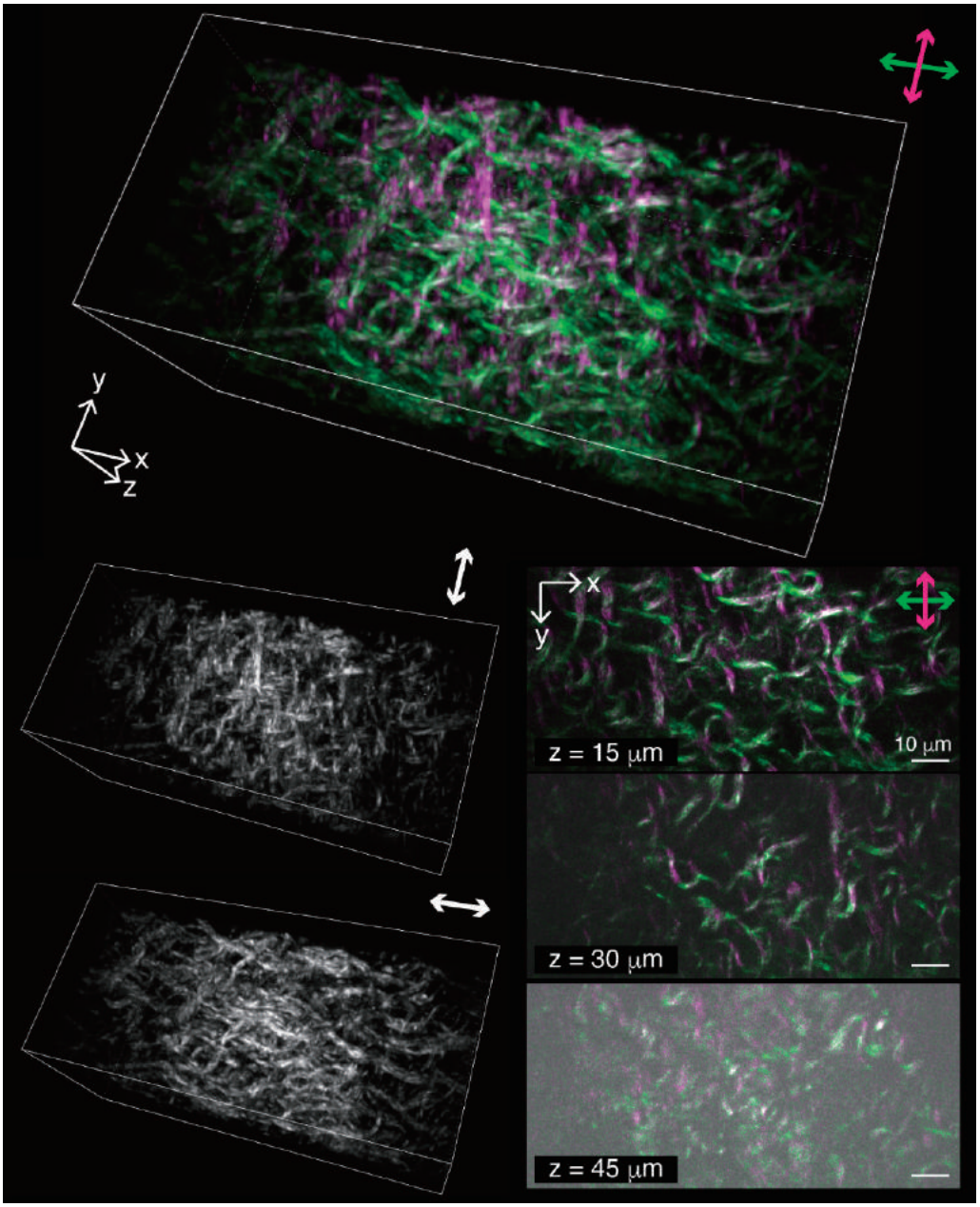

Polarization-resolved SHG imaging of living tissues based on multi-point scanning two-photon excitation microscopy

当社のLED光源でお手持ちの顕微鏡をバージョンアップしませんか?

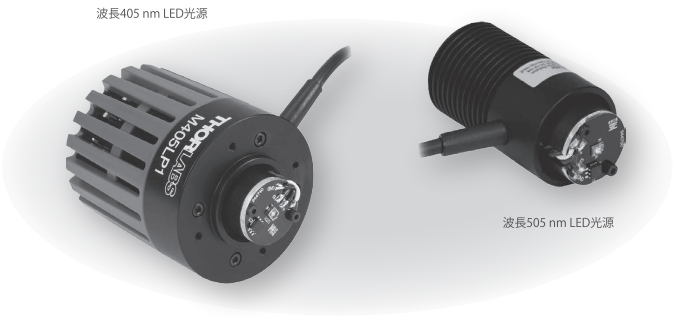

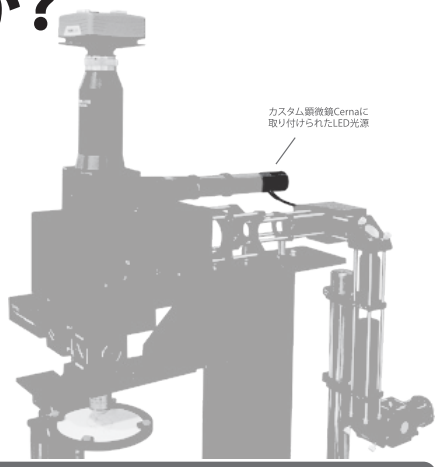

点灯オン・オフ自由自在

水銀ランプと違い、LEDは点灯・消灯ごとの待ち時間を必要としません。また瞬時にスイッチング可能なため、光刺激実験でもシャッターは不要です。

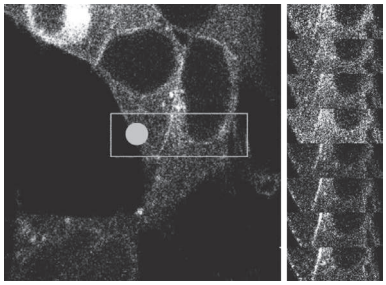

LED光刺激によるCRY2-mCherryの膜局在誘導
画像ご提供：藤岡 容一朗博士、大場雄介博士
(北海道大学 大学院 医学研究院)

高い出力安定性&長寿命

出力が長期に安定し、長寿命。交換頻度が低く、ランニングコストに優れます。

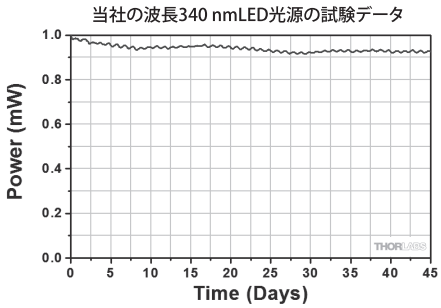

45日間の連続点灯で出力の変動幅は10%以下

豊富な単色波長

UV域から近赤外域まで、LED光源の波長はバリエーションが豊富です。

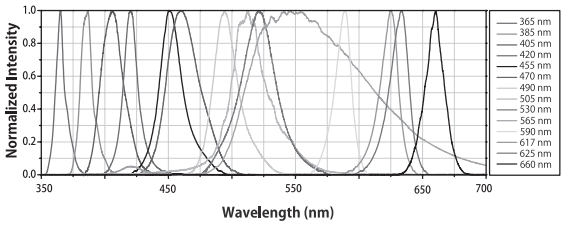

軽量・小型、丈夫な構造

顕微鏡への取付は簡単で安全。特別な技術は不要です。使う道具は六角レンチ1本だけ*。

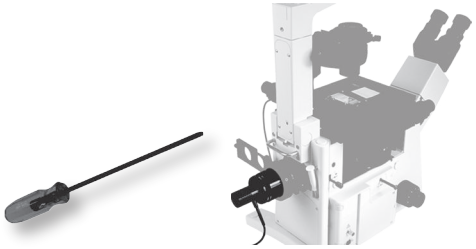

*詳細は当社までお問い合わせください。

www.thorlabs.co.jp E-mail: sales@thorlabs.jp

THORLABS ソーラボジャパン株式会社
〒179-0081 東京都練馬区北町3-6-3 TEL：03-6915-7701 FAX：03-6915-7716

Figure on the front cover

Polarization-resolved SHG imaging of living tissues based on multi-point scanning two-photon excitation microscopy

Ai Goto,[1,2] Kohei Otomo,[1,2,*] Tomomi Nemoto [1,2]

[1] Research Institute for Electronic Science, Hokkaido University, Sapporo, Japan

[2] Graduate School of Information and Technology, Hokkaido University, Sapporo, Japan

E-mail: otomo@es.hokudai.ac.jp

Second harmonic generation (SHG) is a non-linear optical process that can be applied for bioimaging. Two photons from ultrashort high-peak-power laser pulses are converted to a single photon, and its wavelength becomes halved via SHG processes. SHG signals are strongly observed from individual non-centrosymmetric molecules, especially when they are arranged in a crystalline array, such that SHG signals are frequently generated by endogenous fiber-like structures like supercoiled collagens fibers and thick myosin filaments. Moreover, the probability of SHG occurring largely depends on the relative orientation between the polarization of the incident light beam and the orientation axis of the targeted molecules. Therefore, polarization-based SHG imaging, the concept of which is based on analyzing the polarization anisotropy of SHG light or SHG signal intensity as a function of the polarization state of the incident light beam, can be implemented to reveal the structural assembly information of targeted molecules and has been used as a tool for medical and biological analyses. However, most of polarization-based SHG microscopy requires a specialized optical setup to irradiate the sample with the excitation laser light beam, capture, and/or analyze the SHG light signals.

Simple SHG images can be acquired by using a laser scanning microscope equipped with an ultrashort high-peak-power laser light source such as a conventional two-photon excitation fluorescence microscope (TPM). Since most of TPM systems employ a single-point laser scanning method using moving mirrors, their temporal resolution depends on the speed of the physical movement of the mirrors. However, since early 21st century, multi-point laser scanning methods have been attempted to achieve high-speed TPM imaging. Recently, a TPM system equipped with a spinning-disk confocal scanning unit (TPM-SD), which incorporates a micro-lens array disk and a Nikpow disk containing a set of confocal pinholes, has been developed. However, the insufficient energy of conventionally-used mode-locked titanium-sapphire (Ti-Sa) laser light sources restricted the effective field of view (FOV) of TPM utilizing the spinning-disk scanning unit (TPM-SD) to a narrow region. Although Shimozawa *et al.* modified spinning-disks to increase near infrared laser light power throughput, the system using a Ti-Sa laser light source could use a 10% region of the effective area of the detector, which corresponded to approximately 40 μm diameter FOV with a 60× objective lens [Shomozawa *et al., Proc. Natl. Acad. Sci. USA*, 2013]. In order to enlarge the FOV further, we introduced a higher-peak-power ytterbium (Yb)-based laser light source to the TPM-SD system, achieving approximately 10-times larger FOV [Otomo *et al., Anal. Sci.*, 2015].

In this study, we introduced a polarization-resolving detection methodology for the TPM-SD system [Goto *et al., Front. Phys.*, 2019], enabling high-speed SHG imaging of living tissue to reveal the structural orientation of collagen fibers. By utilizing developed system, we visualized three-dimensional objects from cross-sectional images of non-labeled biological specimens. We irradiated a linearly polarized beam to a fixed mouse skin sample from the dermal side and acquired a pair of orthogonally-resolved polarization SHG images from the surface to a depth of 50-μm. As shown in a figure on the front cover, complicated collagen fiber network structures were visualized, and the signal ratios between the two channels appeared to reflect their orientations. In addition, we also demonstrated *in vivo* polarization-resolved SHG imaging of the collagen fibers in the mouse skeletal muscles at video-rate temporal resolution. This technique will enable monitoring of the distribution of biological molecular orientations responding to intracellular dynamics with a superior temporal resolution.

The 6th International Symposium on Bioimaging
The 28th Annual Meeting of the Bioimaging Society

September 21 – 23, 2019
Teikyo University, Tokyo, Japan

Main Organizer
Bioimaging Society

Co-organizers
Teikyo University
National University of Singapore
(Mechanobiology Institute, MBI)

Welcome Messages

Dear colleagues,

The Bioimaging Society was established in 1991 in Japan and is the scientific organization of the bioimaging field. The society contributes to the development of interdisciplinary research over broad fields such as medicine, pharmacy, agriculture, physical science, engineering etc. The research in connection with bioimaging technology such as "Green Fluorescent Protein (GFP) imaging", "Super-resolution Microscopy" and "Cryo-Electron Microscopy", has won the Nobel Prize in chemistry, and bioimaging research has accomplished fast development in response to the benefits. At the present time, bioimaging is an important tool in innovative research in the natural sciences.

The society has held annual scientific meetings since the establishment and international symposia on bioimaging about every two years since 2006. This time, we have a joint meeting of the international symposium and the Annual Meeting of the Bioimaging Society in Tokyo. The main theme is “Leading to the Future with Bioimaging”. This joint meeting will focus on recent progress in bioimaging research from basic research to clinical applications. In this joint meeting, we would like to discuss the future of bioimaging technologies and their applications.

Please join us for discussions of bioimaging research in Tokyo, Japan, and enjoy the Japanese culture and foods. We will do our very best to make you feel welcome to Tokyo and Teikyo University.

Sincerely,

Ryo Suzuki, Ph.D.

Chairman of
The 6th International Symposium on Bioimaging
The 28th Annual Meeting of the Bioimaging Society
Professor, Faculty of Pharma-Science, Teikyo University

Table of Contents

Organization

Main Organizer

Bioimaging Society

Co-organizers

Teikyo University
National University of Singapore (Mechanobiology Institute, MBI)

Partnership

The Society of Chemical Engineers, Japan
The Visualization Society of Japan
The Chemical Society of Japan
The Japanese Society of Microscopy
Japan Society for Cell Biology
The Japan Neuroscience Society
The Japanese Society of Neurochemistry
The Biophysical Society of Japan
The Physiological Society of Japan
Japan Society of Histochemistry and Cytochemistry
Protein Science Society of Japan
The Japan Society of Ultrasonic in Medicine
The Japan Society of Drug Delivery System
The Physical Society of Japan
The Molecular Biology Society of Japan
Japanese Society for Immunology
The Pharmaceutical Society of Japan
The Academy of Pharmaceutical Science and Technology, Japan
The Japanese Pharmacological Society
Japan Society for Laser Surgery and Medicine

Endorsement

The Japan Society of Applied Physics
Japan Society for Bioscience, Biotechnology, and Agrochemistry

Organizing Committee

Chair

Ryo SUZUKI Teikyo Univ., Fac. Pharma-Sci.

President of Bioimaging Society

Takashi FUNATSU The Univ. of Tokyo, Grad. Sch. Pharm.Sci

Vice President of Bioimaging Society

Etsuko SUZAKI Shujitsu Univ., Sch. Pharmacy
Kotaro OKA Keio Univ., Fac. Sci. & Tech.

Director, General Affair of Bioimaging Society

Kotaro OKA Keio Univ., Fac. Sci. & Tech.

Director, Treasurer of Bioimaging Society

Yoshihiro OHTA Tokyo Univ. of Agriculture Tech., Grad. Sch. Eng.

Members

Kazuo SUZUKI Teikyo Univ., Asia International Institute of Infectious Diseases Control (ADC)

Hiroshi KIHARA Himeji Hinomoto College

Takeharu NAGAI Osaka Univ., The Institute of Scientific and Industrial Research

Kohei SOGA Tokyo Univ. of Sci., Fac. Industrial Sci. & Tech.

Naoko TANAKA Otsuma Women's Univ., Fac. Home Economics

Tomomi NEMOTO Hokkaido Univ., Res. Institute for Electronic Sci.

International Organizing Committee

Paul MATSUDAIRA National Univ. of Singapore, Mechanobiology Institute (MBI)

Latha Krishnarajpet SHIVA
National Univ. of Singapore, Mechanobiology Institute (MBI)

Organizing Committee

Secretary General

Daiki OMATA Teikyo Univ., Fac. Pharma-Sci.

Supporting members (Teikyo University)

Sanae ODA
Tadamitsu SHIMA
Yuno SUZUKI
Sara ZAKARIA
Haruka INOUE
Toshiki KUROSAWA
Saori KAGEYAMA
Eri CHIBA
Sekihito SAITO
Lisa MUNAKATA
Fumiko HAGIWARA
Tamotsu MARUYAMA
Tomoyuki FUKUZAWA

Secretariat

Lab. of Drug and Gene Delivery Res.,
Fac. of Pharm-Sci, Teikyo Univ.
2-11-1 Kaga, Itabashi-ku, Tokyo Japan
int-symp-bioimaging2019@pharm.teikyo-u.ac.jp

Map

Area Map

Teikyo University
2-11-1 Kaga, Itabashi-ku, Tokyo 173-8605, JAPAN

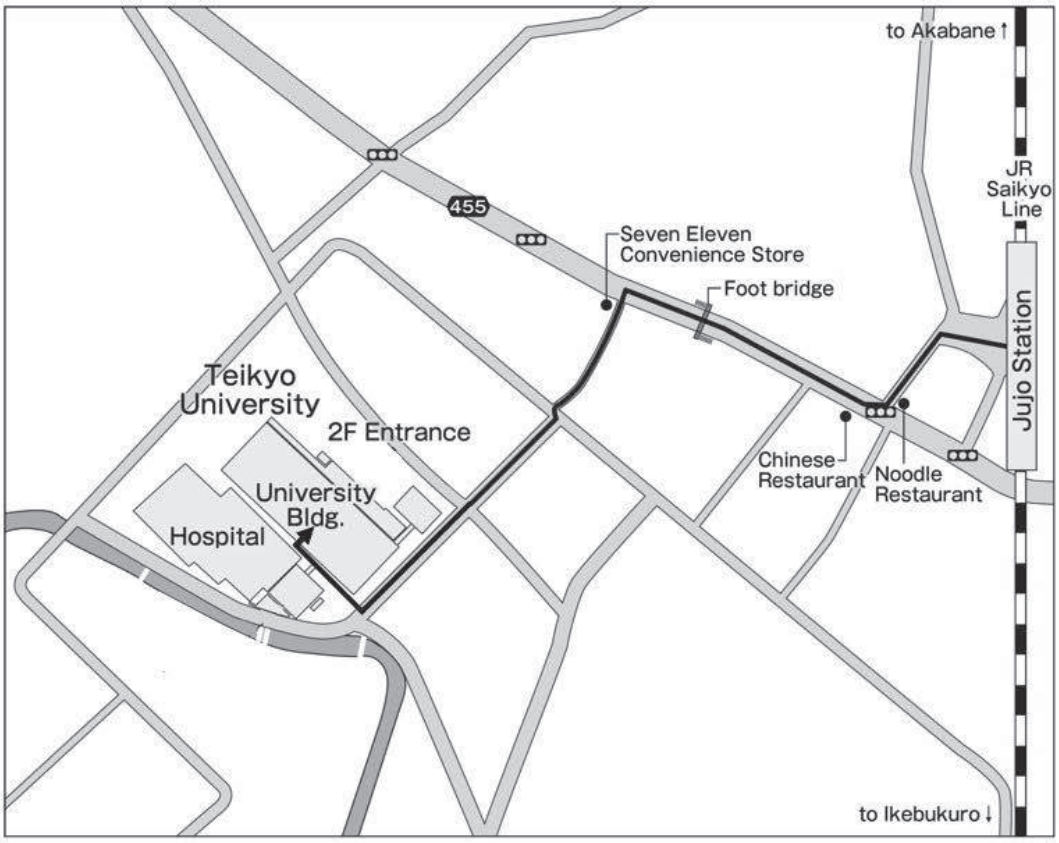

* The nearest station: Jujo Station (10 minutes walk), JR Saikyo Line

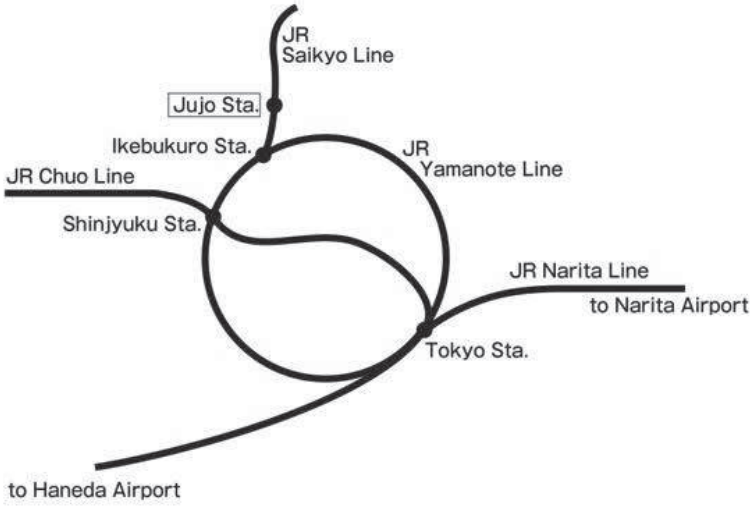

Map (continued)

Access

Teikyo University

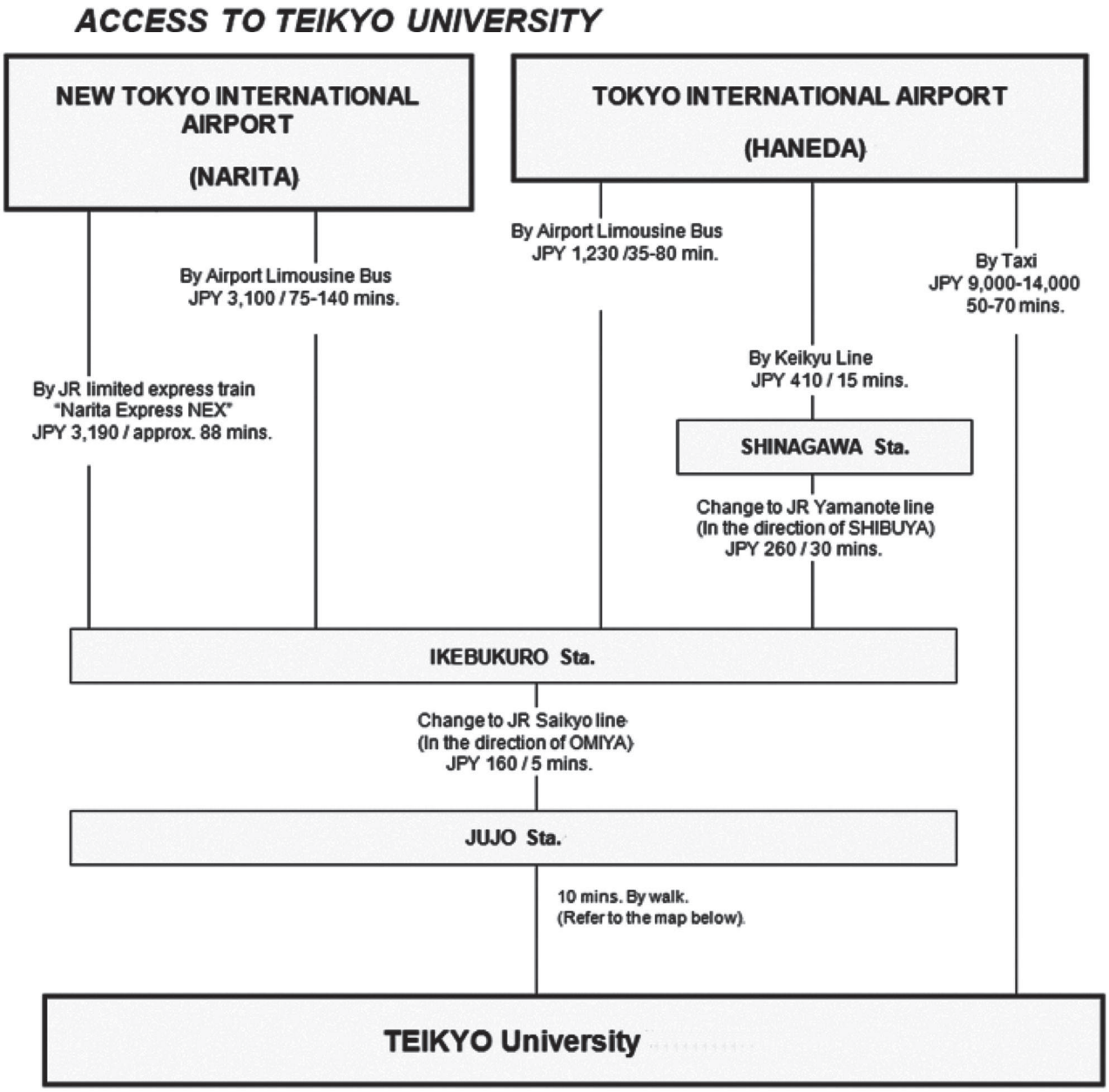

Map (continued)

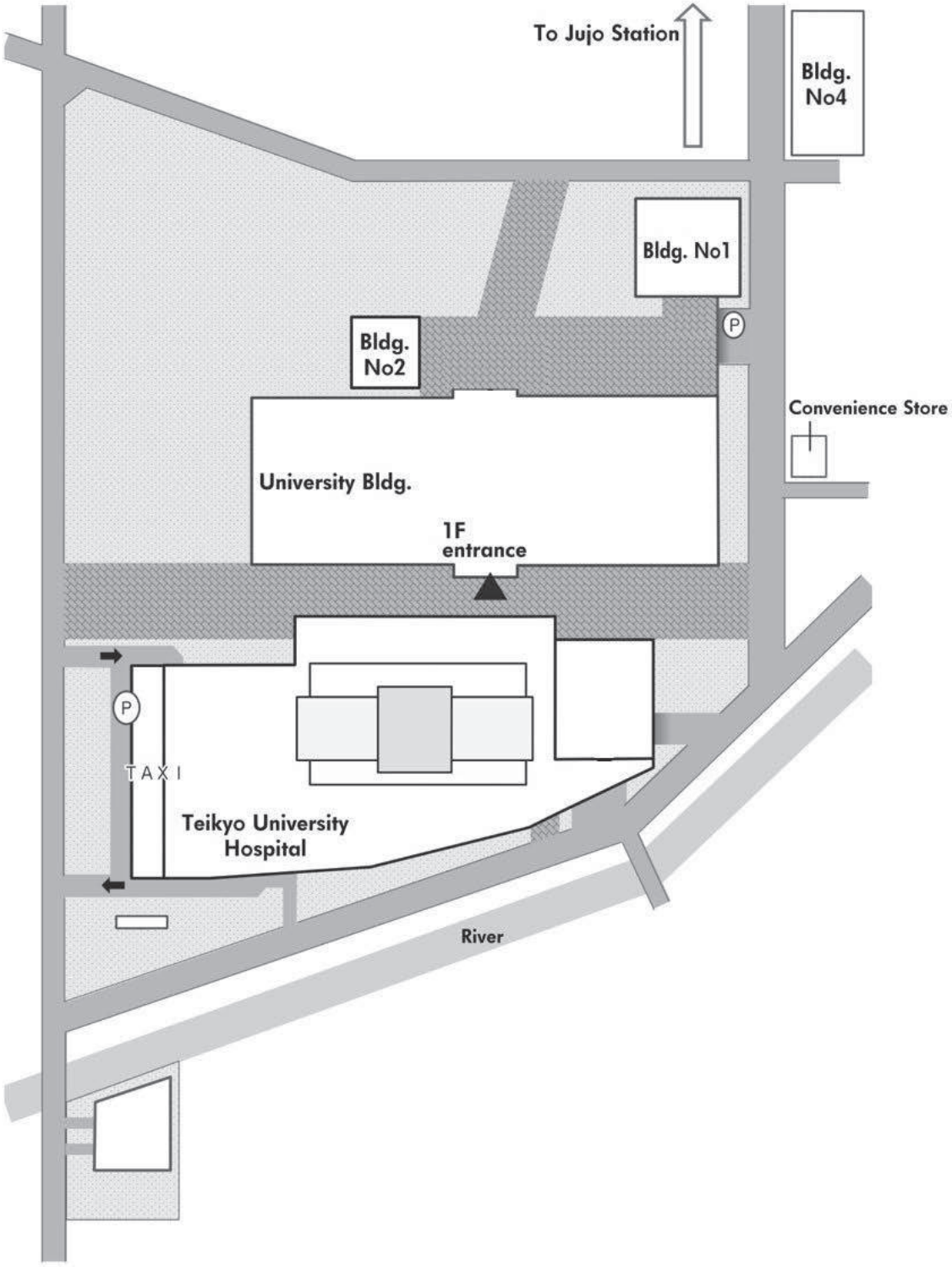

You can use 1F entrance at University Bldg.

Map (continued)

University Bld. 3rd Floor

Room 301 : Poster viewing and Exhibition
Room 302 : Oral presentation

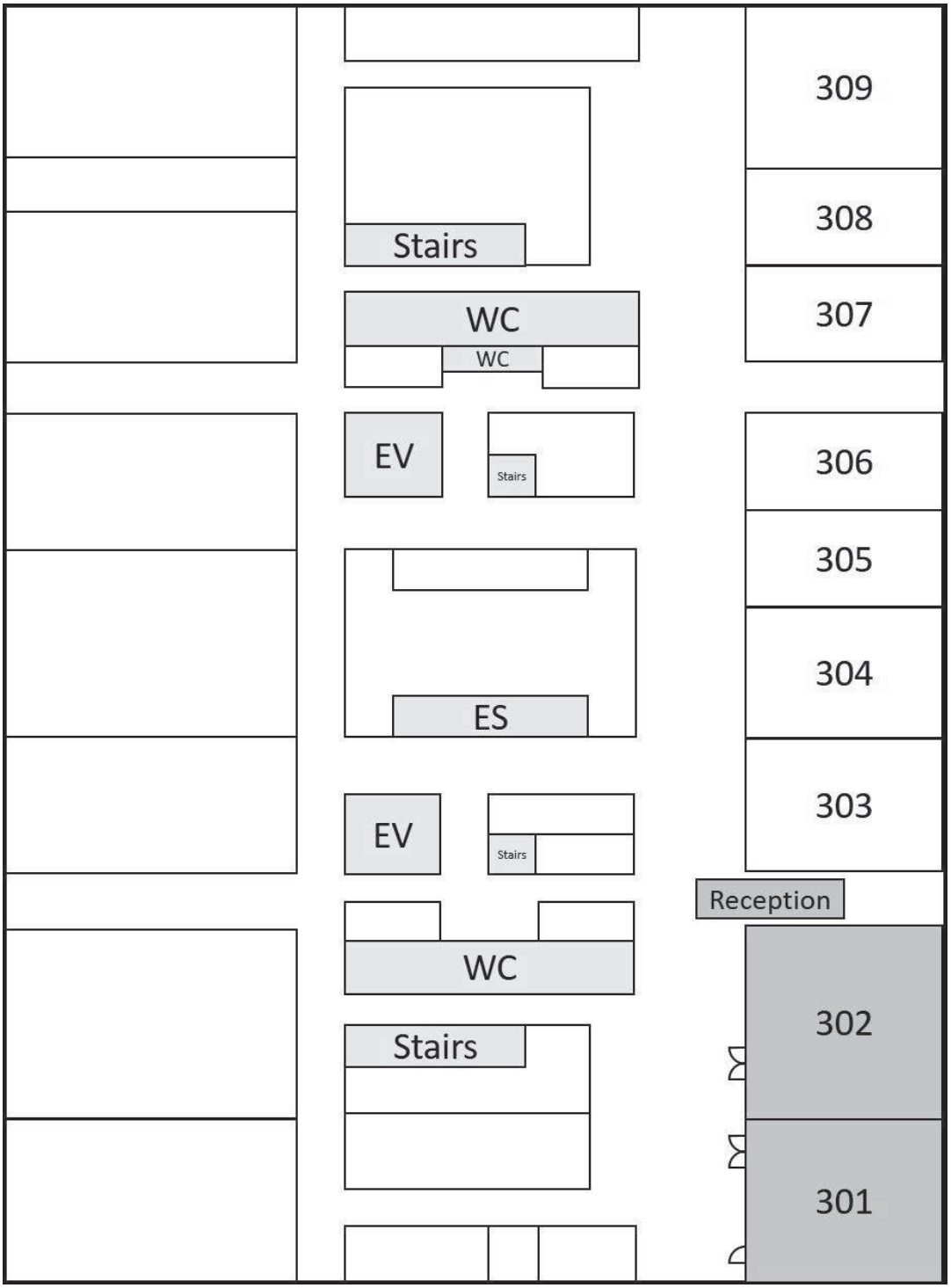

Map (continued)

Room 301 : Poster viewing and Exhibition

(

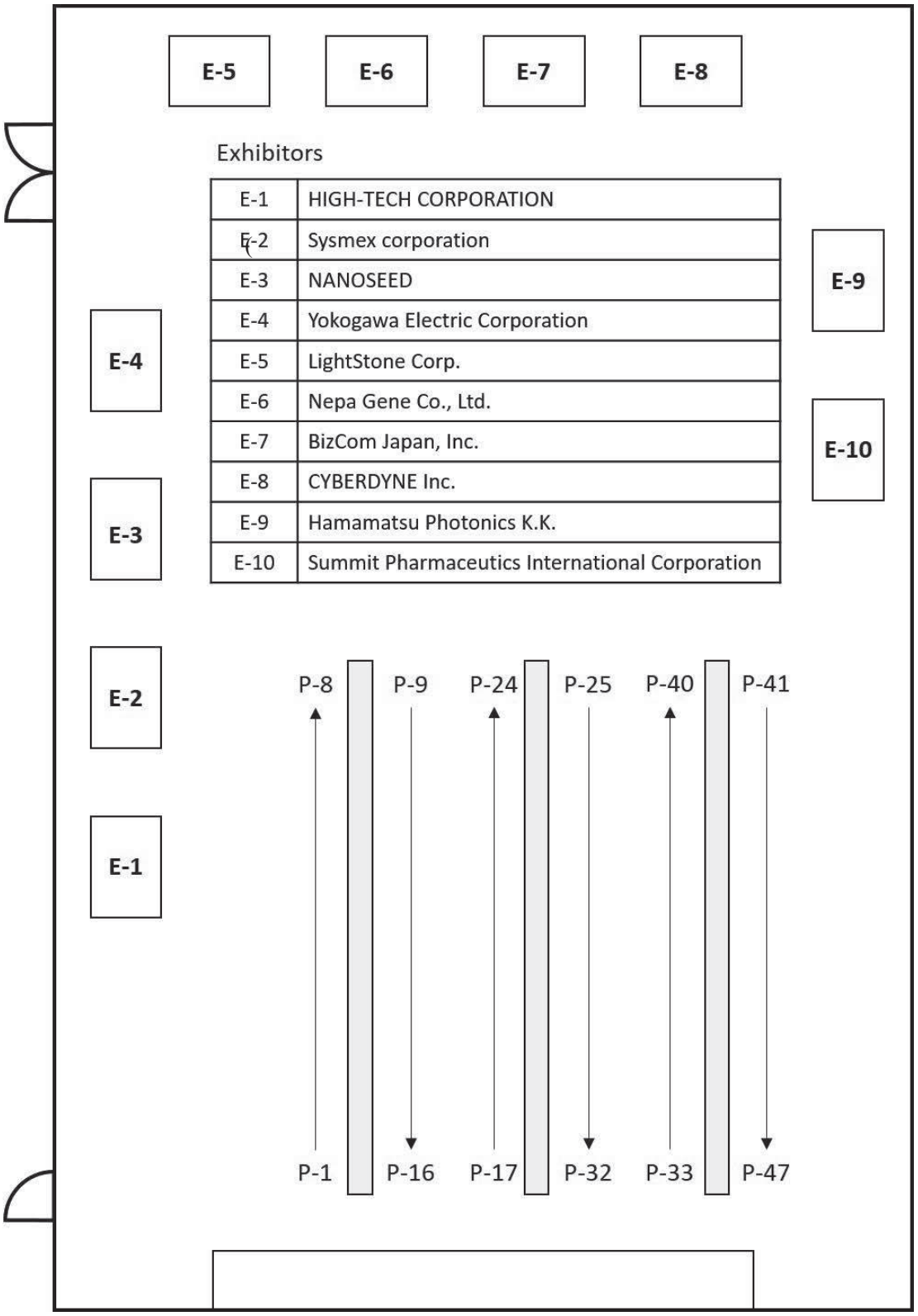

General Information

Registration

Open Hours

September 21 (Sat) 9:00 – 18:30
September 22 (Sun) 8:30 – 18:00
September 23 (Mon) 8:30 – 15:30

Registration Fees

Member: 8,000 yen (Active Participant)*
3,000 yen
(Graduate Student or Undergraduate Student (Over 5th grade))**
Free (Under 4th grade)**

Non-member: 10,000 yen
5,000 yen
(Graduate Student or Undergraduate Student (Over 5th grade))**
Free (Under 4th grade)**

* Member of Bioimaging Society, Partnership & Endorsement
** For students, please show your student ID at the reception desk

Banquet (on September 22): 4,000 yen (General), 2,000 yen (Student)

General Information (continued)

Symposium Information

Name Badges
Please wear your name badge at all the times during the congress for identification and security purpose. Only registered participants wearing a name badge will be allowed access to the session rooms.

Cloak
Located in 3rd Floor

September 21 (Sat)	9:00 – 18:30
September 22 (Sun)	8:30 – 18:00
September 23 (Mon)	9:00 – 15:30

Banquet
Date and Time : 18:00 September 22
Venue: Cafeteria “Godereccio”, 1st Floor, University Bldg.
Style: Buffet Dress code: Casual *Registered applicants only

No Smoking
Smoking is prohibited in all areas of Itabashi campus, Teikyo University.

No Photos, No Audio Recording
Photos and audio recording are prohibited.

Cellular Phones
Using cellular phones during the sessions is prohibited. Cellular phones must be turned off or set to silent moder during the sessions.

Electricity

Electric current is uniformly 100 volts, AC, two leg plug, throughout Japan, but with two different cycles: 50 Hz in eastern Japan including Tokyo and 60 Hz in western Japan including Kyoto and Osaka.

Speakers' Instruction

For oral session

All speakers are requested to come to the speaker's preparation area 15 minutes prior to your presentation.

All the oral presentations are to be made on the PC, and all the speakers are requested to make their presentation data in English.
Please save your presentation data following the guidelines below, and save on a USB flash drive. Windows is the only operating system available for the presentations. If you have prepared the presentation data on a Macintosh, you are advised to bring you own PC.
For smooth progression of the sessions, speakers are requested to follow the guidelines.

- If you have prepared the presentation data on a Macintosh, you are advised to bring you own computer.
- The 6th International Symposium on Bioimaging will not be responsible for any troubles caused by the operation or actions that do not follow the guidelines.

OS and Application

OS: Windows 10
Application: PowerPoint 2016

Monitor Size (Resolution)

XGA (1024 x 768) *Please check in advance that all the data appear properly under the specified conditions.

Backup Data

Please bring backup data to the meeting site if at all possible.

Fonts

Please use default-setting fonts of Windows 10.

Movies

For those who wish to show a movie, it is recommended to bring their own PC to run the presentation slide.

Speakers' Instruction (continued)

For Speakers bringing their own PC

- Please bring an AC adapter for your PC
- For PC with different pin types, please make sure to bring a conversion cable to D-sub 15 pins type or HDMI.
- Please prepare backup data either with USB flash drive.

Chairpersons' Instruction

All chairpersons are asked to be in their session room no later than 15 minutes prior to the beginning of the session.

Speakers' Instruction (continued)

For poster session

Poster Presenters are requested to follow the schedule below in mounting their posters on their assigned boards. Your poster program number will be posted on your assigned board. Board size will be 90 cm × 200 cm (width × Height). Pins for mounting will be available. During the poster session time, presenters are requested to stand in from of your poster board to be asked questions.

Poster Mounting/Presentation/Removal Schedule

Mounting	9:00 – 14:00, September 21st (Sat)
Presentation	September 22nd (Sun)
	Odd number : 13:00 – 13:40
	Even number : 13:40 – 14:20
Removal	13:00 – 15:00, September 23rd (Mon)

Poster Summary Oral Presentation

Preparation:
Please fit the summary slide to slides of ISO A4 size (210 mm × 296 mm) in PowerPoint file. The summary slide must be within three slides (including title page). Bioimaging 2019 office will combine all summary slides in one file. The summary presentation will be performed using Windows 10 and Microsoft PowerPoint 2016. Please make sure the slide is correctly shown in the environment. After the conference, the office will discard all slides and data. First slide must include the title, authors and affiliations. Second and third slide can show your poster summary. It is possible to include images, videos and animations. If you use videos, the videos should be embedded in the slides. The data size must be less than 20 MB.

Presentation:
Summary presentation must be within 2 minutes. If exceed 2 minutes, the presentation will be forcibly closed. The summary presentation will be performed using Windows 10 and Microsoft PowerPoint 2016 in the windows PC of Bioimaging 2019 office.

Awards

Best Imaging Awards (NIKON Award provided by NIKON INSTECH CO., Ltd., OLYMPUS Award provided by Olympus Corporation, HAMAMATSU Award provided by Hamamatsu Photonics K.K., Carl Zeiss Award provided by Carl Zeiss Co., Ltd.) will be presented to four poster presenters of member of the Bioimaging Society.

Best Imaging Award (Bioimaging 2019 Award provided by organization of the 28th Annual Meeting of the Bioimaging Society) will be presented to one person of all poster presenters.

All attendees will vote to select Best Imaging Awards.

Message from Sponsors Providing Best Imaging Award

NIKON Award

Nikon brings to people the fresh surprise and inspirations through excellent microscopic images and conveys the importance of cutting-edge science and technology. We will present the Nikon Award to researchers and their microscopic images that will inspire new impressions at this conference.

NIKON INSTECH CO., LTD.

OLYMPUS Award

OLYMPUS CORPORATION was founded in 1919, this year we cerebrate 100th Anniversary. We have supported bio imaging with many researchers over the years as the first manufacturer of commercializing microscopes in Japan. In this conference, every year we award the best imaging prize to support your research.

Olympus Corporation

HAMAMATSU Award

The letter "イ" was projected on television about 80 years ago for the first time. The light technology is evolving rapidly, and we call the 21st century "the age of light". Hamamatsu Photonics, along with light, in pursuit of the unexplored technology, we will continue to develop in the future. We are engaged in research like "grabbing the goddess's forehead".

Hamamatsu Photonics K.K.

Carl Zeiss Award

There are many different ways in which ZEISS promotes science. In 2002, the company created the Carl Zeiss Research Award to honor outstanding achievements in the field of bioimaging. ZEISS will be presenting a research award with a focus on up-and-coming talent: the Zeiss Award for Young Researchers.

Carl Zeiss Co., Ltd.

Program

Program at a glance

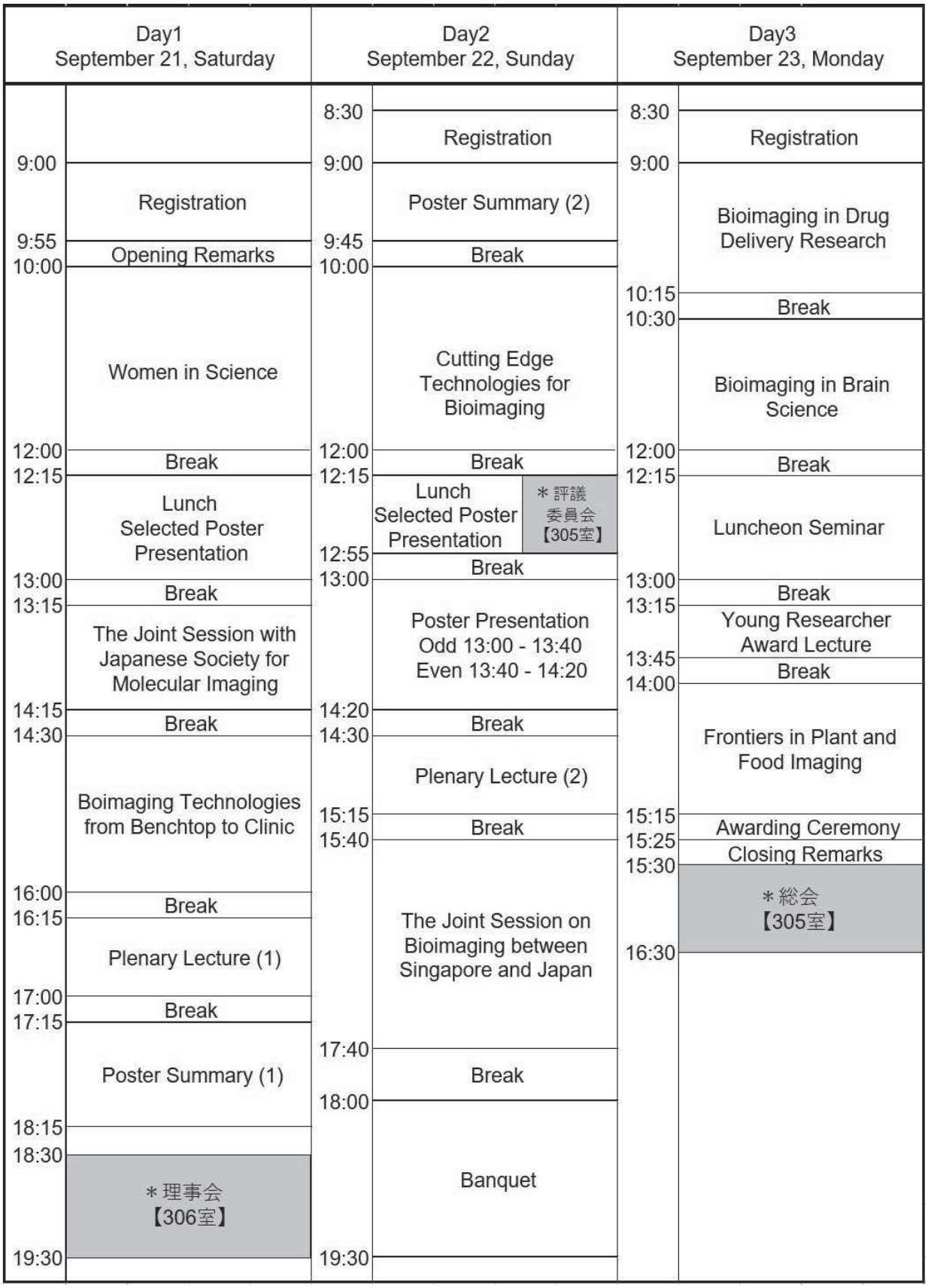

＊These are for members of the Bioimaging Society and related persons.

September 21 (Sat)

9:55 – 10:00 Opening Remarks

Ryo Suzuki (Chair, Teikyo Univ., Japan)

10:00 – 12:00 Women in Science

Chairpersons; Etsuko Suzaki (Shujitsu Univ., Japan)
Shee-Mei Lok (National Unvi. of Singapore (NUS),
Duke-NUS Med. Sci., Singapore)

S1-1 Teikyo University Support Center Activities for Women Physicians and Researchers

Kiyoko Kaneko, Yoko Nakayama, Haruko Sekiya, Hiroko Okinaga *
Teikyo University Support Center for Women Physicians and Researchers, Teikyo University, Japan

S1-2 Rapid cancer imaging by rationally designed fluorescence probes

Mako Kamiya,[1,]* Yasuteru Urano[1,2,3,]*
[1]Grad. Sch. Med. and [2]Grad. Sch. Pharm. Sci., The Univ. of Tokyo, [3]AMED CREST

S1-3 Capsid protein structure in Zika virus reveals the flavivirus assembly process

Ter Yong Tan[1,2,7], Guntur Fibriansah[1,2,7], Victor A. Kostyuchenko[1,2], Thiam-Seng Ng[1,2], Xin-Xiang Lim[3], Shuijun Zhang[1,2], Xin-Ni Lim[1,2], Jiaqi Wang[1,2], Jian Shi[4], Marc C. Morais[5], Davide Corti[6], Shee-Mei Lok[1,2]
[1]Program in Emerging Infectious Diseases, Duke–National University of Singapore Medical School, Singapore.
[2]Centre for BioImaging Sciences, Department of Biological Sciences, National University of Singapore, Singapore.
[3]Department of Biological Sciences, National University of Singapore, Singapore.
[4]CryoEM unit, Department of Biological Sciences, National University of Singapore, Singapore.
[5]Department of Biochemistry and Molecular Biology, Sealy Center for Structural and Molecular Biophysics, University of Texas Medical Branch, Galveston, Texas, United States of America.
[6]Humabs BioMed SA, a subsidiary of Vir Biotechnology, Inc., Bellinzona, Switzerland.

S1-4 Therapeutic strategies using image-guided focused ultrasound for neurodegeneration.

Isabelle Aubert*[1,2]
[1]Sunnybrook Research Institute, [2]University of Toronto, Ontario, Canada.

12:15 – 13:00 Lunch & Selected Poster Presentation

Chairperson; Yoshihiro Ohta (Tokyo Univ. of Agriculture Tech., Japan)

P-1 Whole-organ cell profiling accelerated by CUBIC combined with MOVIE imaging

Tomoki T. Mitani[1,2], Katsuhiko Matsumoto[1], Shuhei A. Horiguchi[1], Junichi Kaneshiro[1], Tatsuya C. Murakami[3], Tomoyuki. Mano[3], Hiroshi Fujishima[1], Ayumu Konno[4], Tomonobu M. Watanabe[1], Hirokazu Hirai[4], Hiroki R. Ueda[1,3]*
[1]RIKEN Ctr. For Biosystems Dynamics Res., [2]Osaka Univ. Hosp., [3]Grad. Med., Univ. Tokyo,
[4]Grad. Med., Gunma Univ.

P-2 Real-time cellular imaging of lung T-lymphocyte accumulation and focus formation in a mouse asthma model

Akihiro Hasegawa,[1]* Hidetaka Ogino,[1] Toshinori Nakayama[2]
[1] Department of Microbiology and Immunology, Yamaguchi University Graduate School of Medicine,
[2] Department of Immunology, Graduate School of Medicine, Chiba University

P-3 From Nano to Macro: Advanced Imaging Techniques for Neuroscience Applications

Shinya Komoto*, Paolo Barzaghi, Koji Koizumi, Toshiaki Mochizuki, Bruno Humbel
Imaging Section, Research Support Division Okinawa Institute of Science and Technology (OIST)

13:15 – 14:15 The Joint Session with Japanese Society for Molecular Imaging

Chairpersons; Tomomi Nemoto (Hokkaido Univ., Japan),
Kenjiro Hanaoka (Univ. of Tokyo, Japan)

S2-1 Chemical design of $^{67/68}$Ga-labeled antibody fragments for low renal radioactivity levels

Tomoya Uehara
Graduate Sch. Pharma-Sci., Chiba Univ.

S2-2 Development of Far-Red to Near-Infrared Small-Molecule Fluorophores and Their Application to Fluorescent Probes

Kenjiro Hanaoka [1,*]
[1]Graduate School of Pharmaceutical Sciences, The University of Tokyo

14:30 – 16:00 Bioimaging Technologies from Benchtop to Clinic

Chairpersons; Kohei Soga (Tokyo Univ. of Sci. Japan)
Yasuaki Kumamoto (Osaka Univ., Japan)

S3-1 Label-free peripheral nerve detection and imaging by Raman scattering

Yasuaki Kumamoto,[1,*] Tetsuro Takamatsu[2]
[1]Dept. of Pathology and Cell Regulation, Kyoto Pref. Univ. of Medicine,
[2]Dept. of Medical Photonics, Kyoto Pref. Univ. of Medicine

S3-2 New methodology for examining the light-microscopic glass slide specimen by a Low-vacuum Scanning Electron Microscope (LVSEM)

Nobuaki Yamanaka
Tokyo Kidney Research Institute

S3-3 Near Infrared Biomedical Imaging for Visualizing Subcutaneous and Submucosal Information

Kohei Soga[1-3], Karina Nigoghossian[1], Gil Yeroslavsky[2], Thi Kim Dung Doan[3],
Masakazu Umezawa[1], Kyohei Okubo[1,2], Masao Kamimura[1,2], and Naoko Ohtani[4]
[1]Dept. of Mater. Sci. and Tech., Tokyo Univ. of Sci., Katsushika, Tokyo, Japan
[2]Imaging Frontier Center, Tokyo Univ. of Sci., Noda, Chiba, Japan
[3]Res. Inst. for Biomed. Sci., Tokyo Univ. of Sci., Noda, Chiba, Japan
[4]Dept. of Pathophysiology, Osaka City Univ., Osaka, Japan

16:15 – 17:00 Plenary Lecture

Chairperson;　Kazuo Suzuki (Teikyo Univ., Japan)

PL-1　Imaging the mechanics of early zebrafish development

Jun Zhong[1], Dipan Bhattacharya[1,3], Sahar Tavakoli[1,4], Alexandre Kabla[2], Paul Matsudaira[1]
[1]MechanoBiology Institute, Centre for BioImaging Sciences, Department of Biological Sciences, National University of Singapore, Singapore
[2]Department of Engineering, Cambridge University, Cambridge, UK
Current address:
[3]Institute FIRC of Molecular Oncology (IFOM), Milan 20139, Italy
[4]Harvard University, Department of Stem Cell and Regenerative Biology, Harvard University, Cambridge 02138, USA
Boston Children's Hospital, Boston 02115, USA
Harvard Stem Cell Institute, Harvard University, Cambridge 02138, USA

17:15 – 18:15 Poster Summary

Summary oral presentation (P-8 ~ P-30)

September 22 (Sun)

9:00 – 9:45 Poster Summary

Summary oral presentation (P-31 ~ P-47)

10:00 – 12:00 Cutting Edge Technologies for Bioimaging

Chairpersons; Takeharu Nagai (Osaka Univ., Japan)
Takeaki Ozawa (Univ. of Tokyo, Japan)

S4-1 Systematic Approach for Live Cell Selective Imaging Probe Development

Young-Tae Chang [1,2]
[1]POSTECH Chemistry and [2]Center for Self-Assembly & Complexity, IBS

S4-2 Imaging and controlling membrane receptor activities in living cells

Takeaki Ozawa[1]
[1]Department of Chemistry, School of Science, University of Tokyo

S4-3 Characterization of Photoacoustic Imaging in Bioimaging

Miya Ishihara,[1]
[1]Dept. of Medical Engineering, National Defense Medical College

S4-4 Trans-Scale Imaging for Singularity Biology

Takeharu Nagai[1,2]
[1]The Institute of Scientific and Industrial Research, Osaka Univ.,
[2]Institute for Open and Transdisciplinary Research Initiative., Osaka Univ.

12:15 – 12:55 Lunch & Selected Poster Presentation

Chairpersons; Takuya Miyakawa (Univ. of Tokyo, Japan)
Yoshitaka Matsumura (Tokyo Univ. of Pharm. and Life Sci., Japan)

P-4 New evaluation technique for micro-environment using translational and rotational diffusion

Johtaro Yamamoto,[1,]* Akito Matsui,[2] Masataka Kinjo [2]
[1]Biomed. Res. Inst., AIST, [2] Fac. Adv. Life Sci.., Hokkaido Univ.

P-5 Simultaneous Tracking of Multiple Biomolecules in a Living Filamentous Fungus by Confocal Raman Microspectroscopic Imaging

Mitsuru Yasuda,[1] Norio Takeshita,[2] Shinsuke Shigeto [1,]*
[1] School of Science and Technology, Kwansei Gakuin University, Japan
[2] Faculty of Life and Environmental Sciences, University of Tsukuba, Japan

P-6 Attempt to observe the structure of schizophyllan monomer by Small Angle X-ray Scattering and Molecular Dynamics simulation

Yoshitaka Matsumura and Masaki Kojima
Sch. of Life Sci., Tokyo Univ. of Pharm. and Life Sci.

P-7 Structural basis for the substrate specificity of phosphoenolpyruvate carboxykinases as phosphodiester energy-conversion enzymes

Takuya Miyakawa,[1,*] Yoko Chiba,[2] Yasuhiro Shimane,[2] Masaru Tanokura[1]
[1]Grad. Sch. Agric. Life Sci., Univ. Tokyo, [2]D-SUGAR, JAMSTEC

13:00 – 14:20 Poster Presentation (P-1 ~ P-47)

Odd number : 13:00 – 13:40
Even number : 13:40 – 14:20

14:30 – 15:15 Plenary Lecture

Chairperson; Takashi Funatsu (Univ. of Tokyo, Japan)

PL-2 Theranostics (Imaging and Therapy) by Lipid Bubbles and Ultrasound

Kazuo Maruyama
Faculty of Pharma-Science, Teikyo University

15:40 – 17:40 The Joint session on Bioimaging between Singapore and Japan

Chairpersons; Yusuke Toyama (National Univ. of Singapore (NUS), MBI, Singapore)
Kaoru Katoh (National Institute of Advanced Industrial Science and Technology (AIST), Japan)

S5-1 Mechanical impact of apoptosis in tissue homeostasis

Yusuke Toyama[1, 2]
[1]Mechanobiology Institute, National University of Singapore, Singapore
[2]Department of Biological Sciences, National University of Singapore, Singapore

S5-2 Visualizing and Controlling Cell Adhesion Complexes at the Molecular Scale

Tony Kanchanawong [1, 2]
[1]Mechanobiology Institute, National University of Singapore, Singapore
[2]Department of Biomedical Engineering, National University of Singapore, Singapore

S5-3 Fine structures of the cells revealed with conventional and super resolution microscopy

Kaoru Katoh,[1,2]* Minami Tanaka,[1] Totai Mitsuyama [2]
[1]Biomed. Res. Inst, AIST, [2] AI Res. Center, AIST

S5-4 Mg ion as a novel candidate for second messenger

Kotaro Oka[1]*, Ryu Yamanaka[2], Yutaka Shindo[1]
[1]Dept. Biosci. & Informat., Keio Univ. [2]Fac. Pharm., Sanyo-Onoda City Univ.

18:00 – 19:30 Banquet (at Godereccio, Cafeteria, 1F)

September 23 (Mon)

9:00 – 10:15 Bioimaging in Drug Delivery Research

Chairpersons; Alexander L. Klibanov (Univ. of Virginia, USA)
Yuriko Higuchi (Kyoto Univ, Japan)

S6-1 Intravital Microscopy for Drug Delivery Research

Yu Matsumoto
Department of Otolaryngology and Head and Neck Surgery, The University of Tokyo

S6-2 Mechanical interactions of oscillating microbubbles with cells and a capillary under ultrasound exposure

Nobuki Kudo
Faculty of Information Science and Technology, Hokkaido University

S6-3 Targeted Ultrasound for Imaging and Drug Delivery

Siva Dasa[2], Akshaya Meher[2], Pingyu Zhang[2], Arshad Khan[2], Johnny Chen[3], Adam Dixon[3], Justin Farry[3], Zhongmin Du[2], Galina Diakova[2], John Hossack[3], Alexander L Klibanov[1,2,3]*
[1]Cardiovascular Division, Department of Medicine, [2]Cardiovascular Research Center,
[3]Department of Biomedical Engineering, University of Virginia, Charlottesville USA

10:30 – 12:00 Bioimaging in Brain Science

Chairpersons; Tomomi Nemoto (Hokkaido Univ., Japan)
Mutsuo Nuriya (Keio Univ., Japan)

S7-1 Imprinting Primes Learning : Thyroid Hormone is the Determining Factor for the Critical Period.

Koichi J. Homma
Faculty of Pharmaceutical Sciences, Teikyo University, Tokyo, JAPAN

S7-2 Visualizing neuronal circuits controlling circadian and ultradian rhythms in mammals

Ryosuke Enoki [1,*]*
[1]Hokkaido University, Research Institute for Electronic Science, Lab of Molecular and Cellular Biophysics

S7-3 Multimodal multiphoton imaging of solutes and solvents in the brain tissue

Mutsuo Nuriya [1, 2, 3]
[1]Department of Pharmacology, Keio University School of Medicine, [2] Graduate School of Environment and Information Sciences, Yokohama National University, [3] JST PRESTO

12:15 – 13:00 Luncheon Seminar

Chairperson; Kazuo Maruyama (Teikyo Univ., Japan)

LS **Brain hippocamp us synthesize s estrogen and androgen which rapidly modulate dendritic spines in non genomic manner**

Suguru Kawato, Mika Soma, Mari Ogiue Ikeda
Dep of Cognitive Neuroscience Sch. Pharma Sci., Teikyo Univ.

13:15 – 13:45 Young Research Award Lecture

Chairpersons; Naoko Iida-Tanaka (Otsuma Women's Univ., Japan)

AL **Design and synthesis of functional small molecule probes for fluorescence imaging**

Toshiyuki Kowada[1,2,3]
[1] Institute of Multidisciplinary Research for Advanced Materials ,
[2] Grad uate Sch ool of Science, [3] Grad uate Sch ool of Life Sciences, Tohoku University

14:00 – 15:15 Frontiers in Plant and Food Imaging

Chairpersons; Kazuyuki Kuchitsu (Tokyo Univ., of Sci., Japan)
Masatsugu Toyota (Saitama Univ., Japan)

S8-1 **Real-time imaging of whole-plant calcium and glutamate dynamics**

Masatsugu Toyota,[1,2]
[1] Department of Biochemistry and Molecular Biology, Saitama University, Japan
[2] Department of Botany, University of Wisconsin-Madison, USA

S8-2 **Mass Spectrometry Imaging of Metabolites in Agricultural Products**

Hirofumi Enomoto*
Dept. Biosci., Teikyo Univ. Grad. Sch. Sci. Eng., Teikyo Univ. Adv. Inst. Analysis Ctr., Teikyo Univ.

S8-3 **Visualizing the Plant Life: Regulation of Development and Stress Responses by the ROS-Ca^{2+} Signaling Network and Autophagy**

Kazuyuki Kuchitsu[1,2], Kenji Hashimoto[1,2]
[1]Dept. Appl. Biol. Sci. & [2]Imaging Frontier Center, Tokyo Univ. of Science, Noda, Japan

15:15 – 15:25 Awarding Ceremony

15:25 – 15:30 Closing Remarks

Ryo Suzuki (Chair, Teikyo Univ., Japan)

Abstracts

PL1

Imaging the mechanics of early zebrafish development

Jun Zhong[1], Dipan Bhattacharya[1,3], Sahar Tavakoli[1,4], Alexandre Kabla[2], Paul Matsudaira[1]

1.MechanoBiology Institute, Centre for BioImaging Sciences, Department of Biological Sciences, National University of Singapore, Singapore
2. Department of Engineering, Cambridge University, Cambridge, UK

Current address:
3. Institute FIRC of Molecular Oncology (IFOM), Milan 20139, Italy
4. Harvard University, Department of Stem Cell and Regenerative Biology, Harvard University, Cambridge 02138, USA
Boston Children's Hospital, Boston 02115, USA
Harvard Stem Cell Institute, Harvard University, Cambridge 02138, USA

The major morphogenetic movement during gastrulation is convergence and extension when the spherical symmetry of the blastula is transformed into the bilateral symmetry of the adult body plan. Gastrulation is powered by the motility, reordering, and shape changes of individual embryonic cells under the guidance of chemical morphogen gradients. The motility of individual cells is mechanically translated into motions of the embryonic tissues over the entire dorsal and ventral hemispheres. We have mapped the mechanical coupling over the surface of the zebrafish embryo during gastrulation from changes in cell density. The resulting strain maps identify the mechanical signatures of compression when cells converge to the dorsal midline, expansion when cells extend to form the head and tail structures, and compression during somite formation. Interestingly, the two step linear motions of convergence and extension can be more simply represented by strain as curl or rotation of the dorsal and ventral hemispheres. What else can be learned from mechanical maps? The strain maps also indicate stationary points and saddle points which are coincident with key morphological locations on the embryo surface such as the dorsal organizer and morphogen gradient source and sinks. This correspondence with the positions of developmentally important regions of the embryo highlights a possible significance between developmental, mechanical, and mathematical features.

PL2

Theranostics (Imaging and Therapy) by Lipid Bubbles and Ultrasound

Kazuo Maruyama

Faculty of Pharma-Science, Teikyo University

OBJECTIVE

"Theranostics" is a treatment strategy that combines therapeutics with diagnostics. The combination of microbubble and ultrasound (US) is a good tool for "theranostics" due to have multi-potency both of imaging with enhanced echo signal from bubble and therapeutics with sonoporation of bubble. We have developed a new lipid bubble suitable for sonoporation. For good storage stability and ease of handling, lipid bubbles were made into freeze-dried formulations. Here we investigate neovascular imaging and enhancement of ERP effect by combination of lipid bubbles and ultrasound and describe a new drug delivery technology.

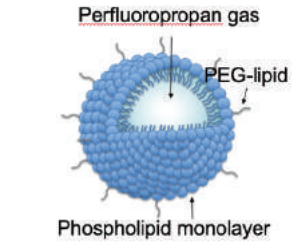

Fig.1 Illustration of lipid stabilized

METHODS

Microbubble : Lipid-stabilized bubbles (LB) were prepared by homogenization of a lipid dispersion in the presence of perfluoropropane gas (Figure 1).

Animal experiments 1: Doxorubicin (DOX) and LB were administered to osteosarcoma-bearing mice via tail vein. Immediately after injection, linear imaging US was exposed to solid tumor site transdermally to take the neovascular imaging. Then, therapeutic US probe was placed directly on the tumor surface and therapeutic US was exposed (2MHz, 2W/cm^2, Duty cycle, 50 %, burst rate, 2Hz). This treatment was repeated three times, on days 1, 2 and 4. Animal experiments 2: DOXIL® and LB were co-administered to thyroid cancer dog and ultrasound treatment (1MHz, 2W/cm^2) was done four times.

RESULTS

LBs were in the size range 1-3 μm and could be preserved by freeze-drying and re-constituted by simple addition of water. LBs were well suited for imaging of blood flow in tumor. The US theranostics capabilities of LB for the solid tumor were studied in osteosarcoma-bearing mice. LB was injected to mice via tail vein and linear imaging US was exposed to solid tumor site transdermally. The flow of LB in blood was observed and neovasuculature of tumor tissue was imaged clearly. Following, therapeutic US was exposed transdermally over the site of solid tumor tissue. Oscillation and cavitation of LB induced by low intensity US exposure showed transiently open the tumor blood vessels and allowing DOX co-injected with LB was delivered into deep area in the tumor tissue. This system achieved an equivalent antitumor effect at about 1/5 the dose in monotherapy of DOX. A thyroid cancer dog was admini-stered DOXIL® and LB and ultrasonic treatment was performed four times. This cancer is a good experiment for proof of concept because it is close to human cancer from the viewpoint of spontaneous onset. From the CT image, the primary tumor volume was clearly reduced (Figure 2). In contrast, because lung metastases were not irradiated with ultrasound, no reduction was observed. From these results, it was considered that DOXIL® was efficiently delivered to the tumor tissue from the blood circulation by LB and ultrasound.

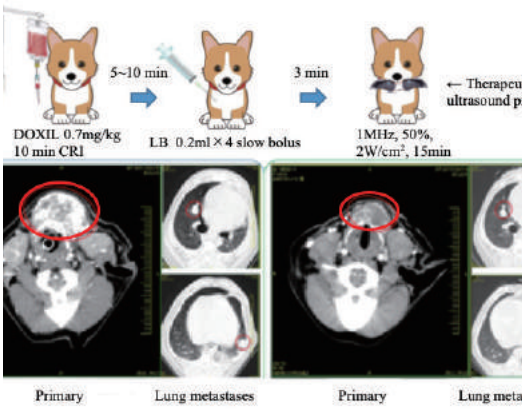

2 Antitumor effect of DOXIL+LB+US in thyroid cancer

CONCLUSIONS

New freeze-dried LB was stable in vivo for long time. Oscillation of LB induced by therapeutic US exposure showed transiently open the neovasucular of tumor tissue and allowing DOX or DOXIL® co-injected with LB was delivered into deep area in the tumor tissue. This new approach by the combination of LB and US could delivery medicines and gene into tumor tissue and work better.

REFERENCES

Scale-up production, characterization and toxicity of a freeze-dried lipid-stabilized microbubble formulation for ultrasound imaging and therapy. J. Unga, S. Kageyama, R. Suzuki, D. Omata, K. Maruyama. J. Liposome Res. 2019 β

AL

Design and synthesis of functional small-molecule probes for fluorescence imaging

Toshiyuki Kowada*

[1]Institute of Multidisciplinary Research for Advanced Materials, [2]Graduate School of Science, and [3]Graduate School of Life Sciences, Tohoku University

Fluorescence imaging is one of the most powerful techniques for visualizing biomolecules in living systems, and many fluorescent sensors and probes have been developed to monitor their activities and concentrations. However, for example, there is nothing universal, even if you could get imagined what the most useful pH probe is. We still need to optimize the properties of the probes, such as pK_a value of turn-ON fluorescence response, chemical stability, photostability, and targetability in living organisms. In such a circumstance, we have so far designed and synthesized fluorescent probes for visualizing cellular functions and ion dynamics by considering structure-optical property relationship from a physicochemical point of view. In this presentation, I will introduce the research on the development of pH-activatable fluorescence probes for intravital imaging of osteoclasts and of fluorescent probes for the quantitative analysis of zinc ion in intracellular organelles.

***Intravital imaging of osteoclasts*:**[1–3] Osteoclasts are multinucleated macrophage-derived cells responsible for bone resorption in the bone marrow. It is well-known that abnormal bone turnover caused by osteoclast dysfunction strongly relates to bone diseases, such as osteoporosis and rheumatoid arthritis. The differentiation and function of osteoclasts are regulated by the surrounding osteoblasts or T cells. Therefore, the development of imaging techniques and chemical probes for both cell motility and activity in living animals have been required for understanding the real behavior of osteoclasts during bone resorption.

We designed and developed pH-activatable fluorescent probes with bone-targeting delivery function and increased photostability, which enabled long-term monitoring of the bone-resorptive activity of osteoclasts in vivo using two-photon excitation microscopy. We also demonstrated the quantitation analysis of osteoclast activity. Consequently, real-time imaging using our probes revealed heterogenic behaviors of osteoclasts in vivo and provided insights into the mechanism of bone resorption.

***Zinc ion imaging in intracellular organelles*:** Zinc is an essential trace element abundantly present next to iron in the human body. While most part of zinc ion (Zn^{2+}) strongly binds to proteins such as metalloproteins and transcriptional factors, free Zn^{2+} is also present at low concentration in organs such as brain and pancreas. In recent years, it has been pointed out that intracellular free Zn^{2+} may function as a second messenger in various biological phenomena. Furthermore, zinc transporters have been shown to regulate the concentration of Zn^{2+} in individual cellular organelles. Therefore, the analysis of Zn^{2+} dynamics in each organelle would be important for understanding Zn^{2+}-mediated biological phenomena.

To date, various Zn^{2+} fluorescent probes based on either small-molecule or protein have been developed, and quantitative analysis of free Zn^{2+} concentration ($[Zn^{2+}]_{free}$) in cells has been conducted using fluorescent protein-based FRET probes. However, the resulting $[Zn^{2+}]_{free}$ values in ER or mitochondria varies between reports probably because of the difference of the type of probes used or influence from the intraorganellar environment, such as pH variation and oxidative environment. To provide more credible insights, we developed pH-insensitive fluorescent probes for visualizing free Zn^{2+} in subcellular compartments and demonstrated quantitative analysis of $[Zn^{2+}]_{free}$ in several organelles.

1) Kowada, T.; Kikuta, J.; Kubo, A.; Ishii, M.; Maeda, H.; Mizukami, S.; Kikuchi, K. *J. Am. Chem. Soc.* **2011**, *133*, 17772–17776.
2) Kikuta, J.; Wada, Y.; Kowada, T.; Wang, Z.; Sun-Wada, G-H.; Nishiyama, I.; Mizukami, S.; Maiya, N.; Yasuda, H.; Kumanogoh, A.; Kikuchi, K.; Germain, R. N.; Ishii, M. *J. Clin. Invest.* **2013**, *123*, 866–873.
3) Maeda, H.; Kowada, T.; Kikuta, J.; Furuya, M.; Shirazaki, M.; Mizukami, S.; Ishii, M.; Kikuchi, K. *Nat. Chem. Biol.* **2016**, *12*, 579–585.

LS

Brain hippocampus synthesizes estrogen and androgen which rapidly modulate dendritic spines in non-genomic manner

Suguru Kawato*, Mika Soma, Mari Ogiue-Ikeda
[1]Dep of Cognitive Neuroscience, Sch. Pharma-Sci., Teikyo Univ.

OBJECTIVE

Brain hippocampus locally synthesizes sex steroids (estrogen and androgen) which can modulate synapses in a rapid non-genomic manner. These processes are essential for memory encoding ability of glutamatergic neurons in the hippocampus.

METHODS

We analyzed dendritic spines (= postsynapses) in isolated hippocampal slices via visualization of spines with super-resolution confocal microscopic imaging. The density of spines and their head diameters were obtained by mathematical and automated software Spiso-3D which identifies spines by calculating geometrical parameters.

RESULTS

Estradiol (E2) at 1 and 10 nM rapidly increased the density of spines, in CA1 glutamatergic neurons. Androgen [testosterone (T) and dihydrotestosterone (DHT)] at 10 nM also increased the density. Using selective kinase inhibitors, we identified the involvement of individual protein kinases (MAPK, LIMK, PKA, PKC and Src) in spine modulation signaling through the observation of kinase inhibitor-induced suppression of E2-induced spine increase as well as suppression of androgen-induced spine increase. Using receptor inhibitors, we identified the involvement of estrogen receptor (ER) and androgen receptor (AR) in spine modulation signaling through the observation of receptor inhibitor-induced suppression of E2-induced spine increase as well as suppression of androgen-induced spine increase. These ER and AR bind spine-membrane via palmitoylation, and they are different from cytosolic/nuclear ER and AR.

CONCLUSIONS

Pathways of spine modulation signaling are as follows: synaptic ERalpha or AR → activation of LIMK, MAPK, Src, PKA, PKC → phosphorylation of cofilin or cortactin (actin binding proteins) → actin polymerization→ new spine formation (non-genomic). These pathways are completely different from slow genomic steroid-actions via cytosolic/nuclear ER and AR.

S1-1

Teikyo University Support Center Activities for Women Physicians and Researchers

Kiyoko Kaneko, Yoko Nakayama, Haruko Sekiya, Hiroko Okinaga *

Teikyo University Support Center for Women Physicians and Researchers, Teikyo University, Japan

BACKGROUND AND OBJECTIVES

The Gender Gap Index is a yearly global ranking of the disparities between the genders published by the World Economic Forum. Iceland ranked number 1 in 2018, and Japan ranked 110th out of the targeted 149 countries. The gender gap ranking of Japan is the lowest among member countries of the Organization for Economic Co-operation and Development. While the gender gap of Japan is small in the fields of education and health, the proportion of women assuming responsibility for roles such as politicians, corporate managers, and managerial staff is extremely low.

The number of female research professionals is increasing every year in Japan, and the relative proportion of female researchers has also increased by about 15.7%. But compared with other countries around the world, this ratio is rather low. A questionnaire survey of researchers in academic societies and associations revealed the following reasons for the low proportion of women researchers: (1) difficulty achieving work-life balance, (2) difficulty returning to work after maternity leave, (3) difficult work environments, (4) few role models, (5) gender division of labor, and (6) a culture of male privilege.

On this background, we established the Teikyo University Support Center for Women Physicians and Researchers in April 2013 at our university. In August of the same year, we were entrusted with the "Program for Supporting Research Activities of Female Researchers" commissioned by MEXT. This is a government-funded program that provides support for female researchers.

TEIKYO UNIVERSITY SUPPORT CENTER ACTIVITIES FOR WOMEN RESEARCHERS

Our goal is to foster the professional development of women physicians and researchers so they can engage in high-quality research activities for the rest of their careers. We also want female physicians and researchers to reach their full potential, while still balancing their social roles outside of work.

The 5 basic components in supporting the development of the potential of women are "Environmental Arrangement", "Improving Education and Research Capabilities", "Awareness Raising", "Investigation / Gathering Evidence", and "Improving the Proportion of Women".

Under our efforts on "Environmental Arrangement", we have opened an in-house nursery school as well as an infant and postnatal childcare facility on the university premises to provide care when a child is ill. We have also introduced the "Concierge Teacher" service, to provide consultations about balancing pregnancy, delivery, child-rearing, and nursing care. To further assist female researchers during life events and to support the balance between research activities and family life, we established the "Researchers' Support System" where a research assistant supports a female researcher. Regarding our efforts on "Improvement of Research Abilities", we organize programs such as seminars on obtaining external funding, career advancement, and role models. Because of the importance of "Awareness Raising", we hold an annual symposium on gender equality and workplace reform themes. In response to the President's statement on gender equality, faculty development seminars on gender equality have been held at several faculties, with discussions on creating awareness of men and women working together and recognizing the need to promote women.

As a result of these activities, the number of female researchers applying for external funding has doubled and the acceptance rate of women for Grants-in Aid for Scientific Research in 2018 also increased at Teikyo University. In addition, the total number of women in senior positions (professors and associate professors) has increased, with the proportion rising by 5.2% over the past 6 years.

Rapid cancer imaging by rationally designed fluorescence probes

Mako Kamiya,[1,*] Yasuteru Urano[1,2,3,*]

[1]Grad. Sch. Med. and [2]Grad. Sch. Pharm. Sci., The Univ. of Tokyo, [3]AMED CREST

OBJECTIVE

It has been a long-term goal to develop cancer-imaging techniques that have sufficient specificity and sensitivity, since early detection and complete resection are an important prognosticator for cancer treatment. Since fluorescence-guided diagnosis is one of the most powerful techniques for real-time in situ cancer detection, we have focused on developing a new cancer-imaging method with activatable fluorescent probes targeted to enzymes that are overexpressed in cancer.

METHODS and RESULTS

We first focused on cancer-associated aminopeptidases as imaging targets, since they play essential roles in many diseases and some of them exhibit altered expression levels in the pathological context. By utilizing our rational design strategies for activatable fluorescence probes based on the concept of intramolecular spirocyclization, we prepared a series of fluorogenic substrates for various aminopeptidases which have unique characteristics that the probes themselves are colorless and almost non-fluorescent due to the formation of spirocyclic structures, but can be converted to highly fluorescent molecules by the target enzymes, thus showing drastic fluorescence activation. By applying these probes to the resected specimen from cancer patients, followed by the subsequent assessment of fluorescence signals, we found that gGlu-HMRG (a probe for γ-glutamyltranspeptidase, GGT) can be selectively activated at certain types of cancers such as breast cancer, oral cancer, head and neck cancer, and liver cancer. We also found that EP-HMRG targeting dipeptidylpeptidase-IV (DPP-IV) is effective for detecting esophageal cancer in resected tissue from patients.

In order to expand the target cancer, we next focused on cancer-associated carboxypeptidases. Especially, we focused on the glutamate carboxypeptidase activity of prostate-specific membrane antigen (PSMA), which is a type II transmembrane glycoprotein that is overexpressed in prostate cancer. Based on our finding that aryl-glutamate conjugates with an azoformyl linker are recognized by PSMA and have a sufficiently low LUMO (lowest unoccupied molecular orbital) energy level to quench the fluorophore through photo-induced electron transfer, we established a new design strategy for activatable fluorescence probes to visualize carboxypeptidases activity, and developed a first-in-class activatable fluorescence probe for carboxypeptidases activity of PSMA. We confirmed that the developed probe allowed us to visualize the CP activity of PSMA in living cells and in clinical specimens from prostate cancer patients, and is expected to be useful for rapid intraoperative detection and diagnosis of prostate cancer.

CONCLUSIONS

In conclusion, the fluorescence-guided diagnosis by our activatable probes can be used as an imaging guidance during surgical procedures to help surgeons for efficient tumor inspection. In particular, due to its rapid and strong activation upon reaction with the target enzyme at cancer site just by topical spraying, we believe that it should have a great potential for clinical application to realize early detection and complete resection of cancer.

S1-3

Capsid protein structure in Zika virus reveals the flavivirus assembly process

Ter Yong Tan[1,2,7], Guntur Fibriansah[1,2,7], Victor A. Kostyuchenko[1,2], Thiam-Seng Ng[1,2], Xin-Xiang Lim[3], Shuijun Zhang[1,2], Xin-Ni Lim[1,2], Jiaqi Wang[1,2], Jian Shi[4], Marc C. Morais[5], Davide Corti[6], Shee-Mei Lok[1,2]

Affiliations:

[1]Program in Emerging Infectious Diseases, Duke–National University of Singapore Medical School, Singapore.

[2]Centre for BioImaging Sciences, Department of Biological Sciences, National University of Singapore, Singapore.

[3]Department of Biological Sciences, National University of Singapore, Singapore.

[4]CryoEM unit, Department of Biological Sciences, National University of Singapore, Singapore.

[5]Department of Biochemistry and Molecular Biology, Sealy Center for Structural and Molecular Biophysics, University of Texas Medical Branch, Galveston, Texas, United States of America.

[6]Humabs BioMed SA, a subsidiary of Vir Biotechnology, Inc., Bellinzona, Switzerland.

Structures of flavivirus (dengue, Zika virus) particles are known to near-atomic resolution, and show detailed structure and arrangement of their surface proteins (E and, prM in immature or M in mature virus). In contrast, the arrangement of the capsid proteins:RNA complex, which forms the core of the particle, is poorly understood, likely due to inherent dynamics. Here we stabilized immature Zika virus via an antibody that binds across the E and prM proteins, resulting in a subnanometer resolution structure of capsid proteins within the virus particle. All secondary structural elements are visible, including a helix that was previously thought to be removed via proteolysis. This structure illuminates capsid protein quaternary organization, including its orientation relative to the lipid membrane and the genomic RNA, and its interactions with the trans-membrane regions of the surface proteins. Results show the capsid protein plays a central role in the flavivirus assembly process.

S1-4

Therapeutic strategies using image-guided focused ultrasound for neurodegeneration.

Isabelle Aubert*[1,2]

[1]Sunnybrook Research Institute, [2]University of Toronto, Ontario, Canada.

Pr. Aubert will discuss the importance of equity, diversity and inclusion (EDI), focusing on women as one of the marginalized groups in science. She will provide examples on how EDI strengthens research excellence, innovation and creativity, and how progress comes from leadership with strong EDI commitments, policies and tangible actions that are seen publicly.

Pr. Aubert will then present an overview of her ongoing collaborative work at Sunnybrook, in which she leads the preclinical development of therapies for neurodegenerative disorders using transcranial image-guided focused ultrasound (FUS).

OBJECTIVES

The primary objectives are (1) to provide background knowledge on image-guided FUS applications for brain disorders, and (2) to present key preclinical work in FUS that led to clinical trials for patients with Alzheimer's disease.

METHODS

Transcranial FUS guided by magnetic resonance imaging (MRI) can target disease-specific brain regions. As examples, FUS modalities can be used to treat brain areas affected by cancer cell growth, or a specific thalamic nucleus in patients with essential tremors, or the hippocampal formation in patients with Alzheimer's disease. Pr. Aubert will discuss the application of FUS in the context of neurodegenerative disorders, where FUS is used to increase the permeability of the blood-brain barrier (BBB), transiently and non-invasively. FUS-induced BBB permeability has been characterized for the delivery of therapeutics to the brain, with more recent discoveries on neural modulation. Preclinical work will be presented, using MRI-guided FUS (MRIgFUS) for BBB permeability in models of neurodegenerative disorders, particularly on the development of therapeutic strategies for Alzheimer's disease. Quantitative biochemical and imaging methods are used to evaluate the efficacy of FUS to deliver therapeutics, and to establish the impact of FUS on neuronal and glial plasticity in the brain, with and without intravenously administered therapeutics.

RESULTS

MRIgFUS efficiently delivers small molecules, shRNAs, and recombinant adeno-associated viruses (rAAVs) used for gene therapy to targeted brain areas in animal models of neurodegenerative disorders. In preclinical models of Alzheimer's disease, FUS-induced BBB permeability reduced pathology and increased brain plasticity. In patients with Alzheimer's disease, FUS-induced BBB permeability has now been shown to be reversible and safe.

CONCLUSION

The modulation of the BBB for increased permeability with FUS has moved from preclinical models to patients with brain disorders and it shows promises for drug delivery and potentially for inducing neural plasticity.

S2-1

Chemical design of $^{67/68}$Ga-labeled antibody fragments for low renal radioactivity levels

Tomoya Uehara
Graduate Sch. Pharma-Sci., Chiba Univ.

OBJECTIVE

Radiolabeled low molecular-weight antibody fragments (LMW Abs) such as Fab exhibit high and persistent localization of radioactivity in the kidney when they are labeled with metallic radionuclides, which has hindered tumor visualization near kidney regions and limited therapeutic effectiveness. Persistent renal radioactivity levels were attributed to the long residence time of radiometabolites generated after lysosomal proteolysis of radiolabeled LMW Abs, following glomerular filtration and subsequent reabsorption in renal cells. To solve the problem, we hypothesized that the renal radioactivity levels after injection of radiolabeled LMW Abs would be improved by liberating a radiometal chelate of urinary excretion from the LMW Abs by enzymes in the lysosome or on the renal brush border membrane (BBM). In this presentation, I will talk the evaluation of the renal radioactivity levels of newly designed $^{67/68}$Ga-labeled antibody fragments with linkages cleaved by enzymes present in the lysosome or on the BBM.

METHODS

Di- or tri-peptide, methionine-isoleucine (MI) sequence or methionine-valine-lysine (MVK) sequence were conjugated to a ^{67}Ga-labeled S-2-(4-isothiocyanatobenzyl)-1,4,7-triazacylononane-1,4,7-triacetic acid (^{67}Ga-NOTA-SCN) and evaluated as enzyme-cleavable linkages (^{67}Ga-NOTA-MI and ^{67}Ga-NOTA-MVK). In these molecular designs, ^{67}Ga-NOTA-Met would be liberated from ^{67}Ga-NOTA-MI or ^{67}Ga-NOTA-MVK by the enzymes presented in lysosomes or on the BBM, respectively. Biodistribution of radioactivity after injection of ^{67}Ga-NOTA-MI-Fab, ^{67}Ga-NOTA-MVK-Fab and ^{67}Ga-NOTA-Fab (a conventional thiourea linkage; no enzyme-cleavable linkage) in mice were evaluated.

RESULTS

^{67}Ga-NOTA-MI-Fab was obtained at radiochemical yields of over 95% and was stable in murine serum for 24 h. In the biodistribution study using normal mice, ^{67}Ga-NOTA-MI-Fab showed significantly lower renal radioactivity levels from 1 to 6 h postinjection than those of ^{67}Ga-NOTA-Fab. Analysis of urine obtained 6 h postinjection of ^{67}Ga-NOTA-MI-Fab in normal mice showed that ^{67}Ga-NOTA-Met was the main radiometabolite. In the biodistribution study using tumor-bearing mice, ^{67}Ga-NOTA-MI-Fab showed significantly lower renal radioactivity levels without impairing the tumor radioactivity levels at 3 h postinjection than those of ^{67}Ga-NOTA-Fab. However, further studies are required to reduce renal radioactivity levels shortly after the injection of ^{67}Ga-labeled Fabs. To liberate ^{67}Ga-NOTA-Met at an earlier stage of antibody metabolism in the kidney, ^{67}Ga-NOTA-MVK-Fab that contained BBM enzyme-cleavable linkage was designed. ^{67}Ga-NOTA-MVK-Fab was obtained at radiochemical yields of over 95% and was stable in murine serum for 24 h. The MVK sequence conjugated ^{67}Ga-NOTA was recognized by enzymes of renal BBM to liberate ^{67}Ga-NOTA-Met. ^{67}Ga-NOTA-MVK-Fab showed significantly lower renal radioactivity levels from 30 min to 6 h postinjection than those of ^{67}Ga-NOTA-Fab and ^{67}Ga-NOTA-MI-Fab. Analysis of urine obtained 6 h postinjection of ^{67}Ga-NOTA-MVK-Fab in normal mice showed that ^{67}Ga-NOTA-Met was the main radiometabolite. In the biodistribution study using tumor-bearing mice, ^{67}Ga-NOTA-MVK-Fab showed significantly lower renal radioactivity levels without impairing the tumor radioactivity levels at 3 h postinjection than those of ^{67}Ga-NOTA-Fab and ^{67}Ga-NOTA-MI-Fab. In the SPECT/CT images, ^{67}Ga-NOTA-MVK-Fab provided a much higher contrast tumor image when compared with ^{67}Ga-NOTA-Fab and ^{67}Ga-NOTA-MI-Fab.

CONCLUSIONS

These findings indicated that the strategy of liberating a radiolabeled compound to urinary excretion from antibody fragments at the renal BBM to reduce the renal radioactivity levels was useful for the $^{67/68}$Ga-labeled antibody fragments of low renal radioactivity levels.

S2-2

Development of Far-Red to Near-Infrared Small-Molecule Fluorophores and Their Application to Fluorescent Probes

Kenjiro Hanaoka [1,*]

[1]*Graduate School of Pharmaceutical Sciences, The University of Tokyo*

OBJECTIVE

Fluorescence imaging is one of the most powerful techniques for visualizing temporal and spatial changes of biological phenomena in living cells, and many fluorescent probes have been developed. In particular, xanthene dyes such as fluorescein and rhodamines have favorable characteristics, such as high water solubility, high fluorescence quantum yield and high molar extinction coefficient, and they have been utilized as fluorescent cores for fluorescent probes working in the green to red wavelength region. Recently, silicon-substituted xanthene dye, 2,7-*N,N,N',N'*-tetramethyl-9-dimethyl-10-hydro-9-silaanthracene (TMDHS)[1], has been reported, and we have also designed and synthesized Si-rhodamines (SiRs)[2,3] and TokyoMagentas (TMs)[4], in which the O atom at the 10-position of xanthene is replaced with a Si atom, as far-red to near-infrared (NIR) fluorescent cores[5,6].

In biological systems, the pH in intracellular organelles is strictly regulated, and differences of pH are deeply related to key biological events such as protein degradation, intracellular trafficking of cell components. To perform these reactions efficiently, intracellular organelles are maintained at specific pH values appropriate for each process. Ratiometric fluorescence imaging is useful for determination of precise pH values, but existing fluorescent probes have substantial limitations, such as inappropriate pK_a for imaging in the physiological pH range, inadequate photobleaching resistance, and insufficiently long excitation and emission wavelengths. So, we set out to develop a novel ratiometric pH fluorescent probes.

METHODS

Recently, we have established the synthetic scheme for asymmetric SiRs.[7] Among them, we discovered the dye scaffold that shows an absorption wavelength change of about 80 nm in response to pH change. Rhodamines are often used for fluorescence imaging because of their high resistance to photobleaching, high water solubility, and high fluorescence quantum yields. In addition to these advantages, SiRs have longer absorption and emission wavelengths, which enable multi-color imaging with widely used fluorescent proteins such as GFP and YFP.

RESULTS

We have developed a fluorescent probe, **SiRpH5**, based on the asymmetric SiR scaffold, which can be used for imaging of intracellular organelle pH.[8] To demonstrate its usefulness for biological applications, we achieved time-lapse imaging of pH in endocytic compartments during protein trafficking by using transferrin tagged with **SiRpH5**.

CONCLUSIONS

We have found that asymmetric rhodamines bearing a piperazine ring show a large, pH-dependent blue shift of the absorption spectra upon protonation of the piperazine ring. **SiRpH5** is a fluorophore whose excitation and emission wavelengths lie in the far-red to NIR region. This provides a new color window for multi-color pH imaging with GFP and YFP. In addition, **SiRpH5** has a higher resistance to photobleaching compared to conventional ratiometric probes, suggesting that **SiRpH5** would be a suitable probe for long-term tracking of intracellular organelle pH. Conjugation of **SiRpH5** to macromolecules was an effective strategy for specific imaging of intracellular organelles, and **SiRpH5** could be delivered to the targeted intracellular organelles by choosing an appropriate macromolecule for conjugation. These chemical tools should be useful for studying the influence of intracellular pH on biological processes, as well as for *in vivo* imaging.

REFERENCES: 1) *Chem. Comm.,* 1780 (2008); 2) *ACS Chem. Biol.*, **6**, 600 (2011); 3) *Bioorg. Med. Chem. Lett.*, **22**, 3908 (2012); 4) *Chem. Commun.*, **47**, 4162 (2011); 5) Review article: *Analyst*, **140**, 685 (2015); 6) Review article: *Chem. Asian J.*, **12**, 1435 (2017); 7) *Chem. Commun.*, **54**, 6939 (2018); 8) *J. Am. Chem. Soc.*, **140**, 5925-5933 (2018).

S3-1

Label-free peripheral nerve detection and imaging by Raman scattering

Yasuaki Kumamoto,[1,*] Tetsuro Takamatsu[2]

[1]Dept. of Pathology and Cell Regulation, Kyoto Pref. Univ. of Medicine, [2]Dept. of Medical Photonics, Kyoto Pref. Univ. of Medicine

OBJECTIVE

Peripheral nerves are essential tissues for organs and limbs to function properly. There is a risk of peripheral nerve injury in surgery by tumor resection, although nerve sparing surgery is widely conducted; in nerve sparing surgery, a surgeon tries to identify peripheral nerves by appearance and anatomical knowledge but a peripheral nerve thinner than 1 mm in diameter is hard to identify. To address this issue, we are aimed at development of a label-free and nondestructive method for accurate peripheral nerve detection and imaging.

METHODS

For label-free and non-destructive peripheral nerve detection, we employed Raman scattering spectroscopy. Raman scattering spectra of peripheral nerves are different from those of adjacent tissues such as skeletal muscle, adipose, fibrous connective, and blood vessel tissues. We utilized this difference for discriminating peripheral nerves from non-nerve tissues in a label-free and non-destructive manner. To quantify the discrimination, we collected a number of spectra of nerve and non-nerve tissues excised from rats, including 2000 spectra from myelinated and unmyelinated nerves and 3000 spectra from skeletal muscle, fibrous connective, and adipose tissues, and subsequently analyzed them with principal component regression and quadratic discrimination by leave-one-out cross-validation.

We further expanded the Raman spectroscopic approach to peripheral nerve imaging. In considering the importance of rapidness in an intraoperative nerve imaging process, we developed a multipoint Raman measurement apparatus. In the apparatus, an excitation laser at λ = 532 nm emission is subdivided into 32 multiple beams by a microlens array. The beams are focused on a sample and Raman scattering light generated at the 32 foci was collected with 32 optical fibers without significant cross talk. By aligning the arrangement of the fibers at exit to the entrance slit of a spectrometer, we detected multiple spectra with a two-dimensional CCD camera in parallel. Through the principal component regression and quadratic discrimination analysis, a nerve-prediction distribution was obtained. The distribution was overlaid with a bright-field image for virtual nerve imaging by image analysis.

RESULTS

By the principal component regression and quadratic discrimination analysis, we classified nerve and non-nerve tissues with the accuracy of 97.8%. This accuracy is sufficiently high for intraoperative nerve detection. For intraoperative nerve detection where plural target tissues are to be inspected, however, a rapid nerve imaging technique is required. This requirement was satisfied by our multipoint apparatus; we acquired 32 spectra in 5 seconds successfully. The overlay of the nerve-prediction distribution with a bright-field image allowed counting of the numbers of nerve-positive prediction points to the total measurement points at individual target tissues. By setting a threshold for the ratio of these two values, we realized at-a-glance identification of peripheral nerves in the field of view. Of 278 target tissues including 158 peripheral nerves and 120 connective tissues analyzed, 97.5% were true predictions.

CONCLUSIONS

These results indicated that the multipoint Raman spectroscopic technique was capable of rapid and accurate peripheral nerve imaging. Remaining issues of the presented technique for intraoperative uses include fusion with an endoscopic technique as well as optimization of multipoint arrangement and excitation laser wavelength.

S3-2

New methodology for examining the light-microscopic glass slide specimen by a Low-vacuum Scanning Electron Microscope (LVSEM)

Nobuaki Yamanaka, ***Tokyo Kidney Research Institute***

OBJECTIVE

Recently an innovative histopathological examination method has been invented. This method enables the light microscopic glass slide specimen to be directly observed by low-vacuum scanning electron microscope(LVSEM). To obtain the contrast for EM examination, the light microscopic specimen should be stained by heavy metal. At present, as the heavy metal staining, silver staining and platinum-bleu staining are available for light microscopic paraffin sections to be observed by LVSEM. This study is to verify the usefulness of this method as correlative light and electron microscopic (CLEM) analysis in the routine morphological examination.

METHODS

For the renal biopsy diagnosis, silver staining (PASM staining) is routinely implemented, then PASM-stained glass slide tissue is directly available for observation with LVSEM. For Platinum-blue staining, usual paraffin section for light microscopy is deparaffinized and immersed with Platinum-blue solution for 10-20 minutes. These metal-stained sections on the glass slide is observed with Hitachi LVSEM TM3030 for various light microscopic tissue specimens.

RESULTS

In observation of the specimen with silver staining, the ultrastructural fine details of silver-positive components, such as basement membrane and collagen fibers, are clearly depicted. In contrast, silver-negative components, such as endothelial cells and podocytes, are finely shown in their cytoplasmic details by the platinum-blue staining. Several new unexpected ultramicroscopic findings were observed in examining the light microscopic tissue specimens.

CONCLUSIONS

This methodology is highly beneficial for obtaining electron microscopic level information from usual light microscopic specimens with the higher magnification and higher resolution. The properties of scanning electron microscopy of LVSEM provide additional 3D information on the entire specimen thickness and further contribute to clear, detailed perception of the morphological changes.

The examination procedures are fairly simple, comparing to the conventional special technique required for usual EM examination. It is expected this CLEM method will contribute to improve the quality of histopathological analysis of LM specimens.

S3-3

Near Infrared Biomedical Imaging for Visualizing Subcutaneous and Submucosal Information

Kohei SOGA[1-3], Karina NIGOGHOSSIAN[1], Gil YEROSLAVSKY[2], Thi Kim Dung DOAN[3], Masakazu UMEZAWA[1], Kyohei OKUBO[1,2], Masao KAMIMURA[1,2], and Naoko OHTANI[4]

[1]Dept. of Mater. Sci. and Tech., Tokyo Univ. of Sci., Katsushika, Tokyo, Japan
[2]Imaging Frontier Center, Tokyo Univ. of Sci., Noda, Chiba, Japan
[3] Res. Inst. for Biomed. Sci., Tokyo Univ. of Sci., Noda, Chiba, Japan
[4] Dept. of Pathophysiology, Osaka City Univ., Osaka, Japan
email: mail@ksoga.com, web site: http://www.ksoga.com

A child draws a line drawing on sand. This is one of the most primitive "imaging" to show something in his or her mind. The essential information is a "shape." Even with this primitive way of imaging, one can receive some "meaning" or "information" such as happy or sad with smiling ☺ or crying ☹. Photography may give much more information with gradual contrast. Color photography was innovative to give much more information as the person is heathy or ill. Now a day, the mission of the development of the imaging techniques contains to show "meaning" or "information" with viewgraphs. Not only the existence or/and the shape of a matter, but information like oxygen or glucose concentration and the meaning as "cancer." The pixel information is no more in one dimension.

The spatial dimension also becomes higher. 3D is normal. The viewgraph may contain "time" is called movie or video. The information of a pixel is becoming higher and higher. The information processing is no more in the hands of human being. In this sense, computer science is one of the essence of the development of the imaging techniques.

One of the kind of lights, near infrared (NIR) light, is attractive with two reasons. One is the transparency. The optical loss is caused by resonance with a light and electric dipole moment in substance for absorption and bending. It occurs in ultraviolet by electronic transition and infrared by molecular vibration. The absorption of course dims the light for normally changing the energy into heat. The bending, containing reflection, refraction and scattering, is caused by the change of refractive index (light speed) along with the propagation of a light. As a consequence, the NIR light is transparent because the wavelength (or frequency) is far both from the ultraviolet or infrared. The other characteristic is week absorption due to overtone and combination bands of the vibration of ions or molecules, which are essentially forbidden for a harmonic oscillator. The absorption intensity is roughly hundred times less than that of normal vibration bands in the infrared range. The fact means the NIR light reflection or transmission may contain the information of molecules on the pathway.

The authors have developed various methods for visualizing information of biological objects by using the NIR light. Fluorescence thermometry can give temperature of a deep part of a body as a 3D image. Hyper spectral imaging (HSI) combined with machine learning can exhibit the distribution of fat concentration. The presentation will review the NIR biomedical imaging for visualizing subcutaneous and submucosal information.

References

1) S. Sekiyama, K. Soga et al., *Langmuir*, **35** (2019) 831-837. DOI: 10.1021/acs.langmuir.8b03789.
2) S. Sekiyama, K. Soga et al., *Sci. Rep.*, **8** (2018) 16979-. DOI: 10.1038/s41598-018-35354-y.
3) M. Kamimura, K. Soga et al., *Polym. J.*, **49** (2017) 799-803. DOI: https://doi.org/10.1038/pj.2017.59.
4) D. Jaque, K. Soga et al., Adv. Opt. Photon., **8** (2016) 1-103. DOI: 10.1364/ · AOP.8.000001.

S4-1

Systematic Approach for Live Cell Selective Imaging Probe Development

Young-Tae Chang [1,2]

[1]POSTECH Chemistry and [2]Center for Self-Assembly & Complexity, IBS

Conventional cell imaging probe development is based on a holding target in the cell, such as proteins or carbohydrates. We have developed a Diversity Oriented Fluorescence Library Approach (DOFLA) where a combinatorial synthesis of fluorescent dye is combined with unbiased cell type specific screening. More than 10,000 fluorescent organic dyes were constructed as a tool-box, and more than 20 different cell type specific probes have been developed. Recently, we started to investigate an alternative mechanism of cell selective staining through transporters. In this presentation, the comparison between conventional HOLD (Holding Oriented Live-cell Distinction) and GOLD (Gating Oriented Live-cell Distinction) will be discussed with an example of activated macrophage probe, CDg16. The probes developed in this study will be freely available for the chemical biology community for open academic research.

Imaging and controlling membrane receptor activities in living cells

Takeaki Ozawa[1]

[1]*Department of Chemistry, School of Science, University of Tokyo*

β

OBJECTIVE

Recognition of extracellular stimuli via various cell-surface receptor proteins is indispensable for cells to adapt to surrounding dynamic environments. The amount of receptors on plasma membrane is strictly regulated for the precise modulation of receptor-mediated signaling. To unveil the physiological roles of receptor proteins, direct manipulation of the receptor-mediated signaling in living cells is required. Conventionally, chemical compounds have been used for the regulation of receptor activities; however, the diffusion and technical difficulties hampers precise analysis on their spatiotemporal functions. To control the receptor-mediated signaling in a spatiotemporal manner, we developed an optogenetic system for inducing light-dependent internalization on a variety of G-protein coupled receptors (GPCRs), the largest family of membrane receptors, using an endocytosis fragment of GPCR and its binding protein of β-arrestin.

METHODS

To induce endocytosis with light illumination, a pair of light-dependently dimerizing plant proteins called cryptochrome 2 (CRY2) and CIB was used. β-arrestin was attached to CRY2 ($Arrestin_{CRY}$). $E\text{-}fragment_{CIB}$ was generated by fusing carboxyl-terminal tail of vasopressin 2 receptor (V2Rct) with CIB. $E\text{-}fragment_{CIB}$ was subsequently attached to GPCR of interest. Upon light illumination, cytoplasmic $arrestin_{CRY}$ is recruited to $E\text{-}fragment_{CIB}$ located on plasma membrane by light-dependent CRY2-CIB interaction. Forced interaction between β-arrestin and V2Rct triggers endocytosis of GPCR labeled with $E\text{-}fragment_{CIB}$.

RESULTS

To confirm whether light illumination triggers membrane-tethered $E\text{-}fragment_{CIB}$ ($Myr\text{-}E\text{-}fragment_{CIB}$) endocytosis or not, $Myr\text{-}E\text{-}fragment_{CIB}$ was expressed in HEK293 cells and observed under confocal fluorescent microscope. Upon illumination with blue laser light, endocytic vesicles were clearly observed in cytoplasm. Dyngo4a, a dynamin inhibitor, treatment abolished the light-induced endocytosis, indicating that the light-dependent $Myr\text{-}E\text{-}fragment_{CIB}$ endocytosis was dependent on clathrin-mediated pathway.

To explore the destination of endocytic vesicles containing $Myr\text{-}E\text{-}fragment_{CIB}$, several organelle were fluorescently labeled with green fluorescent protein (GFP) during light-induced $Myr\text{-}E\text{-}fragment_{CIB}$ endocytosis. Confocal microscope observation revealed that endocytic vesicles containing $Myr\text{-}E\text{-}fragment_{CIB}$ colocalized with early-endosome after 30 min illumination, then with lysosome after 60 min illumination. The western blot analysis also revealed that $Myr\text{-}E\text{-}fragment_{CIB}$ was subjected to lysosomal degradation upon illumination, suggesting that endocytic vesicles containing $Myr\text{-}E\text{-}fragment_{CIB}$ were delivered to early-endosome and subsequently degraded in lysosome.

Finally, we investigated whether $E\text{-}fragment_{CIB}$ labeling enables GPCR endocytosis by light or not, several GPCRs labeled with $E\text{-}fragment_{CIB}$. Blue light illumination on cells expressing Adrenoceptor A2α (ADRA2A) labeled with $E\text{-}fragment_{CIB}$ ($ADRA2A\text{-}E\text{-}fragment_{CIB}$) triggered endocytosis of $ADRA2A\text{-}E\text{-}fragment_{CIB}$. Quantitative analysis of the fluorescent intensity on plasma membrane revealed statistically significant decrease of $ADRA2A\text{-}E\text{-}fragment_{CIB}$ compared to ADRA2A upon light illumination. Consequently, $E\text{-}fragment_{CIB}$ labeling enabled light-induced endocytosis of target GPCRs.

CONCLUSIONS

We developed an optogenetic system to induce GPCR endocytosis by light using peptide named $E\text{-}fragment_{CIB}$. Endocytic vesicles containing $Myr\text{-}E\text{-}fragment_{CIB}$ were delivered to early-endosome and then degraded in lysosome. The amount of cell surface GPCRs labeled with $E\text{-}fragment_{CIB}$ decreased by the light-dependent endocytosis. The developed system will enable us to directly regulate the receptor-mediated signal transduction in a spatiotemporal manner by controlling the amount of receptors on plasma membrane by light.

S4-3

Characterization of Photoacoustic Imaging in Bioimaging

Miya Ishihara,[1]

[1]*Dept. of Medical Engineering, National Defense Medical College*

The factors influencing bio-optical imaging performance include spatial resolution, maximum depth, and non-invasiveness. Further, there is a trade-off among these factors, which means that all of these factors are not satisfied at the same time. A technical challenge in bio-optical imaging is the elimination of this bottleneck.

Photoacoustic (PA) imaging (also called optoacoustic imaging), which visualizes the distribution of optical absorption molecules, is based on optical excitation and ultrasound detection through a thermoelastic process. PA imaging has the advantage of being able to use optical spectroscopic characteristics, and this merit can be used for an optical target as well as fluorescence imaging. PA imaging is different from fluorescence imaging, in that PA signal intensity is inversely proportional to fluorescence quantum yield, whereas the signal intensity of fluorescence imaging is proportional to fluorescence quantum yield. The larger absorbance results in greater signal intensity. Another feature of PA imaging is tomography, which has information of depth resolution. Furthermore, because acoustic waves scatter considerably less than optical waves in tissue, PA imaging has the advantage of a deeply penetrating imaging.

Our technical solution to the spatial resolution at the deep region is the expansion of the coverage of ultrasonic and optical focusing technique. We have constructed a PA tomography type device that can observe the whole body of a mouse to obtain a deep region PA image (Figure 1), and a PA microscopic type device with optical spatial resolution.

In the talk, I would like to present the various data acquired thus far, and discuss the role of PA imaging in bioimaging.

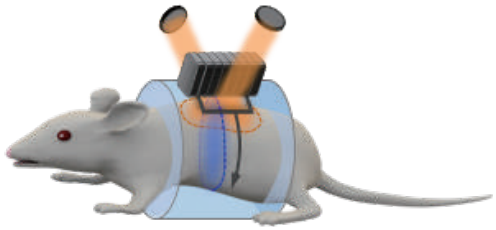

Figure 1 Photoacoustic tomography for whole body mouse imaging

Trans-Scale Imaging for Singularity Biology

Takeharu Nagai[1,2]

[1]*The Institute of Scientific and Industrial Research, Osaka Univ.,* [2] *Institute for Open and Transdisciplinary Research Initiative., Osaka Univ.*

There exist critical moments, such as the 'Big Bang' where "something out of nothing gets created" or in the future, when artificial intelligence might become greater than human intelligence. These points are called *singularities*. In the field of biological science, discontinuous critical phenomena are broadly seen, for example, the emergence of life from the primordial soup, or the evolution and outbreak of diseases. It has been indicated that only a small number of core elements are required to bring about discontinuous changes to an entire multi-component system. However, the mechanism-of-action that generates such singularity phenomena is not yet certain. In our research project, to look deeply into singularity cells, we are developing an imaging platform that will achieve both wide field-of-view high-resolution imaging and high-speed long-term imaging, and corresponding information analysis methods. This will enable us to be at the cutting edge of new scientific fields, where we uncover the underlying mechanisms for the generation of singularity cells as well as their biological functions.

In order to study the processes that singularity cells, considered as minority entities, bring criticality to an entire system (ex: an organ or whole body), it is necessary to measure, analyze, and examine such biological systems in a holistic spatial-temporal manner. For this purpose, an imaging system is required for visualization of *molecules, cells, and organs* across different length scales. In order to achieve this, we are now developing a unique trans-scale imaging device that we call AMATERAS (**A**spired **M**ultimodal **A**nalytical **T**ools for **E**very **R**are **A**ctivities in **S**ingularity) which allows us to capture macroscopic spatiotemporal dynamics with microscopic precision: *not only the composite trees but also the whole forest*.

In this symposium, I will introduce how the trans-scale imaging device will open the new horizon for singularity biology.

Acknowledgements

This work is supported by Grant-in-Aid for Scientific Research on Innovative Areas (18H05408), MEXT, Japan

S5-1

Mechanical impact of apoptosis in tissue homeostasis

Yusuke Toyama[1,2]

[1]*Mechanobiology Institute, National University of Singapore, Singapore*

[2]*Department of Biological Sciences, National University of Singapore, Singapore*

Apoptosis, or programmed cell death, is the most common mechanism of eliminating damaged or unnecessary cells during embryonic development, tissue homeostasis, and certain pathological conditions. When a cell undergoes apoptosis within a tissue, the apoptotic cell is expelled from its neighboring non- dying cells. It has been shown by many labs, including ours, that this mechanical process is driven by the formation and contraction of the actomyosin cables in the dying and the neighboring cells, and/or by the lamellipodial crawling of the neighboring cells. However, how cell mechanics arises upon apoptotic cell extrusion and feedbacks to cellular and molecular function especially in the neighboring non-dying cells is largely illusive. In this presentation, I will present our current understandings of how mechanical tension and biochemical natures are altered in the neighboring cells as a consequence of apoptosis, and how these two factors are related to each other.

Visualizing and Controlling Cell Adhesion Complexes at the Molecular Scale

Tony Kanchanawong [1, 2]

[1] *Mechanobiology Institute, National University of Singapore, Singapore*

[2] *Department of Biomedical Engineering, National University of Singapore, Singapore*

Many complex biological functions are performed by supramolecular assemblies self-organized from a diverse ensemble of proteins. Cell adhesion structures such as the integrin-based focal adhesions and cadherin-based cell-cell junctions are multi-protein complexes known to transmit, sustain, sense, and respond to mechanical force. The knowledge of their physical organization is therefore essential for insights into their mechanobiological functions. Due to the nanometer size scale of the adhesion protein building blocks, the nanoscale is the functionally salient length scale for the spatial organization of these molecular complexes. In this talk, I will discuss our recent studies that sought to 1) decipher the nanoscale architecture of integrin-mediated and cadherin-mediated cell adhesion complexes, using interference-based super-resolution microscopy techniques [1, 2]; 2) control force transmission through specific cell adhesion molecules by chemical biology and optogenetic approaches.

References

1. Liu, J., et al., Talin determines the nanoscale architecture of focal adhesions. Proceedings of the National Academy of Sciences, 2015. 112(35): p. E4864-E4873.

2. Bertocchi, C., et al., Nanoscale architecture of cadherin-based cell adhesions. Nat Cell Biol, 2017. 19(1): p. 28-37.

S5-3

Fine structures of the cells revealed with conventional and super resolution microscopy

Kaoru Katoh,[1,2]* Minami Tanaka,[1] Totai Mitsuyama [2]
[1]Biomed. Res. Inst, AIST, [2] AI Res. Center, AIST

Growth cones are enlargement of thin cytoplasm at the tips of growing neurites. The growth cones crawl about and find the path of neuronal elongation. Their movements depend on the dynamics of actin filaments (actin meshwork), which are too small to observe with conventional optical microscopes. We, therefore, applied polarized light microscope (Polscope), apodised phase contrast microscope, and recently super resolution microscopes (SIM, STED and Spinning disk) to visualize actin cytoskeleton to see actin cytoskeleton and other structures.

In this presentation, we will summarize the images of fine structures of the cell, which we recorded with conventional (polarized light and apodised phase contrast) and super resolution microscopy. Polscope revealed radially aligned actin bundles in the growth cones of living unstained cells. Apodised phase contrast revealed intra nuclear structures and intracellular organelle (mitochondria, ER etc.). Super resolution microscopes revealed fine structures of actin meshwork. SIM (Structure Illumination Microscope) visualized actin meshwork in live cells with resolution of 110 nm as time lapse movie and STED (**St**imulated **e**mission **d**epletion) microscope visualized them in the fixed cells with higher resolution (30-50 nm) and with thin optical section (140 nm thick in each optical slice). Two camera SIM showed co-localization of actin and actin bundling protein (fascin) in live cells with high resolution and dissociation of fascin from actin bundles as time lapse records. Spinning disk type super resolution revealed fine structures in the small fish.

Based on the summarized image data, we will discuss future of the imaging with optical microscopes. This will include big image data (of several TB size (1 million frame images)), AI and robots in biomedical imaging with optical microscopy.

Mg ion as a novel candidate for second messenger

[1] Kotaro Oka*, [2] Ryu Yamanaka, [1] Yutaka Shindo
[1]*Dept. Biosci. & Informat., Keio Univ.* [2]*Fac. Pharm., Sanyo-Onoda City Univ.*

OBJECTIVE

Mg^{2+} is recognized as a multi-target analogue regulator that performs many roles, such as stabilizing biological macromolecules, mediators for enzymatic activity, and also circadian timekeeping. Mg^{2+} has been recognized due to the following physiological properties; (i) it influences wide-ranging biological processes, (ii) its concentration is tightly controlled within a narrow sub-millimolar range, and (iii) its intracellular dynamics are slow and long-lasting; its regulatory manner is not all-or-none in contrast to the switch-like signal transduction by the well-established second messenger Ca^{2+} [1]. Recent studies, however, have reported another role for Mg^{2+} as a second messenger in immune cells. These multifaceted characteristics of Mg^{2+} raise the question of how Mg^{2+} processes information and how common its role is as a signaling molecule. We, therefore, investigated the role of Mg^{2+} as a second messenger in early developmental stages of neurons with several fluorescent-imaging techniques [2].

METHODS

For visualizing intracellular Mg^{2+}, we have developed KMG-series dyes. In this work, we used KMG104 for visualizing the cytosolic Mg^{2+} levels with simultaneously imaging the cytosolic Ca^{2+} by Fura-red. We focused on the effects of γ-aminobutyric acid (GABA) and its functional changes during developmental transition. We show that in neurons, $GABA_A$ signaling, whose action is not inhibitory but excitatory at early developmental stages of neurons, triggers Mg^{2+} release from mitochondria specifically with several fluorescent Mg indicators. By using several FRET-based sensors for specific phosphorylation, we also demonstrate that released Mg^{2+} from mitochondria regulates the ERK, CREB and mTOR signaling pathways. Finally, the Mg^{2+} function for neural network maturation was also investigated as the neuronal functional connectivity by Ca^{2+} imaging and synaptic activity by FM dye imaging.

RESULTS

We found that cytosolic Mg^{2+} fluctuations within physiological ranges is enough to crucially regulate ERK, CREB, and mTOR activities; quantitative analysis of the Mg^{2+} concentration-response curves demonstrates that cytosolic Mg^{2+} regulates the signaling activities of ERK negatively, CREB positively, and mTOR sigmoidally. Together, intracellular Mg^{2+} physiologically integrates and coordinates cellular information and Mg^{2+} is a novel signal transducer for organizing neural networks.

CONCLUSIONS

We succeed to demonstrate the Mg^{2+} as a second messenger in neurons. Mg^{2+} has an important role for facilitating structural and functional maturation of neural networks.

REFERENCES

1) Yamanaka R, Shindo Y, Oka K. *Int. J. Mol. Sci. 20*(14): 3439 (2019).
2) Yamanaka R, Shindo Y, Hotta K, Suzuki K, Oka K. Curr Biol. 28(24): 3984-3991 (2018).

Intravital Microscopy for Drug Delivery Research

Yu Matsumoto

Department of Otolaryngology and Head and Neck Surgery, The University of Tokyo

OBJECTIVE

To understand and develop the site-specific (targeted) drug delivery, it is essential to observe the extravasation, tissue penetration and cellular internalization of drug carriers *in vivo*. In this regard, we have established an **i**ntra**v**ital **c**onfocal **l**aser **s**canning **m**icroscopy (IVCLSM) technique for spatiotemporal and quantitative *in situ* analyses of the drug carrier's behavior in a living animal.

METHODS

IVCLSM utilizes a Nikon A1R confocal laser scanning microscope system attached to an upright ECLIPSE FN1. The setup was optimized through various inventions such as custom-designed mouse stage and coverslip holder, exposure surgery and stabilization under appropriate anesthesia, and tail vein catheterization for timed injection.

RESULTS

(1) Size-Dependent Distribution

Extravasation, penetration, and microdistribution of the different sized nanoparticles were compared in hypovascular human pancreatic BxPC3 tumors. The 30- and 70-nm nanoparticles were labeled with Alexa 488 and Alexa 594 fluorescent probes, respectively, and concurrently injected into tumor-bearing mice. The 30-nm nanoparticles penetrated into the interstitium, whereas the 70-nm nanoparticles formed perivascular clusters and failed to move toward the interstitial space. We demonstrated that the enhanced targeting of drugs to cancer cells within tumors by nanoparticles largely depends on the size.

(2) Nanoparticles Erupts into the Interstitium

To study extravasation and interstitium penetration in detail, we performed longitudinal observation at 10-minute intervals, which greatly increased time resolution. This led us to image, for the first time, an interesting phenomenon where tumor vasculature bursts and nanoparticles erupt out into the interstitium. This phenomenon occurred randomly throughout the study, in scattered and unspecified areas of tumor blood vessels, for durations of 30-60 minutes. Our discovery should trigger awareness and close investigation of the microdistribution behavior of nanoparticles.

CONCLUSIONS

As described above, IVCLSM can serve as a powerful tool for investigating the *in situ* behavior of nanoparticles. IVCLSM can thereby ascertain key barriers in a residing in a living body, facilitating the development of nanoparticles optimized for sufficient drug delivery.

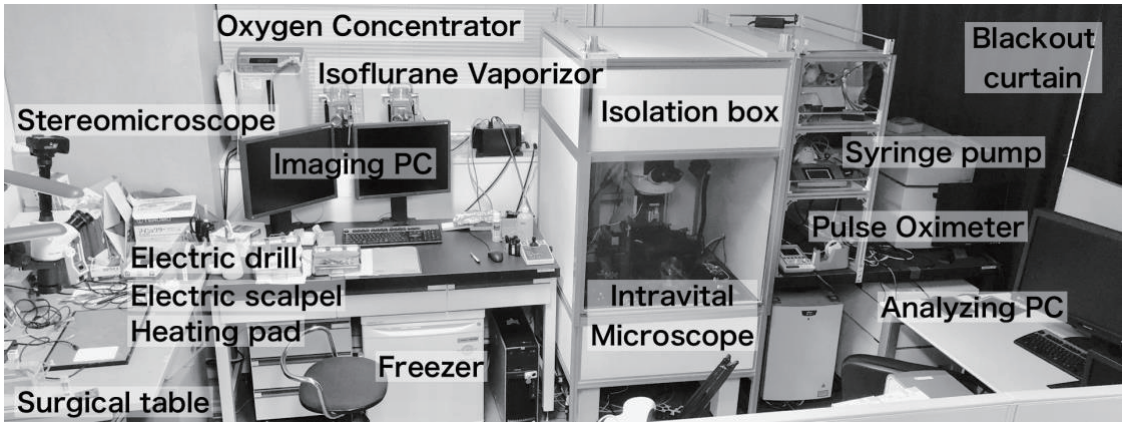

Mechanical interactions of oscillating microbubbles with cells and a capillary under ultrasound exposure

Nobuki Kudo
Faculty of Information Science and Technology, Hokkaido University

OBJECTIVE

Contrast ultrasonography, a technique in which an ultrasound scanner is used for visualizing microbubbles of several microns in diameter that have been introduced inside vessels, is now widely used for non-invasive diagnosis. The pressure range of diagnostic ultrasound pulses reaches several MPas; however, there is almost no volume change in biological tissue that mainly consist of incompressible water, causing no mechanical stress by deformation. On the other hand, microbubbles of a contrast agent easily make a large radial oscillation, causing cavitation effects in their surrounding tissue. Much interest has recently been shown in cavitation effects, especially for applications to ultrasound therapy such as introduction of a gene or drug into a cell through a perforation created on a plasma membrane (sonoporation), opening of the blood brain barrier that exists between cerebral endothelial cells (BBB opening), and modulation of neurons deep inside the brain (neuromodulation). The mechanisms underlying therapeutic applications, however, have still not been fully elucidated, and we have been studying interactions between a bubble and a cell and a bubble and endothelial cells inside a capillary under condition of ultrasound exposure. In this presentation, an observation system equipped with a confocal microscope and a high-speed camera is introduced, and results of recent observations are shown.

METHODS

A confocal unit (C2si, Nikon) and a high-speed video camera (HPV-X2, Shimadzu) were connected to side ports of an inverted-type microscope (ECLIPSE Ti, Nikon). Human prostate cancer cells (PC-3 cells) were cultured on a soft gel scaffold, and a cell with an attached microbubble (bubble liposome) of several microns in diameter was observed. A focused transducer of 1 MHz in resonant frequency was used to generate a one-shot burst pulse of 3 to 50 cycles in duration and 0.2 to 1.0 MPa in peak-negative pressure. The microbubbles and cells were stained using NBD, Cellmask deep red, and Cytox blue, and z-stacked confocal images were captured before and after the ultrasound exposure. Bubble oscillation and interaction with the cell during ultrasound exposure were captured as 256 high-speed frames of 400×250 in pixels, and the framing rate was set to 10 Mfps, which allows 10 frames to be taken in one cycle of 1-MHz ultrasound.

RESULTS

To clearly visualize the interaction, a cultured cell sample was arranged on an observation chamber to enable observation of the interaction from a lateral direction. Figure 1 shows the frames selected from high-speed images of an oscillating microbubble initially adhering to the surface of a cell. The sample was irradiated by a 50-cycle burst pulse of 0.2 MPa in peak-negative pressure. The 4 frames in Fig. 1(a) show bubble oscillation in the early two cycles and those in Fig. 1(b) show bubble oscillation in later two cycles of the pulse, indicating that the bubble that initially adhered to the cell surface was introduced inside the cell during bubble oscillation.

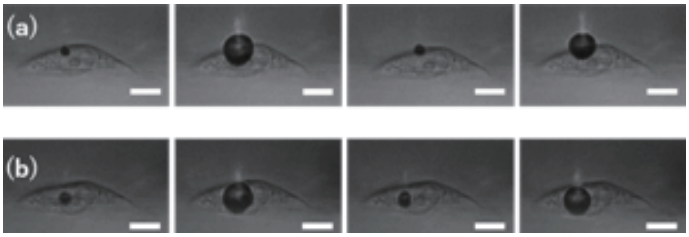

Figure 1. Bubble-cell interaction captured by the high-speed camera. Images were captured at an expansion phase of (a) initial 2 cycles and (b) the last 2 cycles of irradiated ultrasound. The size of the scalebar is 10 μm.

CONCLUSIONS

A biological system always maintains its function in the presence of mechanical stress. Our observations of the reaction of cultured cells to ultrasonically applied mechanical stress are therefore important for elucidating the mechanisms by which cells change their nature. Our system can apply a force not only in the presence but also in the absence of a microbubble by changing ultrasound exposure parameters, suggesting the usefulness of the system also for basic studies on mechanotransduction of cells.

Targeted Ultrasound for Imaging and Drug Delivery

Siva Dasa[2], Akshaya Meher[2], Pingyu Zhang[2], Arshad Khan[2], Johnny Chen[3], Adam Dixon[3], Justin Farry[3], Zhongmin Du[2], Galina Diakova[2], John Hossack[3], Alexander L Klibanov[1,2,3]*

[1]Cardiovascular Division, Department of Medicine, [2]Cardiovascular Research Center, [3]Department of Biomedical Engineering, University of Virginia, Charlottesville VA 22908 USA

OBJECTIVE

Ultrasound, unlike other imaging modalities, is capable of not just providing images of biological tissues and organs: it can also deposit significant amounts of energy to the area of disease, in a focused or unfocused manner. With ultrasound, we can observe the delivery process in real time, and also trigger release of the sequestered drug from the carrier systems. Other imaging modalities, such as MRI, optical and photoacoustic imaging, combined with ultrasound, provide guidance for spatial targeting of therapeutic action, and help assess delivery efficacy.

METHODS

Microbubbles (perfluorobutane gas) were prepared by sonication or amalgamation and stabilized with a lipid monolayer of DSPC and PEG stearate. For targeting to tumor neovasculature, cyclic RGD-PEG-DSPE was added to the bubble preparation medium, or inserted in the RBC membrane. Biotinylated liposomes were remote-loaded with doxorubicin driven by ammonium citrate, and attached to biotinylated microbubbles via a streptavidin link. Superheated nanodroplets (perfluoropentane or perfluorobutane) with a phospholipid shell were prepared by Nuclepore filtration, and attached to RBCs by electrostatic interaction. Doxorubicin was loaded into RBCs by remote loading. Fluorescent dyes, ICG and calcein, were loaded into RBCs by osmotic shock. Magnetic targeting of RBCs was achieved by placement of a ½" N52 Neodymium magnet. For tumor targeting and imaging studies, MC38 colon adenocarcinoma cells (a generous gift of Dr. J. Schlom, NCI) were injected subcutaneously in the hind leg of C57BL/6 mice. Ultrasound was applied either with the focused Philips TIPS unit (1 – 1.2 MHz, 1 Hz pulses), or an unfocused Birtcher Megason physical therapy clinical unit (1 MHz, 3 sec on, 10 sec off intervals), following biweekly intravenous administration of therapeutic agents. Imaging was performed with Sequoia c512 with 15L8 probe in CPS mode (7 MHz, MI 0.2). Fluorescence microscopy was applied to monitor doxorubicin delivery to the tissues. Tumor size following therapy was assessed with a caliper. Photoacoustic studies were performed with a Spectraphysics tunable nanosecond pulse laser.

RESULTS

Delineating tumor mass by ultrasound imaging of tumor vasculature molecular biomarker $\alpha_v\beta_3$ has been accomplished with cRGD-PEG-DSPE microbubbles. Monitoring tumor perfusion is easily achievable by ultrasound imaging; we were able to observe influx of ultrasound contrast material in a murine tumor model, as well as blood pool ultrasound signal replenishment following destruction of microbubbles by ultrasound. It was also noticed that high-MI ultrasound tumor treatment in combination with intravascular microbubbles leads to transient cessation of blood flow in the tumor, which may be detrimental for tumor drug delivery. Conversion to low-power prolonged pulses from a physical therapy ultrasound, in combination with doxorubicin-liposome-microbubble complexes resulted in the suppression of tumor growth. Intravascular perfluoropentane nanodroplets in combination with high pressure focused ultrasound did not result in the immediate cessation of tumor blood flow; however, tumor growth was still slowed down in relation to controls.

As the next step, we are investigating RBCs, a natural drug delivery vehicle with longer circulation time. We have developed tools to entrap doxorubicin inside RBCs, up to 0.9 pg per cell. Co-entrapment of magnetic nanoparticles allows magnetic targeting of drug-loaded RBCs (confirmed by photoacoustic imaging). Molecular targeting with RGD-decorated RBCs to recombinant $\alpha_v\beta_3$ Petri dish has been achieved in vitro in a flow chamber study. Perfluorocarbon nanodroplets were successfully attached to RBC membrane. Fluorescent dyes (ICG and calcein) were entrapped by osmotic shock and resealing; ultrasound-triggered dye release from nanodroplet-RBCs has been demonstrated.

CONCLUSIONS.

Ultrasound, in combination with other imaging modalities, offers a set of tools to guide and perform targeted therapeutic interventions, and assesses the efficacy of therapeutic interventions in real time.

S7-1

Imprinting Primes Learning

: Thyroid Hormone is the Determining Factor for the Critical Period.

Koichi J. Homma

Faculty of Pharmaceutical Sciences, Teikyo University, Tokyo, JAPAN

OBJECTIVE

Avian species has highly cognitive functions comparable to those of mammals. In order to reveal the molecular mechanism of early learning in brain such as imprinting behavior, we are using domestic chicks as an experimental model.

METHODS & RESULTS

Filial imprinting in birds is the process of forming a social attachment during a sensitive or critical period, restricted to the first few days after hatching. Imprinting is considered to be part of early learning to aid the survival of juveniles by securing maternal care. Newly hatched chicks follow the first conspicuous moving object and learn the color and shape of the object and become attached to it. This is the biological mother under normal conditions. However, under experimental conditions it can be any other object. We are investigating the molecular mechanism of the sensitive period using chicks as a model to memorize the plastic bricks for their mother.

We showed that the thyroid hormone determines the start of the sensitive period. Imprinting training causes rapid inflow of thyroid hormone (T_3) into brain, converted from circulating plasma thyroxine. The hormone thus initiates and extends the sensitive period to last more than 1 week via non-genomic mechanisms. Even in non-imprinted chicks whose sensitive period has ended, exogenous thyroid hormone enables imprinting. In the brain neurons, we showed that actin polymerization and depolymerization were occurring simultaneously in the dendritic spines during imprinting using the imaging method of F-actin dynamics. It can also confer "Memory Priming" (MP). Once chicks have achieved MP, it is maintained for long periods, driving subsequent other learning. MP endowed by imprinting or exogenous T_3 clearly enhanced behavioral flexibility in task-switching and reversal learning paradigms in which chicks adjust to the switch or reversal of task contingencies, while the MP-induced chicks did not show the enhancement under non-switch or non-reversal condition.

This suggests that avian species may develop highly cognitive functions via MP in order to adapt to environmental changes. It is possible that the sensitive period for learning closes only if MP is not conferred at an appropriate time of development. The closing of the sensitive period may not exist under usual physiological conditions as long as MP is acquired.

CONCLUSIONS

Our study elucidates the critical role of imprinting to subsequent learning as being governed by the acute action of thyroid hormone. There may exist determining factors for the sensitive period among higher intelligent animals as well. The implications of this study reach beyond the sensitive period of imprinting in chicks and deepen our understanding of the processes of learning.

References

Nat. Commun. **3**, 1081 (2012), ***Neuroscience*** **308**, 115-24 (2015), ***Neurosci. Lett.*** **612**, 32-37 (2016), ***PLoS One*** **12(1)**, e0169643 (2017), ***Behav. Brain Res.*** **349**, 25-30 (2018), ***Horm. Behav.*** **102**, 120-128 (2018), ***Front. Physiol.*** **9**,1837, eCollection (2018), ***Front. Physiol.*** **9**, 1740, eCollection (2018)

S7-2

Visualizing neuronal circuits controlling circadian and ultradian rhythms in mammals

Ryosuke Enoki [1,*]

[1]*Hokkaido University, Research Institute for Electronic Science, Lab of Molecular and Cellular Biophysics*

OBJECTIVE

In mammals, most physiological and behavioral events are subjected to well-controlled daily oscillation, and these circadian (ca. 24 hr) rhythms are controlled by the hypothalamic suprachiasmatic nucleus (SCN) located in deep region of the brain. The SCN is composed of nearly 20,000 neurons, and each of which is thought to contain circadian oscillator. The SCN is considered to be a hierarchical and multi-oscillator system, in which neuronal network plays a critical role in expressing robust and coherent circadian rhythms.

The SCN sends major output signals to the subparaventricular zone (SPZ) and further to the paraventricular nucleus (PVN). The PVN is composed of a group of neurons including neurosecretory cells and synthesizes various hormones. The SPZ is known as a hub region which relays the circadian information from the SCN to other brain regions and ultimately controls the circadian rhythms of various physiological processes, such as sleep-wake cycles and locomotor activities.

In vivo studies have revealed that various functions of mammalian physiology fluctuate in a range from one to several hours (ultradian), such as rapid eye movement (REM)-non-REM sleep cycles. However, despite the broad recognition of ultradian cycles and their functional importance, we know very little about the pacemaker loci and mechanisms of the ultradian rhythms. Interestingly, the ultradian rhythms persist, and even become more robust after surgical or genetic lesion of the SCN. These results indicate the presence of an ultradian oscillator independent of the SCN circadian pacemaker. A fundamental obstacle in elucidating ultradian mechanisms appears to be a difficulty in identification of ultradian rhythms *in vitro*.

METHODS

To understand the mechanisms of the circadian and ultradian rhythms at neuronal circuit level, we developed a time-lapse fluorescence imaging system composed of a Nipkow-spinning disk confocal microscope and high sensitive EM-CCD camera mounted on an inverted microscope with auto-focusing function (Enoki et al., J.Neurosci Methods, 2012). Using genetically encoded sensors and adeno-associated virus in the cultured brain slices, we characterized the spatial and temporal patterns of circadian and ultradian rhythms in the SCN, PVN and SPZ regions.

RESULTS and CONCLUSIONS

We previously found the topological specificity of the circadian calcium rhythms (Enoki et al., PNAS, 2012) and coherent voltage rhythms in the SCN neuronal network (Enoki et al., PNAS, 2017). We also detected ultradian calcium rhythms in both the SPZ-PVN and SCN regions with periods of 0.5 to 4.0 hours. The ultradian rhythms were synchronous in the entire SPZ-PVN region. Since the ultradian rhythms were detected in the SPZ-PVN-only slices but not in the SCN-only slice, we concluded that the origin of ultradian rhythm was the SPZ-PVN region. In association with an ultradian bout, a rapid increase of intracellular calcium in a millisecond order was detected, the frequency of which determined the amplitude of an ultradian bout. Neurochemical interventions revealed that the glutamatergic mechanism is critical for generation and a TTX-sensitive neural network for synchrony of the ultradian rhythm. GABAergic system could have a role in refining the circadian output signals (Wu et al., PNAS, 2018). The present study provides the first clue to unraveling the loci and network mechanisms of the ultradian rhythm.

S7-3

Multimodal multiphoton imaging of solutes and solvents in the brain tissue

Mutsuo Nuriya [1,2,3]

[1]Department of Pharmacology, Keio University School of Medicine, [2] Graduate School of Environment and Information Sciences, Yokohama National University, [3] JST PRESTO

OBJECTIVE

Dynamics of bioactive molecules in the tissue is the key determinant of tissue physiology, pathophysiology and pharmacology, which are then regulated by the dynamics of solvent, water, that constitute ~70% of the whole body weight. Thus, characterization of solutes and solvents in the tissue is critical in biology and medicine. Importance of water dynamics in the tissue has recently been proposed and caught much attention for the brain tissue. Here, it has been suggested that regulated flow of water in the brain tissue work to clear pathogenic substances and dysfunction of such dynamics may lead to various diseases such as Alzheimer's disease.

Despite such importance, investigation of water dynamics in the brain has been difficult due mainly to the lack of appropriate technique. The major difficulty is to visualize water molecules by microscopy since small size of H2O does not allow conventional fluorescence-tagging methodology. In this regard, Raman microscopy holds great promises because Raman scattering can report the existence of molecular vibration and the major source of O-H in the biological tissues is water. While conventional Raman imaging suffers from low efficiency and poor tissue penetration, coherent Raman scattering microscopy using near infrared lasers realizes highly efficient signal detection and deep tissue penetration. Finally, use of high-power pulsed lasers for coherent Raman scattering simultaneously induces multiphoton phenomena of other modalities, allowing multifaceted characterizations of biological samples. Thus, we attempted to apply this multimodal multiphoton microscopy technique to the brain tissues to visualize the dynamics of solutes and solvents.

METHODS

Acute brain slices were prepared from 2 – 3 -week-old C57/BL6 mice and used for analyses. 300 μm-thick coronal slices of cerebral cortices were prepared and placed in the temperature-controlled chamber under the microscope. The brain slices were perfused with oxygenated artificial cerebrospinal fluid during the imaging period.

Multimodal multiphoton microscopy system was built based on FV1000MPE Olympus multiphoton system. Emerald Engine (A.P.E.) was used as the source laser to emit 1,031 nm Stokes beam as well as 515nm frequency doubled beam that is then fed to optical parametric oscillator to generate ~775 nm Pump laser, both of which were temporally synchronized and introduced to the scanning system. Resulting coherent anti-Stokes Raman scattering (CARS) signals of O-H vibration as well as simultaneously emitted fluorescent signals from two-photon excited fluorescent molecules were collected by the photomultiplier tubes after the narrow band-pass filters.

RESULTS

First, we tested if we could see O-H vibration signal inside the brain tissue by using CARS microscopy. This revealed that O-H vibration signal can be readily observed in the middle of the brain slices where the cellular structures and functions are best preserved. In addition, cellular fluorescent markers such as sulforhodamine 101 that selectively stain living astrocytes can be detected simultaneously, allowing characterization of O-H CARS signals in the context of cellular organizations and structures. Furthermore, live imaging of the CARS signals while exchanging normal water-based external solution with deuterated water-based one reveal the dynamics of water molecules inside the brain tissue. Further characterizations of these images under normal and pathological conditions are currently being undertaken.

CONCLUSIONS

Our preliminary data suggest that multimodal multiphoton microscopy enables simultaneous visualization of solutes and solvents in the brain tissue. Further applications of this system are expected to contribute to the field of physiology, pathophysiology and pharmacology of the brain.

Real-time imaging of whole-plant calcium and glutamate dynamics

Masatsugu Toyota,[1,2]

[1] *Department of Biochemistry and Molecular Biology, Saitama University, Japan*
[2] *Department of Botany, University of Wisconsin-Madison, USA*

OBJECTIVE

Plants, unlike animals, do not have a nervous system, but they can rapidly sense local environmental stresses (i.e., insect attack and mechanical wounding), transmit this information throughout their body and activate plant-wide defense responses. However, the molecular machinery underlying such rapid sensory and long-range signal transduction remains unclear. Here, we show that L-glutamate is a wound signal in plants that leaks from damaged cells/tissues and activates the *GLUTAMATE RECEPTOR LIKE* (*GLR*) family of ion channels in *Arabidopsis thaliana*, resulting in the intracellular Ca^{2+} transmission to distant organs.

METHODS

Using genetically-encoded GFP-based Ca^{2+} and glutamic acid (Glu) indicators (GCaMP and iGluSnFR, respectively) and a motorized fluorescence stereo microscope equipped with a sCMOS camera, we have visualized the plant-wide spatial and temporal dynamics of cytosolic Ca^{2+} and apoplastic Glu in response to wounding stress in *Arabidopsis*.

RESULTS

Mechanical wounding caused immediate Ca^{2+} and Glu increases in the wounded leaf and subsequently this Ca^{2+} increase was transmitted via the phloem to distant target leaves (1089 ± 141 μm/s). In these target leaves, defense marker genes such as *OPR3*, *JAZ5* and *JAZ7* and jasmonic acid/jasmonoyl-isoleucine were highly up-regulated within 2 minutes of mechanical wounding. We also found that the *GLR* family of Ca^{2+}-permeable channels was required for the wound-induced Ca^{2+} transmission and extracellularly-applied Glu in a leaf could trigger the similar systemic Ca^{2+} transmission and resistance responses.

CONCLUSIONS

These data suggest that the plant GLR is a sensor to monitor the apoplastic Glu levels, and when symplastic Glu is leaked out of wounded cells/tissues, GLR rapidly creates the Ca^{2+} signal propagating throughout the entire plant and activates systemic resistance responses in distant organs.

Mass Spectrometry Imaging of Metabolites in Agricultural Products

Hirofumi Enomoto*

Dept. Biosci., Teikyo Univ. Grad. Sch. Sci. Eng., Teikyo Univ. Adv. Inst. Analysis Ctr., Teikyo Univ.

OBJECTIVE

Agricultural products contain various metabolites, such as anthocyanins, flavan-3-ols, sugars, organic acids, phospholipids, and plant hormones. For example, in strawberries, anthocyanins, flavan-3-ols, sugars, and organic acids influence the appearance, taste, and antioxidant properties. In pork meat, sphingomyelins (SMs), the major phospholipids, affect its health-beneficial properties. Plant hormones abscisic acid (ABA) and 12-oxo-phytozienoic acid (OPDA), regulate the development of immature common bean. However, the spatial distributions of these metabolites have not been fully elucidated due to the lack of optimal visualization techniques. Mass spectrometry imaging (MSI) is a powerful technique for visualization of biomolecules in biological tissues. Matrix-assisted laser desorption/ionization (MALDI)-MSI is commonly used for metabolite imaging in plant and animal tissues. Here, we present our studies on MALDI-MSI to investigate the distribution of various metabolites in several biological samples.

METHODS

Frozen sections were prepared from the biological samples, namely ripe strawberry fruit, pork chop, and immature common bean, using a cryostat (CM 1860, Leica Mycrosystems). The sections were mounted onto indium-tin-oxide coated glass slides, and a matrix solution, namely 2,5-dihydroxybenzoic acid (DHB) or 1,5-diaminonaphthalene (DAN), was applied uniformly over the section using an airbrush. ABA and OPDA were derivatized with Girard's Reagent T (GirT) to enhance their detection intensities prior to matrix application. MALDI-MSI was performed using an ultrafleXtreme TOF/TOF instrument (Bruker) at positive or negative ion mode. Ion images of metabolites were constructed using FlexImaging software (Bruker). To identify metabolites, MALDI-tandem MS was also performed.

RESULTS

Anthocyanins containing pelargonidin- and cyanidin-glycosides, hexose, sucrose, and citric acid were visualized by DHB in positive ion mode in ripe strawberry fruit. Pelargonidin-glycosides were distributed on the skin, cortical, and pith tissues, whereas cyanidin-glycosides were distributed only on the skin, suggesting that the different distribution patterns of anthocyanins are dependent on the aglycone moiety rather than the sugar moiety. While hexose was distributed almost equally throughout the fruit, sucrose was mainly distributed in the upper side of the cortical and pith tissues. Flavan-3-ol monomers and oligomers, visualized by DAN in negative ion mode, were mainly distributed in the calyx, vascular bundle, and skin of the ripe strawberry fruit. SMs in pork chops were visualized by DHB containing potassium in positive ion mode. SMs containing stearic acid were predominantly distributed in the loin and spinalis muscle, whereas SMs containing palmitic, lignoceric, and nerbonic acids were predominantly distributed in the transparent tissue, indicating that SM tissue distribution is dependent on the tissue-specific fatty acid composition. ABA and OPDA were visualized by on-tissue derivatization with GirT and DHB in positive ion mode, in common bean. ABA-GirT was mainly distributed in the embryo, while OPDA-GirT was localized in the external structures.

CONCLUSIONS

These results suggest that MALDI-MSI is a valuable technique for visualization of various metabolites in agricultural products. Spatial information of metabolites obtained by MALDI-MSI would be contribute to improve the quality of strawberry fruit, assess the health-beneficial properties of each tissue in pork meat, and elucidate the biological role of plant hormones.

REFERENCES

Enomoto *et al*., *J. Food Sci.*, 2019, *in Press*. Doi: 10.1111/1750-3841.14667

Enomoto *et al*., *Rapid Commun. Mass Spectrom.*, 32, 1565-1572, 2018.

Enomoto *et al*., *J. Agric. Food Chem.*, 66, 4958-4965, 2018.

S8-3

Visualizing the Plant Life: Regulation of Development and Stress Responses by the ROS-Ca^{2+} Signaling Network and Autophagy

Kazuyuki Kuchitsu[1,2], Kenji Hashimoto[1,2]

[1]Dept. Appl. Biol. Sci. & [2]Imaging Frontier Center, Tokyo Univ. of Science, Noda, Japan

Reactive oxygen species (ROS), such as superoxide anion radical ($O_2^{\bullet-}$) and hydrogen peroxide (H_2O_2), are highly toxic molecules produced during photosynthesis and aerobic respiration. However, ROS are enzymatically produced in a highly regulated manner spatially and temporally. ROS play key roles in regulating a broad range of physiological processes, such as growth and development including tip growth of root hairs and pollen tubes, defense responses against biotic and abiotic stresses as well as cell wall metabolism. Respiratory burst oxidase homologues (Rboh) have been identified as ROS-producing NADPH oxidases, which act as key signaling nodes integrating multiple signal transduction pathways in plants. Rbohs are synergistically activated by Ca^{2+} binding to the N-terminal EF-hand motifs and phosphorylation by several families of protein kinases. The ROS-Ca^{2+} positive feedback regulation seems to be conserved not only in polarized cell growth but also various signaling processes in plants. We have recently identified and characterized two Rbohs from an emerging model liverwort *Marchantia polymorpha*. Knockout lines of the two isozymes established by genome editing revealed that they have distinct physiological roles in development, morphogenesis and environmental stress responses. We will discuss various imaging techniques to characterize the morphological phenotypes of the *rboh* mutants such as cell proliferation rate and the cell division pattern during the vegetative development. Evolutionary aspects and molecular regulatory mechanisms of Rboh/ROS-mediated signaling will also be discussed.

In flowering plants, programmed cell death (PCD) of the tapetum, the innermost layer of the anther, is one of the most critical and sensitive steps for pollen maturation and fertility. It is severely affected by various environmental stresses, which cause serious problems in agriculture. We recently discovered that autophagy is induced at the uninucleate stage during pollen maturation and required for tapetal PCD, postmeiotic anther development and nutrient supply to the pollens in rice. We also established an *in vivo* imaging system to analyze the dynamics of autophagic flux in rice tapetum cells, and revealed the dynamics of autophagy during pollen maturation. Possible involvement of Rboh/ROS-mediated signaling and transcriptional network in the regulation of autophagy and the proper timing of tapetal PCD during anther development will be discussed.

Numerous pigments plants contain in many organelles such as chloroplasts, cell wall and vacuoles prevent fluorescence imaging. We are applying various cutting-edge non-invasive imaging techniques for plant research. Stimulated Raman scattering (SRS) microscopy is a method to obtain the spatial distributions of various constituents by detecting their characteristic molecular vibrations. High-speed SRS microscope enables rapid image acquisition with molecular vibrational spectra in the CH-stretching region (2,800 to 3,100 cm^{-1}), and is expected to be widely useful in medical diagnoses and biological researches. In collaboration with Dr. Yasuyuki Ozeki, we have applied the imaging system to various plant tissues and cells. Intracellular and extracellular distribution of biological constituents (e.g., fatty acids, starch granules and phenolic metabolites) was distinctively visualized without any staining processes. We will discuss prospects for application of the high-speed SRS imaging to plant sciences. Application of laser-induced surface deformation microscope to analyze the cell surface of plant cells in collaboration with Dr. Toshinori Morisaku and Prof. Hiroharu Yui will also be discussed.

Poster Abstracts

P-1 Whole-organ cell profiling accelerated by CUBIC combined with MOVIE imaging

Tomoki T. Mitani[1,2], Katsuhiko Matsumoto[1], Shuhei A. Horiguchi[1], Junichi Kaneshiro[1], Tatsuya C. Murakami[3], Tomoyuki. Mano[3], Hiroshi Fujishima[1], Ayumu Konno[4], Tomonobu M. Watanabe[1], Hirokazu Hirai[4], Hiroki R. Ueda[1,3]*
[1] RIKEN Ctr. For Biosystems Dynamics Res., [2] Osaka Univ. Hosp., [3]Grad. Med., Univ. Tokyo, [4] Grad. Med., Gunma Univ.

P-2 Real-time cellular imaging of lung T-lymphocyte accumulation and focus formation in a mouse asthma model

Akihiro Hasegawa,[1]* Hidetaka Ogino,[1] Toshinori Nakayama[2]
[1] Department of Microbiology and Immunology, Yamaguchi University Graduate School of Medicine,
[2] Department of Immunology, Graduate School of Medicine, Chiba University

P-3 From Nano to Macro: Advanced Imaging Techniques for Neuroscience Applications

Shinya Komoto*, Paolo Barzaghi, Koji Koizumi, Toshiaki Mochizuki, Bruno Humbel
Imaging Section, Research Support Division Okinawa Institute of Science and Technology (OIST)

P-4 New evaluation technique for micro-environment using translational and rotational diffusion

Johtaro Yamamoto,[1,]* Akito Matsui,[2] Masataka Kinjo [2]
[1]Biomed. Res. Inst., AIST, [2] Fac. Adv. Life Sci.., Hokkaido Univ.

P-5 Simultaneous Tracking of Multiple Biomolecules in a Living Filamentous Fungus by Confocal Raman Microspectroscopic Imaging

Mitsuru Yasuda,[1] Norio Takeshita,[2] Shinsuke Shigeto [1,]*
[1] School of Science and Technology, Kwansei Gakuin University, Japan
[2] Faculty of Life and Environmental Sciences, University of Tsukuba, Japan

P-6 Attempt to observe the structure of schizophyllan monomer by Small Angle X-ray Scattering and Molecular Dynamics simulation

Yoshitaka Matsumura and Masaki Kojima
Sch. of Life Sci., Tokyo Univ. of Pharm. and Life Sci.

P-7 Structural basis for the substrate specificity of phosphoenolpyruvate carboxykinases as phosphodiester energy-conversion enzymes

Takuya Miyakawa,[1,]* Yoko Chiba,[2] Yasuhiro Shimane,[2] Masaru Tanokura[1]
[1]Grad. Sch. Agric. Life Sci., Univ. Tokyo, [2]D-SUGAR, JAMSTEC

P-8 Analysis of myosin II localization during cytokinesis of sea urchin eggs using super-resolution microscopy

Natsumi Hosoya[1,]*, Issei Mabuchi[2]
[1]Faculty of Social Information Studies, Otsuma Women's University,
[2]Department of Life Sciences, Graduate School of Arts and Sciences, The University of Tokyo

P-9 Measurement resolution of diffraction phase microscopy as investigated with reflection interference microscopy

Shota Ueki,1 Hisashi Hujiwara [1,]*
[1] Graduate School of Information Sciences, Hiroshima City University

P-10 Development of evaluation method of cell morphology using Digital In-line Holographic Microscope (D-IHM)

Shuhei Yamamoto[1], Ryuji Sawada[1], Toru Ezure[1], Kanna Nagaishi[2]
[1]Analytical & Measurements Division, Shimadzu Corporation
[2]Second Department of Anatomy, Sapporo Medical University

P-11 Development of the imaging methods for phenotyping of knockout mice with the X-ray Computed Tomography

Hirotoshi Shibuya[1], Taku Gotoh[2], Ruriko Tanabe[2], Shintaro Nomura[2], Masaru Tamura[1,*]
[1] RIKEN BRC, [2] Nagahama Inst. of Bio-Sci. and Tech.

P-12 Open Source Local Gene Induction System by IR Laser Irradiation

Joe Sakamoto,[1,*] Yuko Kamikawa,[1] Yasuhiro Kamei [1,2]
[1] Spectrography and Bioimaging Facility, NIBB Core Research Facilities, NIBB,
[2] School of Life Science, SOKENDAI

P-13 Microwave-antenna-integrated cell dishes for nanodiamond quantum thermometry

Keisuke Oshimi[1], Yushi Nishimura[1], Masuaki Tanaka[2], Eiji Shikoh [2], Masazumi Fujiwara[1], Yoshio Teki[1]
[1]Grad. Sch. Sci. of Osaka City Univ., [2]Grad. Sch. Eng. of Osaka City Univ.

P-14 Titanium Dioxide Nanoparticle is a Brilliant Perfusion Contrast Agent for Visualization and Diagnosis of Small-Animal Microvessel.

Ruriko Tanabe[1], Taku Gotoh[1], Hirotoshi Shibuya[2], Masaru Tamura[2], Shintaro Nomura[1,*]
[1] Nagahama Inst. of Bio-Sci. and Tech., [2] RIKEN BRC

P-15 Multimodal OTN-NIR/MRI imaging with IR-1061@Gd-DOTA imaging molecules

Doan Thi Kim Dung[1,4], Masakazu Umezawa[2], Karina Nigoghossian[2], Gil Yeroslavsky[3], Kyohei Okubo[2,3], Masao Kamimura[2,3], Masayuki Yamaguchi[4], Hirofumi Fujii[4], and Kohei Soga[2,3]
[1] Research Institute of Biomedical Science, Tokyo University of Science,
[2] Department of Material Science and Technology, Tokyo University of Science,
[3] Imaging Frontier Center (IFC), Research Institute for Science and Technology (RIST), Tokyo University of Science,
[4] Exploratory Oncology research & Clinical Trial center, National Cancer Center Hospital East, Japan.

P-16 Development of Functional ^{19}F MRI Contrast Agents Using Perfluorocarbon-Encapsulated Nanoparticle

Yuki Konishi[1], Kazuki Akazawa[1], Rena Akimoto[1], Fuminori Sugihara[2,3], Masafumi Minoshima[1], and Kazuya Kiuchi[1,2]
[1]Graduate School of Engineering, Osaka University, Osaka, Japan
[2]Immunology Frontier Research Center, Osaka University, Osaka, Japan
[3]Research Institute for Microbial Diseases, Osaka University, Osaka, Japan

P-17 Visualization of mitochondrial Ca^{2+} flux in pancreatic INS-1 cells cultured by the medium with high concentration of fatty acids.

Mariko Suzuki,[1] Megumi Kawakubo,[1] Naoko Iida-Tanaka[2,*]
[1] Dept. of Health and Nutr. Sci., Grad. Sch. of Stud. in Hum. Cult., Otsuma Women's Univ.,
[2] Dept. of Food Sci., Otsuma Women's Univ.

P-18 Anti-apoptotic properties of ferulic acid in pancreatic INS-1 cells.

Sumika Takahashi, Megumi Kawakubo, Naoko Iida-Tanaka*
Dept. of Food Sci., Otsuma Women's Univ.

P-19 Cell Morphology and Early-phase Ca^{2+} Transients of Guinea-Pig Pulmonary Vein Cardiomyocytes Compared with Atrial and Ventricular Cardiomyocytes

Iyuki Namekata,[1] Haruhito Hiiro,[1] Tamano Ohmori,[1] Yusuke Tanaka,[1] Shogo Hamaguchi,[1] Hikaru Tanaka[1]
[1]Department of Pharmacology, Toho University Faculty of Pharmaceutical Sciences

P-20 Imaging stress-responsive long-distance ROS-Ca^{2+} signaling in Marchantia

Kenshiro Watanabe,[1] Kota Hasegawa[1], Hiroki Shindo[1], Kenji Hashimoto[1,2], Kazuyuki Kuchitsu[1,2]
[1]Dept. Appl. Biol. Sci. & [2]Imaging Frontier Center, Tokyo Univ. of Science, Noda, Japan

P-21 Regulation of cell proliferation and differentiation by NADPH oxidase-mediated ROS production in the development of a model liverwort Marchantia polymorpha

Kazuyuki Kuchitsu[1,2], Yuki Hagiwara[1], Daisuke Miyamoto[1], Kenji Hashimoto[1,2]
[1]Dept. Appl. Biol. Sci. & [2]Imaging Frontier Center, Tokyo Univ. of Science, Noda, Japan

P-22 Imaging of ROS dynamics and roles of the ROS-producing NADPH oxidase in tapetal programmed cell death during pollen maturation in rice

Togo Fukunaga[1], Jumpei Sawada[1], Kazunori Ogawa[1], Bunki Toh[1], Kenji Hashimoto[1,2], Shigeru Hanamata[2,3], Seijiro Ono[4], Ken-ichi Nonomura[4], Takamitsu Kurusu[2,5], Kazuyuki Kuchitsu[1,2]
[1]Dept. Appl. Biol. Sci. & [2]Imaging Frontier Center, Tokyo University of Science,
[3]Grad. Sch. Sci. & Tech., Niigata Univ., [4]Natl. Inst. Genetics, [5]Fac. Eng., Suwa Univ. of Science

P-23 Imaging autophagy in the anther tapetum cells during pollen maturation in rice

Kazunori Ogawa[1], Jumpei Sawada[1], Togo Fukunaga[1], Bunki Toh[1], Kenji Hashimoto[1,2], Shigeru Hanamata[2,3], Seijiro Ono[4], Kenichi Nonomura[4], Takamitsu Kurusu[2,5], Kazuyuki Kuchitsu[1,2]
[1]Dept. Appl. Biol. Sci. & [2]Imaging Frontier Center, Tokyo University of Science,
[3]Grad. Sch. Sci. & Tech., Niigata Univ., [4]Natl. Inst. Genetics, [5]Fac. Eng., Suwa Univ. of Science

P-24 Dynamic Photocontrol of Biomachines During Cell Division

Kazuya Matsuo[1], Mafy Nusrat Noushaba[1], Shota Hiruma[2], Ryota Uehara[2], Nobuyuki Tamaoki[1]
[1]Research Institute for Electronic Science, Hokkaido university
[2]Graduate School of Life Science, Hokkaido University

P-25 Development of Ratiometric Oxygen Probes Based on Green Fluorophore and Red Phosphor for Visualization of Intracellular Oxygen Level

Mami Yasukagawa, Seiji Tobita, Toshitada Yoshihara*
Department of Chemistry and Chemical Biology, Graduate School of Science and Technology, Gunma University

P-26 Cell cycle dependence of phototoxicity caused by irradiation of blue laser light

Naohiro Kanamaru[1]*, Mikiya Yamaguchi[1], Tetsuya Matsuyama[1], Kenji Wada[1], Koichi Okamoto[1], Ai Kawakita[2], Kaori Murata[2], Kenji Sugimoto[2]
[1] Graduate School of Engineering, Osaka Prefecture University
[2] Graduate School of Life and Environmental Sciences, Osaka Prefecture University

P-27 Development of novel microbubbles for ultrasound imaging

Tamotsu Maruyama[1], Daiki Omata[1], Lisa Munakata[1], Tadamitsu Shima[1], Saori Kageyama[1], Fumiko Hagiwara[1], Yuno Suzuki[1], Kazuo Maruyama[2], Ryo Suzuki[1,*]
[1]Laboratory of Drug and Gene Delivery Research, Faculty of Pharma Science, Teikyo University
[2]Laboratory of Theranostics, Faculty of Pharma Science, Teikyo University

P-28 Contribution of cellular immune response in tumor growth suppression by the combination of microbubbles and ultrasound

Eri Chiba[1], Lisa Munakata[1], Daiki Omata[1], Tadamitsu Shima[1], Saori Kageyama[1], Fumiko Hagiwara[1], Yuno Suzuki[1], Kazuo Maruyama[2], Ryo Suzuki[1,*]
[1]Laboratory of Drug and Gene Delivery Research, Faculty of Pharma Science, Teikyo University
[2]Laboratory of Theranostics, Faculty of Pharma Science, Teikyo University

P-29 Evaluation of Transporter Function in Brain Microvascular Endothelial Cells Derived from Human Induced Pluripotent Stem Cells

Toshiki Kurosawa,[1]Yuma Tega,[1] Tomoko Yamaguchi,[3] Tatsuki Mochizuki,[2] Yasuhiro Hayashi,[1] Atsushi Yamashita,[1] Hiroyuki Kusuhara,[2] Kenji Kawabata,[3] Yoshiharu Deguchi[1,*]
[1]Fac. Pharm-Sci., Teikyo Univ., [2] Grad.Sch. Pharma-Sci., Univ. Tokyo.,
[3]Nat. Instit. Biomed. Innov. Health Nut.

P-30 Development of new anticancer drug delivery system with ultrasound for cancer therapy

Yuno Suzuki[1], Daiki Omata[1], Lisa Munakata[1], Tadamitsu Shima[1], Saori Kageyama[1], Fumiko Hagiwara[1], Kazuo Maruyama[2], Ryo Suzuki [1,*]
[1]Laboratory of Drug and Gene Delivery Research, Faculty of Pharma-Science, Teikyo University
[2]Laboratory of Theranostics, Faculty of Pharma-Science, Teikyo University

P-31 Induction of the accelerated blood clearance (ABC) phenomenon by polyethyrene glycol (PEG) modified microbubbles

Tadamitsu Shima[1], Tamotsu Maruyama[1], Takumi Yamada[1], Daiki Omata[1], Lisa Munakata[1], Saori Kageyama[1], Fumiko Hagiwara[1], Yuno Suzuki[1], Ryo Suzuki[1,*]
[1]Laboratory of Drug and Gene Delivery Research, Faculty of Pharma-Science, Teikyo University

P-32 Development and evaluation of antibody-modified nanobubbles using Fc binding polypeptides for tumor imaging

Nobuhito Hamano[1], Yusuke Yano[1], Yamato Kikkawa[2], Tomomi Kobayashi[1], Yoko Endo-Takahashi[1], Ryo Suzuki[3], Kazuo Maruyama[3], Motoyoshi Nomizu[2], and Yoichi Negishi[1]*
[1] Dept. of Drug Deliv. and Mol. Biopharm., School of Pharmacy, Tokyo Univ. of Pharmacy and Life Sci.,
[2] Dept. of Clin. Biochem., School of Pharmacy, Tokyo Univ. of Pharmacy and Life Sci.,
[3] Lab. of Drug and Gene Deliv. Res., Faculty of Pharma-Sci., Teikyo Univ.

P-33 CpG oligodeoxynucleotide loaded lipid nanoparticles activate $CD8^+$ T cells and exert antitumor effect for murine colon carcinoma

Lisa Munakata[1], Daiki Omata[1], Yasunari Haseda[2], Shohei Koyama[3], Yoshiaki Okada[4], Yasuo Yoshioka[2, 4], Taiki Aoshi[2], Ryo Suzuki[1, *]
[1]Faculty of Pharma-Science, Teikyo University, [2] Research Institute for Microbial Diseases, Osaka University,
[3] Graduate School of Medicine, Osaka University
[4] Graduate School of Pharmaceutical Sciences, Osaka University

P-34 Development of fluorescence / NanoSIMS bioimaging coupled with immunostaining using novel hybrid probe

Naoya Iwano,[1] Wataru Haya,[1] Yasuhiko Fujita,[1] Kohji Shimoda, [2] Yasushi Miyauchi,[3] Takuo Onizuka[1]
[1] Toray Research Center, Inc., [2] Toray Industries, Inc., [3] Kamakura Techno-Science, Inc.

P-35 Promotion of α2,3-Sialylation of Glycoproteins by a Passport Sequence Tag Recognized by Cargo Receptor

Rino Yamada[1], Hirokazu Yagi[1], Rena Honda[2,3,5], Maho Yagi-Utsumi[1,2,3,5], Kazuhiro Aoki[2,4], Koichi Kato[1,2,3,5,]*

[1] Graduate School of Pharmaceutical Sciences, Nagoya City University,
[2] Exploratory Research Center on Life and Living Systems (ExCELLS),
[3] Institute for Molecular Science,
[4] National Institute for Basic Biology, National Institutes of Natural Sciences,
[5] School of Physical Science, SOKENDAI (The Graduate University for Advanced Studies)

P-36 Quantitative analysis of cell cycle progression within heterogeneous cell population using information theory

Ryu Yamanaka,[1, 2] Kotaro Oka[1, 3, 4,] *

[1]Dep. of Biosci. and Info., Fac. of Sci. and Tech., Keio Univ., Japan,
[2]Faculty of Pharm. Sci., Sanyo-Onoda City Univ., Japan,
[3]Grad. Inst. of Med., Col. of Med., Kaohsiung Med. Univ., Taiwan,
[4]Waseda Res. Inst. for Sci. and Eng., Waseda Univ., Japan. *Corr. Auth.

P-37 Simultaneous visualization of intracellular energy substrates by using dual FRET imaging

Yutaka Shindo,[1] Mitsuru Iizumi,[1] Ryu Yamanaka,[2] Kohji Hotta,[1] Kotaro Oka[1,3,4,]*

[1] Biosci Info., Keio Univ., [2] Pharmac. Sci. Sanyo-Onoda City Univ., [3] Inst. Med., Kaohsiung Med. Univ.,
[4] Waseda Res Inst. Sci., Waseda Univ.

P-38 *Intra-vital* fluorescence imaging of interaction between transplanted stem cells and immune cells by quantum nano-materials and tissue clearing (CUBIC) technology

Toshiki Mizumaki,[1,]* Hiroshi Yukawa,[1,2,3] Kodai Kitamura,[1] Daisuke Onoshima, [1,2] Etsuo A. Susaki, [4,5] Hiroki R. Ueda, [4,5] Yoshinobu Baba, [1,2,3,6]

[1]Dept. Biomolecular Eng., Grad. Sch. Eng., Nagoya Univ.,
[2] Inst. Nano-Life-Systems, Inst. Innovation for Future Society, Nagoya Univ.,
[3]National Institute of Radiological Science (NIRS), National Institute for Quantum and Radiological Science and Technology (QST),
[4]Dept. Systems Pharmacology, Grad. Sch. Med., Tokyo Univ.,
[5]Laboratory for Synthetic Biology, Center for Biosystems Dynamics Research, RIKEN,
[6]Health Research Institute, AIST

P-39 Brain-targeted Gene Delivery using Microbubbles and Ultrasound

Daiki Omata[1], Fumiko Hagiwara[1], Lisa Munakata[1], Tadamitsu Shima[1], Saori Kageyama[1], Yuno Suzuki[1], Kazuo Maruyama[2], Ryo Suzuki[1,]*

[1]Laboratory of Drug and Gene Delivery Research, Faculty of Pharma-Science, Teikyo University
[2] Laboratory of Theranostics, Faculty of Pharma-Science, Teikyo University

P-40 Blood-brain barrier opening using 220-kHz transcranial MRI-guided focused ultrasound and microbubbles in mouse and rat

Michiharu Yoshida[1], Kazuo Maruyama[2]*, Yasutaka Kato[3], Rachmilevitch Itay[4], Shuji Suzuki[4], Omer Brockman[4], Yeruham Shapira[4], Kenji Moriyama[5], Daiki Omata[2], Ryo Suzuki[2], Hajime Kamada[1]

[1]Department of Neurosurgery, Hokuto Hospital,
[2]Faculty of Pharma-Sci., Teikyo Univ.,
[3]Laboratory of Cancer Med-Sci., Hokuto Hospital,
[4]InSightec Ltd.,
[5]Department of Radiology, Hokuto Hospital

P-41 Enhanced chemotherapy effects on gynecological cancers by using the combination of lipid bubble and ultrasound

Kohei Yamaguchi[1], Yoko Matsumoto[1] *, Haruka Nishida[1], Daiki Omata[2], Michihiro Tanikawa[1], Kenbun Sone[1], Katsutoshi Oda[1], Yutaka Osuga[1], Ryo Suzuki[2], Kazuo Maruyama[2], Tomoyuki Fujii[1]
[1]The Department of Obstetrics and Gynecology, The University of Tokyo
[2]Laboratory of Drug and Gene Delivery System, Faculty of Pharma-Science , Teikyo University

P-42 Bioimaging of inhalable nanocarriers with aggregation-caused quenching dye to visualize retention in the respiratory system

Kohei Yamada,[1] Tetsuya Matsushita,[1] Kurt D. Ristroph, [2] Hoang D. Lu, [2] Yoshiki Seto, [1] Wei Wu, [3] Hak-Kim Chan, [4] Robert K. Prud'homme, [4] Hideyuki Sato, [1] Satomi Onoue [1,*]
[1] Laboratory of Biopharmacy, School of Pharmaceutical Sciences, University of Shizuoka, Japan,
[2] Department of Chemical & Biological Engineering, Princeton University, USA,
[3] Key Laboratory of Smart Drug Delivery of MOE & PLA, Fudan University, China
[4] Advanced Drug Delivery Group, The University of Sydney, Australia

P-43 Development of Caged Gene Regulators for Application to Control of Genetic Recombination in vivo

Kurumi Yoshida,[1,*] Masafumi Minoshima,[1] Kazuya Kikuchi [1,2]
[1]Graduate School of Engineering, Osaka University. [2] Immunology Frontier Research Center, Osaka Univ.

P-44 Image evaluation of biological tissue using Bio-LSI

Ryoma Kumagai,[1] Ankush Prasad,[2] Teruya Sato,[1] Kosuke Ino,[3] Hitoshi Shiku,[3]Shigenobu Kasai[1]
[1]Graduate Department of Electronic, Tohoku Institute of Technology, Sendai, Japan,
[2]Department of Biophysics, Centre of the Region Haná for Biotechnological and Agricultural Research, Faculty of Science, Palacký University, Olomouc, Czech Republic
[3]Graduate School Department of Applied chemical – electrochemical science and technology, Tohoku University, Sendai, Japan

P-45 Study on Photodynamic diagnosis for micrometastases using photosensitizer Talaporfin sodium

Saito Takuma[1] , Furuya Kazunari[1] , Li Liming[1]
[1]Graduate School of Chitose Institute of Science and Technology

P-46 *In vivo* imaging of exosomes derived from stem cells by using quantum nano-optics for regenerative medicine

Yuka Kumon,[1] Hiroshi Yukawa,[1,2,3] Onoshima Daisuke [1,2], Yoshinobu Baba[1,2,3,4]
[1] Grad. Sch. of Engineering, Nagoya Univ., [2] Institutes of Innovation for Future Society, Nagoya Univ.
[3] National Institutes for Quantum and Radiological Sci. and Tech. (QST), [4] Health Research Institute, AIST

P-47 *Ex vivo* fluorescent imaging of macromolecule kinetics by nose-to-brain delivery with functional arginine-rich peptides

Takumi Kurano[1,2] ,Takanori Kanazawa[1,2], Mami Kaneko[2], Hisako Ibaraki[2], Yuuki Takashima[2], Toyofumi Suzuki[1], Yasuo Seta[2]
[1]School of Pharmacy, Nihon University, [2]Tokyo University of Pharmacy and Life Sciences

P-1

Whole-organ cell profiling accelerated by CUBIC combined with MOVIE imaging

Tomoki T. Mitani[1,2], Katsuhiko Matsumoto[1], Shuhei A. Horiguchi[1], Junichi Kaneshiro[1], Tatsuya C. Murakami[3], Tomoyuki. Mano[3], Hiroshi Fujishima[1], Ayumu Konno[4], Tomonobu M. Watanabe[1], Hirokazu Hirai[4], Hiroki R. Ueda[1,3]*

[1] RIKEN Ctr. For Biosystems Dynamics Res., [2] Osaka Univ. Hosp., [3]Grad. Med., Univ. Tokyo, [4] Grad. Med., Gunma Univ.

OBJECTIVE

Whole-organ cell profiling pipeline combined with CUBIC tissue clearing technologies is an effective tool to obtain comprehensive cell information throughout the organ. Recently, we reported a single-cell-resolution whole-brain atlas (CUBIC-Atlas), which was novel scalable and sharable format for handling the whole-organ data by a point cloud of cells. However, the positions of all detected cells in an organ had to be extracted from a massive image data to compact the data size, and therefore the throughput of data acquisition and analysis remains a critical bottleneck for biomedical applications handling numerous samples.

METHODS

We developed a high-speed volumetric imaging system named as MOVIE (MOVIng observation with Efficient real-time autofocus) system for efficient volumetric imaging, which has integrated 1) continuous acquiring (MOVIE-scan), 2) real-time adaptive autofocusing (MOVIE-focus) and 3) skipping of blank images (MOVIE-skip). MOVIE system was integrated into a custom-built light-sheet fluorescence microscopy. To analyze the large-scale imaging data in a rapid timescale, we also developed a cell detection algorithm based on three-dimensional Hessian-based Difference of Gaussian and a highly parallelization of multiple CPUs and GPUs.

RESULTS

The acquisition time was shortened to within a few hours per mouse whole organ. For example, using a ten-fold expanded adult mouse whole-brain sample, the throughput of 50 ms of exposure time was measured as 0.56 TB/h and total data size was 6.3 TB using 10x objective lens with novel imaging system, comparing with 0.15 TB/h and 14 TB with previous imaging scheme (Murakami et al., 2018). Acquisition time per brain also became 8.5 times shorter than the previous report. Our cell-detection algorithm worked at 1 hour/TB and had over 90% F-scores of nuclear stained cell detection throughout the brain. Using a brain transduced with AAV-PHP.eB (NSE-H2B-mCherry) counterstained by nuclear stain dye, we demonstrated the usability of the developed imaging and analysis pipeline by quantification of mCherry positive cell number in each anatomical region and the ratio of positive cells in each 80 μm voxel. These results showed that the cortex and hippocampus showed higher positive ratio than other areas.

CONCLUSIONS

Thus, the pipeline realizes a novel platform for the high-speed organ-scale analysis of cells and will promote next-generation biomedical research targeting a large number of samples in a practical timescale. This content will be published in Nature Protocols.

Whole-organ cell profiling pipeline.

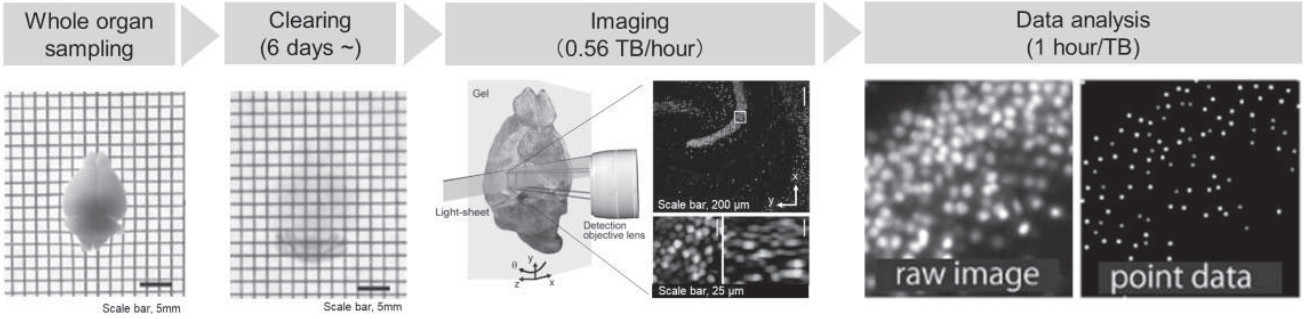

P-2

Real-time cellular imaging of lung T-lymphocyte accumulation and focus formation in a mouse asthma model

Akihiro Hasegawa,[1]* Hidetaka Ogino,[1] Toshinori Nakayama[2]

[1] Department of Microbiology and Immunology, Yamaguchi University Graduate School of Medicine,
[2] Department of Immunology, Graduate School of Medicine, Chiba University

OBJECTIVE

The cardinal features of acute asthma are airway inflammation predominated by eosinophils, hypersecretion of mucus, and airway hyperresponsiveness. A critical role for $CD4^+$ Th2 cells in the pathogenesis of acute asthma has been demonstrated in the studies of human asthma as well as of animal models of asthma. Th2 cell migration into the lung is crucial for the initiation of asthma phenotype, but the *in vivo* dynamics of this process in living animals are poorly understood since it has been difficult to visualize this process. Our aim was to image the cellular dynamics of the migration of Th2 cells into the lung of living animals in a mouse model of asthma and identify the cellular processes required for the initiation of the asthma phenotype.

METHODS

We developed a new *in vivo* color-coded real-time cellular imaging model using green fluorescent protein (GFP) and red fluorescent protein (RFP) transgenic CD4 T cells to visualize the dynamics of migration of T cells in a mouse model of asthma.

RESULTS

Selective accumulation of antigen-specific CD4 T cells in the lungs was quantitatively imaged. The inhibition of accumulation by dexamethasone was imaged. Accumulating GFP^+ Th2 cells formed foci in the lungs from 6 to 20 hours after antigen inhalation. The migration of CD69-deficient CD4 T cells into the asthmatic lung was severely compromised. This process was also inhibited by the administration of anti-ICAM-1 or anti-VCAM-1 mAbs. Two days after inhalation of antigen, GFP^+ Th2 cells were detected in the area of eosinophil infiltration.

CONCLUSIONS

Focus formation generated by accumulating antigen-specific Th2 cells in the lung appeared to be a critical process in the initiation of asthma phenotype. This new model enables the study of *in vivo* cell biology of airway inflammation and novel drug discovery for lung inflammatory diseases.

P-3

From Nano to Macro: Advanced Imaging Techniques for Neuroscience Applications

Shinya Komoto*, Paolo Barzaghi, Koji Koizumi, Toshiaki Mochizuki, Bruno Humbel
(OIST Imaging Section)

Imaging Section, Research Support Division
Okinawa Institute of Science and Technology (OIST)
1919-1 Tancha, Onna-son, Kunigami-gun
Okinawa, Japan 904-0495

OBJECTIVE:

An integrated approach with an array of different sample preparations, imaging technologies and software analysis has been applied to tackle difficult tasks in Neuroscience.
The combination of classical laser scanning fluorescence microscopy with light-sheet microscopy and super resolution imaging techniques has been used to better understand the cellular mechanisms and neural circuitry underlying learning and adaptive behavior in the brain.

METHODS & RESULTS:

Cholinergic system plays a fundamental role in mammal's brain and is involved in neurodegenerative diseases, thus a characterization of cholinergic neurons (number, size and spatial distribution) might contribute to a better understanding of neuronal disorder like Alzheimer. The use of fast laser scanning confocal coupled to high sensitive and with a better spatial resolution detector (Airyscan detector, Zeiss Microscopy) allowed the collection of large volumetric data fulfilling the Nyquist criteria but still maintaining a single cell resolution in an acceptable time frame.

To further develop our imaging techniques to understand the cellular mechanisms of neuronal development, we combined the use of clearing protocols and high-speed confocal system (e.g. light sheet microscopy, multi-point laser confocal system). The latter allows the imaging of large volume specimen. In particular, we have focused on visualizing microglia, the professional phagocytes of the brain serving both immune and glial functions. In details, we have image the brain together with the microglia and determine the number and distribution of microglial cells in post-injured brain.

CONCLUSIONS:

In this work, it has been shown that the complexity of cellular mechanisms and neural circuitry of the brain can be better understand using not only a single approach but an ensemble of different techniques and technologies.

P-4

New evaluation technique for micro-environment using translational and rotational diffusion

Johtaro Yamamoto,[1,*] Akito Matsui,[2] Masataka Kinjo [2]

[1]Biomed. Res. Inst., AIST, [2] Fac. Adv. Life Sci.., Hokkaido Univ.

OBJECTIVE

Macromolecular crowding (MMC) in cells is recently an attractive issue in biology field. However, there are no promising measurement method for the degree of crowding yet. We developed a polarization-dependent fluorescence correlation spectroscopy (Pol-FCS), which enables to measure rotational diffusion and translational diffusion of fluorescent molecules simultaneously. We found the Pol-FCS is capable of evaluation for extent of space, namely microenvironment surrounding target fluorescent molecule. In this work, we suggest a new evaluation technique for micro-environment such as MMC using Pol-FCS.

METHODS

Figure 1 shows a sematic diagram of Pol-FCS system. An excitation laser with a wavelength of 488 nm is reflected by a dichroic mirror and focused into a sample droplet by an objective lens. The droplet is an MMC solution or other solution of 100 nM EGFP. The fluorescence of EGFP in the droplet pass through the dichroic mirror and emission filter. The fluorescence separated into 4 beams by a polarizing beam splitter and two non-polarizing beam splitters. Each fluorescence beam was coupled to multimode optical fibers with a core diameter of 62.5 μm acting as pinhole, and finally detected by four avalanche photo diodes.

Cross-correlation functions of recorded fluorescence intensity signals were obtained using hardware correlator. The characteristic decay time of the cross-correlation functions were analyzed by non-linear least squares method using theoretical cross-correlation function of Pol-FCS.

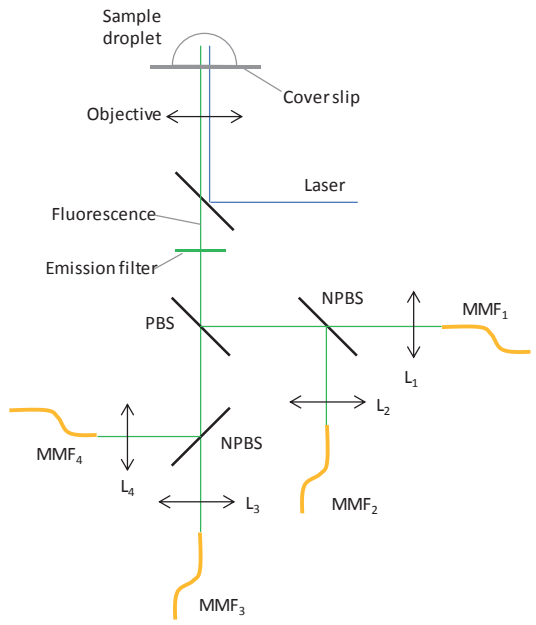

Fig. 1. Experimental setup. L: Lens. MMF: multi-mode optical fiber. PBS: polarizing beam splitter, NPBS: non-polarizing beam splitter.

RESULTS

We compared the characteristic decay time of rotational and translational diffusion (rotational diffusion time and translational diffusion time) of EGFP in various MMC solutions and other solutions. In sucrose solution of phosphate buffer saline (PBS), which is small molecule solution, the ratio of rotational diffusion time and translational diffusion time was always 1 independent of the concentration of sucrose. This was reasonable result because both the rotational and translational diffusion coefficients are inversely proportional to the viscosity of solution according to the Stokes-Einstein relationship and the Debye-Stokes-Einstein relationship. On the other hand, in the MMC solutions such as ficoll or bovine serum albumin in PBS, the ratio was lower than 1, suggesting that the rotation of EGFP molecule is easier than the translation in MMC solution. This indicates the translational diffusion can be disturbed by surrounding crowder molecules, however the EGFP molecules can rotate within gap between crowder molecules.

CONCLUSIONS

In this work, Pol-FCS measurements in MMC solutions were performed and the rotational and translational diffusion were compared. The results indicating that such the comparison gives information about micro-environment around target molecules including MMC condition. We expect Pol-FCS will be a useful tool to quantitatively evaluate MMC.

P-5

Simultaneous Tracking of Multiple Biomolecules in a Living Filamentous Fungus by Confocal Raman Microspectroscopic Imaging

Mitsuru Yasuda,[1] Norio Takeshita,[2] Shinsuke Shigeto [1,*]
[1] School of Science and Technology, Kwansei Gakuin University, Japan
[2] Faculty of Life and Environmental Sciences, University of Tsukuba, Japan

INTRODUCTION: A filamentous fungus known as a mold is composed of thread-like long hyphae, and grows by elongating the tips of the hyphae. In order to investigate the elongation mechanism of the hyphae, we focus on confocal Raman microspectroscopic imaging, which gives spectral information reflecting the molecular structure of biomolecules in a cell *in vivo* and the information on their spatial distributions [1]. Additionally, an integrated approach with stable isotope labeling can be useful for further investigation of the elongation mechanism. The Raman band of a substance of interest with a heavy stable isotope shifts to lower frequency because of the isotope effect. By monitoring this shifted band, the behaviors of multiple intracellular biomolecules associated with metabolism of stable isotope-labeled substances can be tracked simultaneously [2]. Therefore, this integrated approach is expected to provide new insight into the elongation mechanism of the fungal hypha from the viewpoint of metabolism. In this presentation, we report a simultaneous tracking of multiple biomolecules in a living filamentous fungus by stable isotope-labeled confocal Raman microspectroscopic imaging.

MATERIALS AND METHODS: *Aspergillus nidulans* was used in this work, which is widely used as a model filamentous fungus. As stable isotope-labeled substrates, D (deuterium)-labeled glucose and ^{13}C-labeled glucose were used. *A. nidulans* was first cultured in a liquid medium containing the unlabeled glucose instead of D-/^{13}C-labeled glucose at 25 °C for 1–2 days. After removing the medium, a fresh liquid medium containing D-/^{13}C-labeled glucose was then added. Raman imaging experiments of hyphae were performed with a confocal Raman microspectroscopic system (XploRA Nano, HORIBA) while cultivating *A. nidulans*.

RESULTS AND DISCUSSION: Since the Raman spectrum of a cell generally contains Raman bands of various molecules, it is significantly difficult to decode what kind of components Raman imaging data consists of. To first investigate main components constituting Raman imaging data, multivariate curve resolution-alternating least-squares (MCR-ALS) was employed [1]. MCR-ALS allowed us to reveal that the Raman imaging data of *A. nidulans* hyphae are mainly composed of proteins including cytochromes, nucleic acids, polysaccharides, and lipids. The spatial distributions of these intracellular biomolecules were visualized simultaneously [3]. Based on these results, experiments using stable isotope-labeled substrates were then performed. When *A. nidulans* were grown with D-labeled glucose, molecules whose hydrogen atoms were substituted with D were localized along the edge of the hyphal tip. This localization suggests that D-labeled glucose was taken up selectively from the apex of the hypha. Moreover, experiments using ^{13}C-labeled glucose enabled us to track the biosynthetic process of reduced cytochrome *b*/*c*, and showed that metabolic activity is higher at the apex of the hyphae and the inner part of hyphal tips than a part away from the apex and the outer part of hyphal tips. The elongation mechanism inferred from the obtained results is as follows: (i) Glucose is taken up selectively from the apex of the hypha by glucose transporters. (ii) The incorporated glucose diffuses along the edge of the hyphal tip. (iii) Metabolic activity around the tip increases as a result of the high glucose concentration. (iv) Substances necessary for the elongation are synthesized at around the hyphal tip consuming the glucose. (v) The hypha elongates. In conclusion, we have proposed a new hyphal elongation model based on glucose metabolism in this work.

ACKNOWLEDGEMENTS: This work was supported by JST ERATO Grant Number JPMJER1502 (Japan) and the Research Foundation for Opto-Science and Technology (Japan).

REFERENCES:
[1] C.-K. Huang *et al*., *Anal. Chem*. 84, 5661 (2012). [2] H. N. N. Venkata *et al*., *Chem. Biol*. 19, 1373 (2012).
[3] M. Yasuda *et al*., *Anal. Chem.* submitted.

P-6

Attempt to observe the structure of schizophyllan monomer by Small Angle X-ray Scattering and Molecular Dynamics simulation

Yoshitaka Matsumura and Masaki Kojima

Sch. of Life Sci., Tokyo Univ. of Pharm. and Life Sci.

OBJECTIVE

β-glucan is a major component of the pathogenic fungal cell walls. Depending on their composition and structure, it is related to diseases like mycoses and shows good effects as health promotion such as anti-tumor effect *etc*. Since β-glucan is a target molecule for candin antifungal drugs, it is an important molecule from the viewpoint of structure-activity relationship of antibacterial drugs. Dectin-1 and the like have been found as receptors for β-glucan, and are positioned as important molecules also from the viewpoint of infectious immunity and innate immunity.

Schizophyllan, which is a β-glucan derived from *Schizophyllum commune*, has been approved as an anticancer agent because it exhibits antitumor activity, and it has been clarified by X-ray crystal structure analysis that it dissolves in water to form a triple helix structure (Takahashi, Y., *et al*. 1984, Kony, D. B., *et al*., 2007). In contrast, it is known that sonication of schizophyllan reduces the molecular weight and causes a structural change from trimer to monomer, resulting in loss of anticancer activity (Yanaki, T., *et al*. 1983). However, it has been found that the monomeric schizophyllan exhibits activity in the horseshoe crab fluid coagulation reaction (Limulus test, Nagi, N., *et al*. 1993). The Limulus test has been used since 1980's to determine mycosis, a major human disease. However, there is no example in which the structure directly was observed in the solution.

Previously, we have used Physicochemical methods such as Small Angle X-ray Scattering (SAXS), Atomic Force Microscopy (AFM), solution Nuclear Magnetic Resonance (NMR), and molecular dynamics (MD) simulation to investigate the three-dimensional structure of β-glucan derived from *Agaricus brasiliensis*. The results indicated that the β-glucan derived from *Agaricus brasiliensis* in aqueous solution is multi-dispersed state, trimers and/or monomers, the shape of the molecule is globule, the main axis of β-1,6 bond and the side chain of β-1,3 bond (10%) (Matsumura, Y. & Kojima, M., 2018). So, in the present study, we attempted to observe and visualize the three-dimensional structure of the monomeric schizophyllan molecule treated with sonication by SAXS and MD simulation.

METHODS

The SAXS experiments were carried out on beamline BL-6A at the Photon Factory. All data were collected using X-ray of wavelength of 1.5 Å with a PILATUS3 1M dectector (Dectris). The sample-to detector distance was 0.5 m. Equilibrium experiments were performed at 25℃. The SAXS intensities were accumulated for a total of 3.0 s by repeating the measurements for a period of 0.1 s each time in order to ensure enough statistical precision. X-ray scattering data were obtained from schizophyllan and the corresponding aqueous solution. The scattering data of the aqueous solution were subtracted from those of the schizophyllan solutions. X-ray scattering data were analyzed by Guinier approximation, as assuming an exponential dependence of the scattering intensity on h^2, where $h = 4\pi\sin\theta/\lambda$ and θ is half of the scattering angle (Guinier, A. and Fournet, G., in Small Angle Scattering of X-rays. Wiley New York, 1995. The radius of gyration (R_g) and zero angle scattering intensity $I(0)$ were determined using Guinier approximation (Guinier, A. and Fournet, G., Small angle scattering of X-rays. Wiley, 1995).

Molecular dynamics simulation was permormed by AMBER. The details of the simulation are written in the poster.

RESULTS

By SAXS analyses showed that schizophyllan treated with sonication was multi-dispersed state, and the shape was globule. The R_g of major component of the schizophyllan at several concentrations were almost 10 Å. MD simulation of the schizophyllan suggested that the shape was helical structure. As a results, it is suggested that the possibility which the schizophyllan is a good model showing biological activity in any structural form of the trimeric helical structure, monomeric helical structure, and random coil. The details are discussed in the poster.

P-7

Structural basis for the substrate specificity of phosphoenolpyruvate carboxykinases as phosphodiester energy-conversion enzymes

Takuya Miyakawa,[1,*] Yoko Chiba,[2] Yasuhiro Shimane,[2] Masaru Tanokura[1]
[1]Grad. Sch. Agric. Life Sci., Univ. Tokyo, [2]D-SUGAR, JAMSTEC

OBJECTIVE

Inorganic pyrophosphate (PPi) is the simplest compound containing a high-energy phosphate bond between two phosphate (Pi) molecules. PPi can act as an energy and phosphate donor similar to nucleoside di- or tri-phosphates, including adenosine triphosphate (ATP), in cellular reactions. Several enzymes selectively utilize PPi over ATP and other nucleotides to catalyze similar reactions as ATP-dependent functional homologs. Because PPi has the simplest structure among molecules with a high-energy phosphate bond, this molecule has been proposed as an evolutionary precursor of ATP. Phosphoenolpyruvate carboxykinase (PEPCK) is one of the pivotal enzymes that regulates the carbon flow of the central metabolism by fixing CO_2 to phosphoenolpyruvate (PEP) to produce oxaloacetate or vice versa. ATP- and GTP-type PEPCKs were well established to their enzymatic properties including the selectivity of phosphate donor. More recently, PPi-type PEPCK was characterized, which clarified that the amino acid sequence similarity of these PEPCKs was too low to confirm that they share a common ancestor [1]. Here, we attempted to elucidate how the PPi-type PEPCK gained the selectivity of PPi as a phosphate donor and what evolutionary relationship the enzyme has with ATP- and GTP-types.

METHODS

PPi-type PEPCK form *Actinomyces israelii* (AiPEPCK) was produced using the *Escherichia coli* expression system and was then purified by a series of column chromatography experiments. X-ray diffraction data were collected from the crystals of the purified enzyme on the beamline BL-17A at Photon Factory (Tsukuba, Japan). The crystal structure of AiPEPCK was determined at 2.6 Å resolution by using a single-wavelength anomalous dispersion (SAD) method.

RESULTS

AiPEPCK adopted a core structure enveloped by some lobe structures (Lobes 1 to 4). The core structure was divided into two globular α/β domains, N-terminal domain and C-terminal domain. The Co^{2+} ion located in the deep cleft between two domains, indicating that the cleft probably functions as active site of AiPEPCK. The structural superposition with ATP- and GTP-type PEPCKs revealed that AiPEPCK shared a core structure and all of the catalytic residues which directly interact with Co^{2+} and Mg^{2+} ions, γ-phosphate group of ATP or GTP, PEP and oxaloacetate in ATP- and GTP-type PEPCKs. On the other hand, the residues in the purine-binding region were not conserved among three types. Especially, the bulky side chain of His920 sterically hinders the access of ATP or GTP to the active site in AiPEPCK. In addition, the core structure of AiPEPCK was fixed to a closed conformation due to the dimer formation by contacting the AiPEPCK-specific appendage structures, Lobes 2 and 3, which contribute to narrow the purine-binding regions for the PPi selectivity.

CONCLUSIONS

The PPi selectivity of AiPEPCK requires the presence of His920 with bulky side chain in purine-binding region and dimer formation between Lobes 2 and 3. Furthermore, the order of secondary structure elements and residues directly involved in enzymatic function were conserved between these PEPCKs, indicating that they share a common ancestor.

[1] Chiba et al., Discovery of PPi-type phosphoenolpyruvate carboxykinase genes in eukaryotes and bacteria. J. Biol. Chem., 290, 23960–23970 (2015)

P-8

Analysis of myosin II localization during cytokinesis of sea urchin eggs using super-resolution microscopy

Natsumi Hosova[1,*], Issei Mabuchi[2]

[1]Faculty of Social Information Studies, Otsuma Women's University,
[2]Department of Life Sciences, Graduate School of Arts and Sciences, The University of Tokyo

OBJECTIVE

During cytokinesis of animal and fungal cells, the actomyosin contractile ring (CR) is formed at the division site and divides the cell into two by its contraction. Non-muscle myosin II is known to be concentrated in the CR and essential for both formation and contraction of the ring, but the precise localization of myosin II in the CR remains unsolved.

We have been studying structure and function of the CR during cytokinesis of echinoderm eggs, since these eggs divide synchronously and the cell cortex including the CR (cleavage furrow) can be isolated.

Here, we investigated myosin II localization using antibodies raised against sea urchin egg myosin using confocal microscopy and super-resolution microscopy.

METHODS

Cortices containing CR were isolated from dividing sea urchin (*Hemicentrotus pulcherrimus*) eggs as previously described (Mabuchi 1994). Actin filaments were stained with Rhodamine-phalloidin. Indirect immunofluorescence microscopy was performed according to Mabuchi (1994) using rabbit polyclonal antibodies raised against myosin heavy chain (HC) of sea urchin (*Tripneustes gratilla*) egg and mouse monoclonal antibodies raised against monophosphorylated myosin regulatory light chain (1P-MRLC). Confocal microscopy was carried out using Olympus FV1000 laser scanning microscope. Super-resolution images were obtained by N-SIM (Nikon Structured Illumination Microscopy).

RESULTS and DISCUSSION

Both actin and myosin II were localized to the division site of isolated cortices from the very beginning of formation till the full contraction of the CR as seen by confocal microscopy. The actin staining was observed just beneath the plasma membrane (PM) to about 2.0 μm toward cytoplasm. Myosin II-positive layer was seen to be thinner than the actin staining and found at a little deeper region, 1.0 to 2.0 μm away from the PM, than the actin staining.

Next, the staining pattern of myosin II was examined using either anti-myosin HC or anti-1P-MRLC by N-SIM. Myosin HC staining was strong at the cytoplasmic side of the CR. Furthermore, the staining of 1P-MRLC was found in the innermost region of the CR. This specific localization of myosin, especially its activated form, in the CR has never been reported previously. This may suggest that myosin II may interact with actin filaments to drive CR contraction at a region a little distant from the PM, but not just beneath the PM.

It has been shown by electron microscopy that purified sea urchin egg myosin II forms bipolar filaments *in vitro* (Mabuchi, 1973). The length of the filaments was reported to be 370±20 nm. We found that myosin II (myosin HC) in the CR observed by N-SIM formed a structure similar to the bipolar filament. We picked up such images and measured their length using the imaging software (Image J). The average length of 20 images was 394±40 nm, which agreed well with that of the bipolar egg myosin II filaments formed *in vitro*. This result suggests that bipolar myosin filaments may play a key role in formation and contraction of the CR in dividing sea urchin eggs.

REFERENCES

Mabuchi, I. (1973) *J. Cell Biol.* 59, 542-547.
Mabuchi, I. (1994) *J. Cell Sci.* 107, 1853–1862.

P-9

Measurement resolution of diffraction phase microscopy as investigated with reflection interference microscopy

Shota Ueki,[1] Hisashi Hujiwara [1,*]

[1] Graduate School of Information Sciences, Hiroshima City University

OBJECTIVE

Diffraction phase microscopy (DPM) employs a common-path interferometer robust against the mechanical vibration and provides quantitative phase images related to both thickness and refractive index of transparent samples such as living cells [1].

To ensure the phase resolution of DPM, transparent standard samples with well-defined thickness steps have been frequently used; the step sizes are usually larger than 100 nm [2]. Instead of such samples, we propose to use a soap film, because soap films are known to exhibit stepwise thinning called "stratification" where each step is about 10-20 nm [3]. The thickness of a soap film can be monitored with reflection interference microscopy (RIM). Therefore, simultaneous application of DPM and RIM to the soap film during stratification enables us to investigate precise phase resolution of DPM.

METHODS

We have constructed a simultaneous measurement system of both DPM and RIM. The system includes an objective (5× or 20×) and dichroic mirrors. The epi-illumination light source (405 nm) for RIM is a combination of a mercury lamp and an interference filter. For DPM, on the other hand, the transmission light source (682 nm) is a superluminescent diode (FOLS-04, Craft Center SAWAKI). A quantitative phase imaging unit (QPI-U1, Pi Photonics) is used for making interference fringe images, from which the phase delay as a result of the light transmission through the sample can be extracted by two dimensional Fourier transform analysis [4].

To obtain simultaneous images of both DPM and RIM, we have constructed an image recording system where two CCD cameras (SXC10, Baumer) synchronously acquire the images at 100 fps with the synchronization signal from a signal generator.

RESULTS

We recorded the simultaneous DPM and RIM images of a vertical soap film made from 0.1 M sodium oleate aqueous solution. Detailed analysis of both simultaneous images is now still in progress, but even brief analysis of the RIM images confirms that the stratification actually occurred in the observed soap film, which supports the use of a thinning soap film to investigate the phase resolution of DPM.

CONCLUSIONS

We have constructed a system to acquire and record simultaneous DPM and RIM images. The detailed analysis of both DPM and RIM images of a soap film during stratification is expected to reveal the phase resolution of DPM.

REFERENCES

[1] G. Popescu et al., Opt. Lett., **31**, 775 (2006).
[2] T. H. Nguyen et al., Opt. Lett., **39**, 5511 (2014).
[3] A. A. Sonin and D. Langevin, Europhys. Lett., **22**, 271 (1993).
[4] M. Takeda et al., J. Opt. Soc. Am., **72**, 156 (1982)

P-10

Development of evaluation method of cell morphology using Digital In-line Holographic Microscope (D-IHM)

Shuhei Yamamoto,[1] Ryuji Sawada,[1] Toru Ezure,[1] Kanna Nagaishi [2]

[1]Analytical & Measurements Division, Shimadzu Corporation, [2]Second Department of Anatomy, Sapporo Medical University.

OBJECTIVE

In regenerative medicine and cell therapy, the importance of non-invasive evaluation of large numbers of cells is increasing day by day. The most popular non-invasive method for morphological evaluation is the analysis of phase contrast microscopy images, but it is impossible to quantitatively evaluate the three-dimensional shape of cells from phase contrast microscopy images. Because the three-dimensional shape of the cell changes with the accumulation of intracellular organelles and functional proteins, it is very important to evaluate the three-dimensional shape. We measured the optical thickness, which is the product of the refractive index and the three-dimensional shape of the cell, using D-IHM, which has a wide field of view and high resolution. We have developed a method to quantitatively evaluate the gradient of the optical thickness of the cell contour by focusing on the gradient of the cell contour as a shape indicating the state of the cell.

METHODS

Cells are irradiated with coherent light of different wavelengths. CMOS image sensor captures an interference pattern caused by the light passing through the cell and the reference light passing around the cell. Phase information of light is retrieved numerically by using 4 different wavelength images, and reconstructed image at cell surface is calculated by wavefront propagation. The phase delay of thins transparent object, such as cells, are visualized by reconstructed phase images. The brightness of the pixels of the phase image represents the phase change. So, the luminance value of each pixel of a differential image of a phase image indicates the magnitude of the inclination of optical thickness in each pixel. Therefore, the histogram of the differential image shows the distribution of the gradient of the optical thickness, and it is possible to quantitatively evaluate of which gradient of the optical thickness of the cells is steeper in the image.

RESULTS

We evaluated the cell morphology of mesenchymal stem cells with different passage numbers. Cells with different passage numbers had different three-dimensional cell morphologies, and our method was able to quantitatively evaluate the differences.

CONCLUSIONS

We developed a non-invasive and quantitative method to evaluate the optical thickness of a large number of cells using D-IHM. This method is considered to be very useful as a technique for evaluating the cell state in the field of regenerative medicine and cell therapy.

P-11

Development of the imaging methods for phenotyping of knockout mice with the X-ray Computed Tomography

[1] Hirotoshi Shibuya, [2] Taku Gotoh, [2] Ruriko Tanabe, [2] Shintaro Nomura, [1,*] Masaru Tamura
[1] RIKEN BRC, [2] Nagahama Inst. of Bio-Sci. and Tech.

OBJECTIVE

The genome editing technologies such as CRISPR/Cas9 system make it possible to the gene knockout of various animals with unprecedented simplicity and speed. It means that bottleneck of the functional gene analysis will change from generating the knockout animal to the phenotyping. Therefore, we need easy and high-throughput phenotyping method. To overcome this issue, we have developed imaging techniques that used the X-ray computed tomography (CT) and contrast agents.

METHODS

·Ex vivo X-ray CT imaging of the soft tissues

The tissue samples were fixed with suitable formalin-based fixatives and immersed in the contrast agents. After the contrast enhancement, samples were mounted in the plastic tube and scanned with the high-resolution X-ray CT.

·Three-dimensional angiography using the new angiographic agent

Mice were perfused transcardially with contrast agent using a peristaltic pump under deep anesthesia. After the perfusion, tissue samples were isolated and scanned with the high-resolution X-ray CT.

RESULTS

We succeeded the development of imaging techniques to visualize the mouse soft tissues by X-ray CT at high-throughput and high-resolution (Fig.1). Moreover, we developed new angiographic agent, and detected whole vascular and capillary network without structural deformation (Fig.2).

CONCLUSIONS

These methods provide the quantifiable datasets to characterize pathological conditions in disease mouse models.

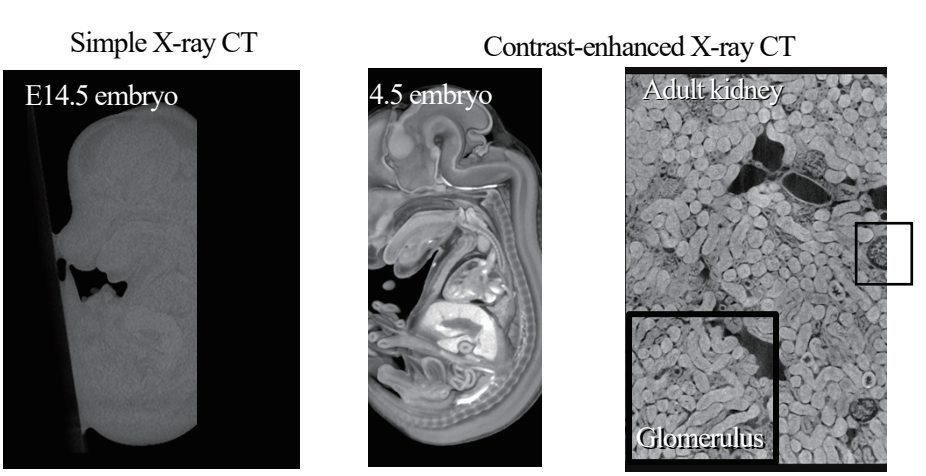

Fig.1, CT images of the mouse soft tissues

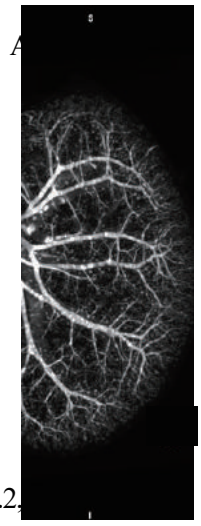

Fig.2,

Open Source Local Gene Induction System by IR Laser Irradiation

Joe Sakamoto,[1, *] Yuko Kamikawa,[1] Yasuhiro Kamei [1, 2]

[1] Spectrography and Bioimaging Facility, NIBB Core Research Facilities, NIBB,
[2] School of Life Science, SOKENDAI

OBJECTIVE

InfraRed Laser Evoked Gene Operator (IR-LEGO) is a spatiotemporal gene induction system via a heat shock response (HSR). HSR is well known as heat protective response of living organisms, and is conserved among various organisms. In HSR, heat shock transcription factor 1 is activated by heat treatment, and promotes expression of a group of chaperone proteins, so called heat shock proteins. Because HSP promoter is easily activated by heat stress, HSP promoter is traditionally used for temporal gene induction. Although temporal gene induction is realized by HSP promoter, spatial control of gene expression is still difficult. To overcome this problem, IR-LEGO utilizes not only HSR, a biological technique, but also microscope, an optical technique. Since living organism is consisted from water, 1,480 nm IR laser which is absorbed by water molecules is used to heat cells for activation of HSP promoter. And IR laser is focused through objective to regulate spatial activation of HSP promoter. Thus, IR-LEGO realized spatiotemporal induction of gene expression. To utilize IR-LEGO effectively, researchers can label single cells by fluorescent protein, and trace cell lineage. Also, researchers can express a functional protein ectopically. Therefore, gain of function experiment can be performed with single-cell resolution. Furthermore, HSR is conservative system, IR-LEGO can be applied to various organisms such as medaka, zebrafish, Iberian ribbed newt, *A. thaliana*, and so on. For these reasons, IR-LEGO has a possibilities to be powerful technique for various research fields. However, almost all research reports which use IR-LEGO is published from Japanese researcher. Recently, a few foreign researchers published reports which use simple self-constructed IR-LEGO system, but still limited. For those who is not professional of optics and microscopy, it is difficult to construct IR-LEGO optical system. In the present study, we show how to construct IR-LEGO by one's self, and introduce its application.

METHODS

We constructed whole optical system of IR-LEGO including inverted microscope. Open source (os) IR-LEGO consists of two optical component, inverted microscope and IR-LEGO optics. In IR-LEGO optics, IR laser was collimated and expanded its beam diameter, and was introduced to inverted microscope component. In inverted microscope optics, IR laser was introduced to objective by a dichroic mirror, and emitted to samples through objective. To adjust an IR laser focal point, we used specific ink pen (Kawakima-pen from Shachihata co., Ltd.) or up-conversion particle. To confirm that osIR-LEGO works heat shock reporter transgenic medaka and cell line was used. Transgenic medaka is expressed Venus fluorescent protein which driven from *hsp* promoter. Heat shock reporter cell line stably has Venus or EGFP driven by *hsp* promoter. To use these transgenic medaka and cell line, we could visualize whether HSR was activated or not.

RESULTS

Because of chromatic aberration of objective, focal point of IR laser is different from visible light. We adjust the focal point of IR laser visualized by specific ink pen or up-conversion particles. We successfully constructed osIR-LEGO. We could also observe fluorescent protein expression as a reporter of heat shock response in both *in vivo* and *in vitro* by irradiating target region using osIR-LEGO.

CONCLUSIONS

Although IR-LEGO has potential abilities to apply to various fields of research, publications which effectively utilizes IR-LEGO are still limited. One problem is that it is difficult for foreign researchers, especially who are not professional of optics, to obtain IR-LEGO. The other is that there are no protocols which describe how to construct IR-LEGO precisely. In the present study, we demonstrated that IR-LEGO can be constructed by one's self. This research will be useful for the potential users of IR-LEGO.

P-13

Microwave-antenna-integrated cell dishes for nanodiamond quantum thermometry

Keisuke Oshimi[1], Yushi Nishimura[1], Masuaki Tanaka[2], Eiji Shikoh [2], Masazumi Fujiwara[1], Yoshio Teki[1]

Grad. Sch. Sci. of Osaka City Univ.[1], Grad. Sch. Eng. of Osaka City Univ.[2]

OBJECTIVE

Fluorescent quantum nanodiamond thermometry is a promising new technology that may enable nanoscale temperature measurement inside cells with a high sensitivity down to milli-Kelvin. In this technique, microwave irradiation to cell is under the optical microscope to exploit optically detected magnetic resonance (ODMR) of luminescent color centers, namely nitrogen vacancy (NV) centers. In order to carry out this operation simply and quickly, we have recently developed culture dishes equipped with microwave antenna [1], where the linear antenna structure was used. However, the linear antenna allowed us to measure ODMR only in a narrow apace range, 100 μm distance from the antenna (Fig. 1(a)), which is a significant drawback for the efficient measurement. In this study, we have developed a wide and broadband microwave antenna that enables observation of ODMR in the wide area on cell culture dishes.

RESULTS

The antenna structure was designed based on a split-ring resonator concept having the resonance frequency of near 2.87 GHz required for the ODMR. We used a finite element method simulation for the antenna design. Figure 2 shows a microscope photograph of cultured-cells with the linear microwave antenna on our dishes. Figure 1(b) shows simulated intensity distribution of the magnetic and electric fields of this antenna. The irradiated area was expanded 10 times or more than that of the conventional linear structure. We also found that it was possible to control the spatial distribution of the electric field by this resonator, which may be toxic to cells. When the conventional linear structure was used, the magnetic-filed spatial distribution was overlapped with the electric field, so that cells were subjected to the electric field irradiation. In the new structure, they do not overlap each other and cells may avoid the electric field irradiation. Figures 2 and 3 show a photograph of cultured cells near antenna structures fabricated by photolithography the simulated spectrum of the reflection coefficient of the antenna. It has a resonance peak at around 2.75 GHz, which means the microwave can be irradiated most efficiently at this resonance point.

CONCLUSIONS

The split ring resonator microwave antenna was designed on culture dishes for the large-area microwave irradiation. The structure was fabricated by photolithography and used for cell culturing.

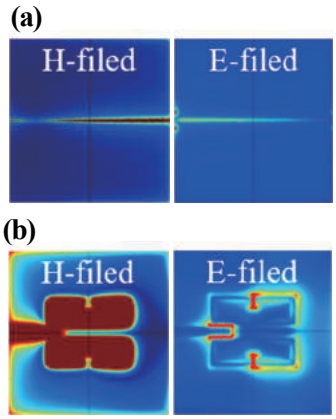

Figure 1. Comparison of linear antenna (a) and antenna with split ring resonators (b).

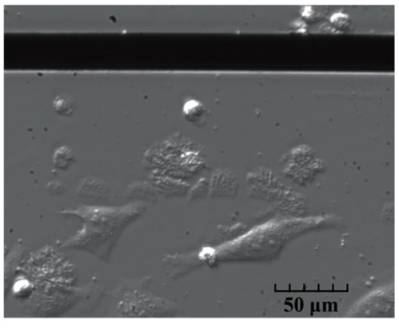

Figure 2. A microscope photograph of cultured-cells near the antenna.

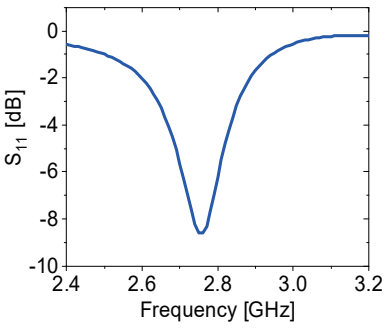

Figure 3. Calculation of reflection coefficient of the antenna structures.

[1] H. Yukawa, M. Fujiwara, K. Kobayashi1, Y. Umehara, Y. Kumon, K. Miyaji, T. Iwasaki, M. Hatano, H. Hashimoto, Y. Baba, submitted.

P-14

Titanium Dioxide Nanoparticle is a Brilliant Perfusion Contrast Agent for Visualization and Diagnosis of Small-Animal Microvessel.

[1] Ruriko Tanabe, [1] Taku Gotoh, [2] Hirotoshi Shibuya, [2] Masaru Tamura, [1,*]Shintaro Nomura

[1]Nagahama Inst. of Bio-Sci. and Tech., [2] RIKEN BRC

OBJECTIVE

It is important to develop highly sensitive contrast agent for visualization and quantification of microvessels in small-animals for preclinical research. Commonly available contrast agents have problems such as rapid clearance and leaking out from vessels due to the small size of molecule, deform the vessels by high pressure in perfusion due to their high viscosity, and stuck the small vessels by the aggregation particularly in small animals. Nanoparticle of titanium dioxide with dispersing reagent, which would dissolve the problems, was examined as promising contrast-enhancing agent in the study.

METHODS

Deeply anesthetized 8 weeks-old mice were perfused with saline (0.9% NaCl) until red-blood cells are not visible. Then nanoparticle of titanium dioxide solution (generously gifted by TAYCA Corp.) containing dispersing reagent was injected left ventricle to visualize systemic arteries of brain, kidney, digestive organs, liver and eye, or right ventricle to visualize pulmonary artery. Dissected organs were analyzed by micro-computed tomography (micro-CT). Three-dimensional reconstitution of CT-imaging was performed by OsiriX software.

RESULTS

As shown in the pictures below, arteries of Brain (left) and Liver (right) were clearly visualized up to 10 micrometers diameter in size without deformation. Furthermore, bleeding area was detected in experimental model of acute hepatitis, and disruptions of arteries were detected in the model of thrombosis.

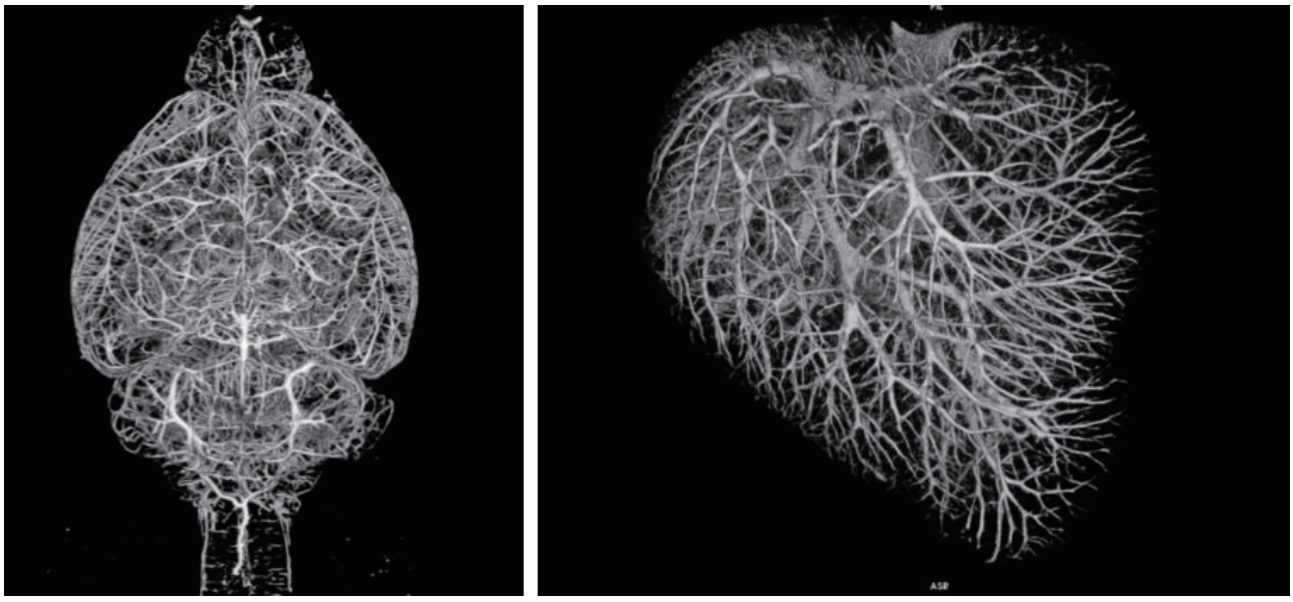

CONCLUSIONS

The perfusion contrast agent developed in this study gave us sensitive and accurate results in angiogram and will be useful for diagnostic research in preclinical field (1, 2).

1. Shibuya H. et al. The 6th International Symposium on Bioimaging. 2019.

2. Shibuya H. et al. Annual Meeting of Genetic Soc. Japan. 2019.

P-15

Multimodal OTN-NIR/MRI imaging with IR-1061@Gd-DOTA imaging molecules

Doan Thi Kim Dung[1,4], Masakazu Umezawa[2], Karina Nigoghossian[2]
Gil Yeroslavsky[3], Kyohei Okubo[2,3], Masao Kamimura[2,3], Masayuki Yamaguchi[4], Hirofumi Fujii[4], and Kohei Soga[2,3]

[1] Research Institute of Biomedical Science, Tokyo University of Science, [2] Department of Material Science and Technology, Tokyo University of Science, [3] Imaging Frontier Center (IFC), Research Institute for Science and Technology (RIST), Tokyo University of Science, [4] Exploratory Oncology research & Clinical Trial center, National Cancer Center Hospital East, Japan.

OBJECTIVE

In recent, multimodal imaging has attracted an enormous attention from researchers in various fields. The combination of individual techniques is expected to provide a comprehensive image from the objects [1]. Among medical imaging techniques currently exploited, magnetic resonance imaging (MRI) is considered the most beneficial one because it is a non-ionizing radiation technique which provides images with high resolution, high tissue contrast as well as great signal-to-noise (SNR) ratios. While optical imaging can obtain functional or molecular information, the overlaying of optical images onto an anatomical map provided by MRI enables the overlaying of optical images on to anatomical maps provided by MRI can promote comprehensive understanding of the object from molecular to anatomical level. Optical imaging with the near-infrared over 1000 nm (OTN-NIR) emission under 980nm excitation is growing as a promising technique because the light has its maximum depth of penetration through biological tissue from several millimeters to centimeters thickness [2, 3] utilizes the so-called biological window [2]. In this work, IR-1061, a molecule emitting over 1000 nm fluorescence under 980 nm excitation is employed as an imaging probe. The probe is then trapped in a micelle composed of PEG-based co-polymer conjugated Gd-DOTA, an MRI contrast agent.

METHODS

Preparation of IR1061@PEG-co-block-polymer@Gd-DOTA probe

170µL of Gd-DOTA solution 17 mg/mL was added in 1 mL of MES buffer at pH 5.5 and mixed and after 5 minutes, 300 µg of EDC and 500µg of NHS were alternately added into the mixture. Finally, 1.5 mg of PEG-co-polymer-NH_2 in 1 mL of MES buffer, pH 5.5 and incubated for 6 hours. The conjugated polymer was dissolved in 1 mL of acetonnitrile (ACN) and 4 mL of water. 40µL of IR1061 in ACN (0.5 mg/mL) was then added to the mixture and stirred overnight.

RESULTS

NIR absorption and emission and imaging

Absorption spectra of the probe was determined by an UV-VIS-NIR v770 spectrometer showed the absorption range from 800-1150 nm with the highest peak around 1050 nm. Emission spectra were obtained by Avaspec-NIR 256-1.7 spectrometer showed the sharp emission around 1200 nm. Size distribution was obtained by DLS and the size distribution is 22 nm. The probe was then injected into mice and observed the NIR imaging by SAI-1000 system and NIR microscope.

T_1 contrast effect

T_1 enhancement effect of the probe was confirmed on spin-echo T_1-weighted images (Fig. 2) and imaging with phantom was conducted with a 3 tesla whole-body scanner (Signa HDx 3T; GE Healthcare). The molecular probe exhibited an enhancement on T_1 relaxation as in phantom.

Further animal images by both OTN-NIR/MRI will be presented at the conference.

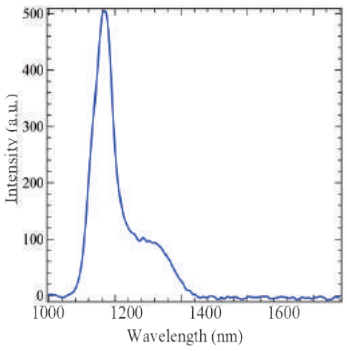

Fig.1: Emission spectrum of the probe.

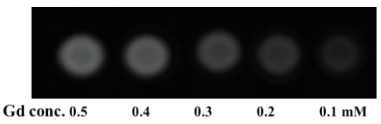

Fig.2: T_1-weighted images of phantoms containing various concentrations of IR-1061-Gd-DOTA probe (TR = 200 ms; TE = 9 ms).

CONCLUSIONS

The multimodal imaging OTN-NIR/MRI is able to materialize with a favor of IR1061@PEG-based-co-polymer@Gd-DOTA multimodal imaging probe. Further functionalization with antibodies heralds advances in areas of cancer diagnosis.

References

[1] K Shah, Gene Therapy **11**, (2004) 1175–1187.
[2] A Schmidt, Nat Nanotechnol. **4** (11), (2009) 710-1.
[3] E Hemmer, Nanoscale Horiz. **1**, (2016) 168.

P-16

Development of Functional ^{19}F MRI Contrast Agents Using Perfluorocarbon-Encapsulated Nanoparticle

Yuki Konishi[1], Kazuki Akazawa[1], Rena Akimoto[1], Fuminori Sugihara[2,3], Masafumi Minoshima[1], and Kazuya Kiuchi[1,2]

[1]Graduate School of Engineering, Osaka University, Osaka, Japan
[2]Immunology Frontier Research Center, Osaka University, Osaka, Japan
[3]Research Institute for Microbial Diseases, Osaka University, Osaka, Japan

OBJECTIVE

Magnetic resonance imaging (MRI) is a molecular imaging method using nuclear magnetic resonance, and can image deep tissues in bodies with high spatial resolution. ^{19}F atom has high relative sensitivity to ^{1}H and a 100% isotopic abundance ratio. In addition, the amount of ^{19}F is very few in body. Thus ^{19}F MRI signals can be monitored with negligible background signal. ^{19}F MRI probes are suitable for tracking specific cells and imaging enzyme activities in living animals. We have developed a perfluorocarbon-encapsulated silica nanoparticle, termed FLAME. FLAMEs show highly sensitive ^{19}F MRI signals, and the surfaces can be modified with various functional groups. However, in vivo targeting of FLAME is limited because nanoparticles are often taken up by phogocytes through opsonization. In this study, we modified the surfaces of FLAMEs with polyethylene glycol (PEG) to reduce the opsonization by forming a fixed aqueous layer on surface of nanoparticle. We evaluated the blood retention and in vivo distribution of the FLAMEs by using ^{19}F MR imaging.

METHODS

PEG was modified on the surface of FLAME-OH in one step by silane coupling with PEG-silane. We compared the blood retention of FLAME-PEG and FLAME-COOH in living mice by ^{19}F MRI. As another approach, we also developed a block copolymer-encapsulated ^{19}F MRI nanoparticle as a ^{19}F MRI contrast agent. The nanoparticles were prepared by living radical polymerization on perfluorocarbon nanoemulsions.

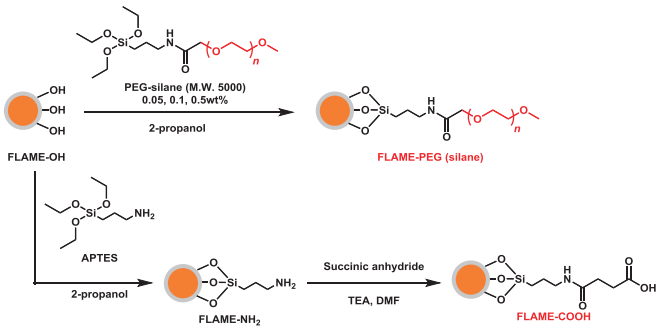

RESULTS

To examine the blood retention of FLAME, the accumulation of FLAME in the liver was evaluated by ^{19}F MRI. In FLAME-COOH, a strong ^{19}F MRI signal was observed from the liver, while in FLAME-PEG, ^{19}F MRI signal in the liver is lower.

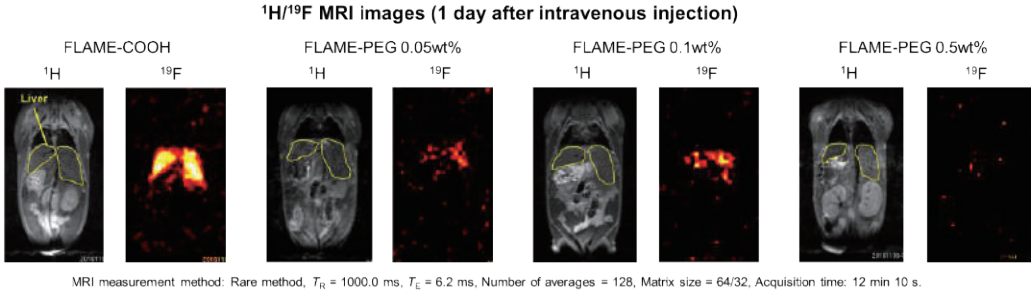

MRI measurement method: Rare method, T_R = 1000.0 ms, T_E = 6.2 ms, Number of averages = 128, Matrix size = 64/32, Acquisition time: 12 min 10 s.

CONCLUSIONS

By modifying FLAME surface with PEG, we achieved decrease of liver accumulation and improvement of blood retention.

P-17

Visualization of mitochondrial Ca^{2+} flux in pancreatic INS-1 cells cultured by the medium with high concentration of fatty acids.

Mariko Suzuki,[1] Megumi Kawakubo,[1] Naoko Iida-Tanaka[2,*]

[1] Dept. of Health and Nutr. Sci., Grad. Sch. of Stud. in Hum. Cult., Otsuma Women's Univ.,

[2] Dept. of Food Sci., Otsuma Women's Univ.

OBJECTIVE

Elevated free fatty acid concentrations in plasma is supposed to decline pancreatic β-cell function and mass, resulting in impaired insulin secretion. The phenomenon, "lipotoxicity", is thought to be responsible for progressive decrease of insulin secretion in type 2 diabetes. Palmitic acid (PA), one of saturated fatty acids has been reported to induce ER stress and apoptosis in INS-1 cells. Concentration of mitochondrial Ca^{2+} has been reported to be affected by Ca^{2+} influx from ER during ER stress and to modulates mitochondrial metabolism and apoptotic threshold. In this study, we visualized mitochondrial Ca^{2+} fluctuation induced by glucose intake, and effects of elevated palmitic acid or oleic acid levels in the culture media on the Ca^{2+} fluctuation were analyzed.

METHODS

INS-1 cells originated from rat pancreatic β-cells were cultured in the medium with 200 μM of palmitic acid (PA-treated cells) or oleic acid (OA-treated cells) for 6-7days. For visualization of mitochondrial Ca^{2+}, a fluorescent protein CEPIA which was Ca^{2+}-binding and mitochondrial targeted protein was used. Cells were transfected with the plasmid encoded CEPIA cDNA and fluorescent images were obtained by using Olympus IX81 equipped with ORCA-AG CCD camera. Expression of proteins related to mitochondrial Ca^{2+} flux, energy metabolism regulation and apoptosis were assessed by mRNA levels obtained from Realtime PCR analyses.

RESULTS

Figure 1 shows that mitochondrial Ca^{2+} was increased up to ~1.4 fold of the start level 30 min after adding glucose in control cells. In the PA-treated cells, in contrast, mitochondrial Ca^{2+} level was kept at the start level, suggesting that the number of ATP generated in mitochondria stayed low after addition of glucose. In the OA-treated cells, mitochondrial Ca^{2+} level was higher than that in the control cells until ~20 min after glucose addition and was decreased quickly to the level ~1.2 fold of the start level.

CONCLUSIONS

A possible hypothesis for those results is that palmitic acids reduce mitochondrial ATP generation and oleic acids, oppositely, accelerate it. To confirm the hypothesis, further experiments, for example, measurement of ATP, mitochondrial membrane potential and oxygen consumption rate are necessary.

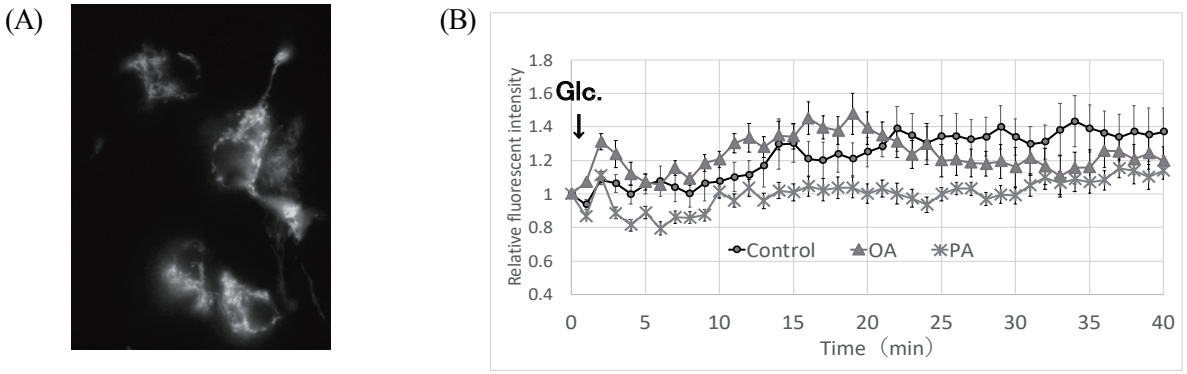

Fig.1. (A) Fluorescent images of mitochondrial Ca^{2+} in INS-1 cells transfected with CEPIA2mt and (B) changes of mitochondrial Ca^{2+} concentration after adding glucose up to 20 mM in the medium. Intensities of green fluorescence of CEPIA2mt were measured and plotted as relative values against those at 0 min. PA, the cells cultured in the medium with 200 μM of palmitic acid; OA, those in the medium with 200 μM of oleic acid.

P-18

Anti-apoptotic properties of ferulic acid in pancreatic INS-1 cells.

Sumika Takahashi, Megumi Kawakubo, Naoko Iida-Tanaka*
Dept. of Food Sci., Otsuma Women's Univ.

OBJECTIVE

Insulin secretion from pancreatic β-cells is strongly affected by various stress, especially oxidation stress and ER stress. Considerable evidences indicate that oxidative stress induced by elevated saturated fatty acid concentration in plasma reduces pancreatic β-cell mass in Type 2 diabetes. Ferulic acid is one of polyphenols and rich in rice bran. Ferulic acid has been reported to have antioxidative and anti-apoptotic effects in pancreatic β-cells. In this study, protective effects of ferulic acid against "lipotoxicity" of palmitic acid were evaluated by insulin secretion, apoptosis induced by H_2O_2 and gene expression of apoptosis- and ER stress- related proteins.

METHODS

INS-1 cells originated from rat pancreatic β-cells were cultured in the medium with 200 μM of palmitic acid (PA) for 6-7days. Treatment of ferulic acid (FlcA) was performed by adding ferulic acid (final conc. of 0 or 10 μM) to the medium with PA. Apoptosis induced by H_2O_2 (final conc. of 1 mM) was evaluated by fluorescent images with Annexin V, and insulin secretion from cells was visualized with FM1-43 fluorescent reagent. Fluorescent images obtained by using Olympus IX81 equipped with ORCA-AG CCD camera or Zeiss LSM510 confocal fluorescence microscope. Expression of proteins related to apoptosis and ER stress was assessed by mRNA levels obtained from Realtime PCR analyses.

RESULTS

Much more apoptosis was induced by H_2O_2 in the PA-treated cells than in the control cell, suggesting that PA-treatment lowers apoptotic threshold. Ferulic acid showed an effect reducing the number of apoptotic cells, that is, the effect canceling toxicity of PA (Fig.1). These results were confirmed by the fact that ferulic acid reduced mRNA level of Ddit3, increased by PA-treatment. Ddit3 is the protein which is induced by ER stress and promoting apoptosis. In addition, ferulic acid recovered the early insulin secretion reduced by PA-treatment.

CONCLUSIONS

Ferulic acid has a protective effect against PA-induced toxicities, that is, lowering insulin secretion and inducing apoptosis in pancreatic β-cells, INS-1. From the analysis of mRNA levels, it was described that Ddit3 which is induced by ER stress and regulates apoptosis is a key protein for lipotoxicity of PA and the protective effect of ferulic acid.

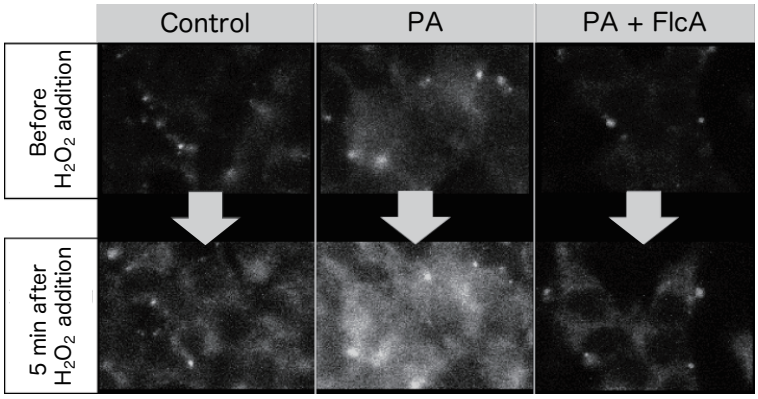

Fig.1. Fluorescent images of H_2O_2-induced apoptosis visualized by Annexin V.
PA, the cells cultured in the medium with 200 μM of palmitic acid; PA+FlcA, the cells cultured in the medium with 200 μM of palmitic acid and 10 μM of Ferulic acid.

P-19

Cell Morphology and Early-phase Ca^{2+} Transients of Guinea-Pig Pulmonary Vein Cardiomyocytes Compared with Atrial and Ventricular Cardiomyocytes

Iyuki Namekata,[1] Haruhito Hiiro,[1] Tamano Ohmori,[1] Yusuke Tanaka,[1] Shogo Hamaguchi,[1] Hikaru Tanaka[1]

[1]Department of Pharmacology, Toho University Faculty of Pharmaceutical Sciences

Pulmonary veins contain a myocardial layer, whose electrical activity is considered to be involved in the genesis and maintenance of atrial fibrillation. To obtain insight into the automaticity of the pulmonary vein myocardium, we studied the cellular morphology and spatio-temporal pattern of the rise in Ca^{2+} during the early-phase Ca^{2+} transients of isolated guinea pig pulmonary vein cardiomyocytes using confocal microscopy and compared with those of ventricular and atrial cardiomyocytes.

Transsarcolemmal Ca^{2+} influx during the action potential plateau triggers Ca^{2+}-induced-Ca^{2+} release (CICR) from the sarcoplasmic reticulum. In ventricular cardiomyocytes with a well-developed T-tubular system, Ca^{2+} concentration rises and rapidly becomes uniform throughout the cytoplasm, while in atrial cardiomyocytes lacking T-tubules, a wave of CICR propagates from the subsarcolemmal region towards the cell center. The pulmonary vein cardiomyocytes had cross striations and were rich in sarcoplasmic reticulum but lacked T-tubules; this was similar to atrial cardiomyocytes but different from ventricular cardiomyocytes, in which T-tubules were present throughout the cell. The sarcoplasmic reticulum was present throughout the cytoplasm in all cell types, which was consistent with the observation that Ca^{2+} sparks occurred throughout the cytoplasm in all cell types. On the induction of Ca^{2+} transients by electrical field stimulation of the pulmonary vein cardiomyocytes, the rise in Ca^{2+} concentration first occurred at the subsarcolemmal region and then spread to the cell interior; this phenomenon was similar to that in atrial cardiomyocytes but different from that in ventricular cardiomyocytes, in which the Ca^{2+} concentration rose simultaneously throughout the cytoplasm. The properties of the Ca^{2+} sparks and Ca^{2+} waves in the pulmonary vein cardiomyocytes were the same as those in atrial and ventricular cardiomyocytes. Thus, the pattern of the rise in Ca^{2+} concentration during the early phase Ca^{2+} transient is not determined by the properties of the Ca^{2+} release unit itself, but rather by the presence or absence of the T-tubules.

In pulmonary vein cardiomyocytes, the percentage of cells showing spontaneous Ca^{2+} transients, as well as the probability of Ca^{2+} spark firing, was higher than in the atrial and ventricular myocytes. In the pulmonary vein cardiomyocytes showing spontaneous activity, the Ca^{2+} transients were preceded by increased firing of Ca^{2+} sparks. SEA0400, an inhibitor of the Na^{+}/Ca^{2+} exchanger, decreased the frequency of the Ca^{2+} transients and eventually inhibited the Ca^{2+} transients completely without decreasing the firing of Ca^{2+} sparks. These results indicate that the guinea-pig pulmonary vein myocardium have a tendency to show spontaneous electrical activity, and that they are mediated by Ca^{2+} released from the sarcoplasmic reticulum and the resulting activation of the Na^{+}/Ca^{2+} exchanger.

In conclusion, in guinea pig pulmonary vein cardiomyocytes that lack T-tubules, Ca^{2+} transients involve the propagation of Ca^{2+} waves, which is similar to that of atrial but not ventricular cardiomyocytes. Ca^{2+} sparks appear to be involved in the generation of spontaneous Ca^{2+} transients of pulmonary vein cardiomyocytes.

P-20

Imaging stress-responsive long-distance ROS-Ca^{2+} signaling in *Marchantia*

Kenshiro Watanabe,[1] Kota Hasegawa[1], Hiroki Shindo[1], Kenji Hashimoto[1,2], Kazuyuki Kuchitsu[1,2]

[1]Dept. Appl. Biol. Sci. & [2]Imaging Frontier Center, Tokyo Univ. of Science, Noda, Japan

Although plants lack the nervous system and brain, as sessile organisms, plants are equipped with numerous sensors to monitor the environmental changes, signal transmission mechanisms throughout the body as well as decentralized information processing systems to reorganize their body for environmental adaptation. In response to biotic and abiotic stresses, long-distance signals are systemically transmitted from the stressed local sites to distant tissues. Such long-distance systemic signals play important roles to prevent the entire plant from further damage by stress. Various signal molecules such as hormones transported through phloem and xylem are involved in slow long-distance signaling. Moreover, plants can also rapidly transmit signals systemically. Possible involvement of Ca^{2+} and reactive oxygen species (ROS) as well as electric signals has been suggested in the rapid long-distance signaling, the molecular mechanisms are largely unknown. We have developed live-imaging systems to monitor cytosolic Ca^{2+} and ROS in a model liverwort *Marchantia polymorpha* and analyzed their dynamics under various stresses.

We established a transgenic plants expressing Ca^{2+} sensor fluorescent proteins GCaMP6f or R-GECO and monitored spatiotemporal dynamics of cytosolic Ca^{2+} concentration. NaCl and wounding treatment induced Ca^{2+} rise not only at the local site but also at distant sites and the Ca^{2+} wave was systemically transmitted throughout the thalli (Fig. 1). The speed of signal transmission was in the range of 1 mm/sec. We also developed the live imaging system of ROS using a fluorescent indicator and observed its dynamics. Wound-induced ROS production was observed not only locally but also at distant sites. These results suggest that the long-distance signaling mechanism involving Ca^{2+} and ROS exist even in a basal liverwort.

In seed plants, the ROS production by NADPH oxidase is synergistically activated by Ca^{2+} and phosphorylation [1-4]. The Ca^{2+}-activated ROS-producing NADPH oxidase and ROS-activated Ca^{2+} permeable channels are postulated to be co-localized at microdomains in the plasma membrane, and constitute a positive feedback mechanism to amplify Ca^{2+} and ROS signals [2-4]. However, molecular identity of Ca^{2+} channels involved in stress responses remain largely unknown. By combining the imaging technique and molecular genetic tools, we are trying to identify molecules involved in the rapid long-distance signaling involving Ca^{2+} and ROS. Inter-relationship between Ca^{2+} and ROS signals in the rapid long-distance signal transmission will be discussed.

1. Ogasawara *et al.* (2008) *J. Biol. Chem.* 283: 8885-8892.
2. Takeda *et al.* (2008) *Science* 319: 1241-1244.
3. Kurusu *et al.* (2013) *Trends in Plant Science* 18: 227-233.
4. Kaya *et al.* (2014) *Plant Cell* 26: 1069-1080.

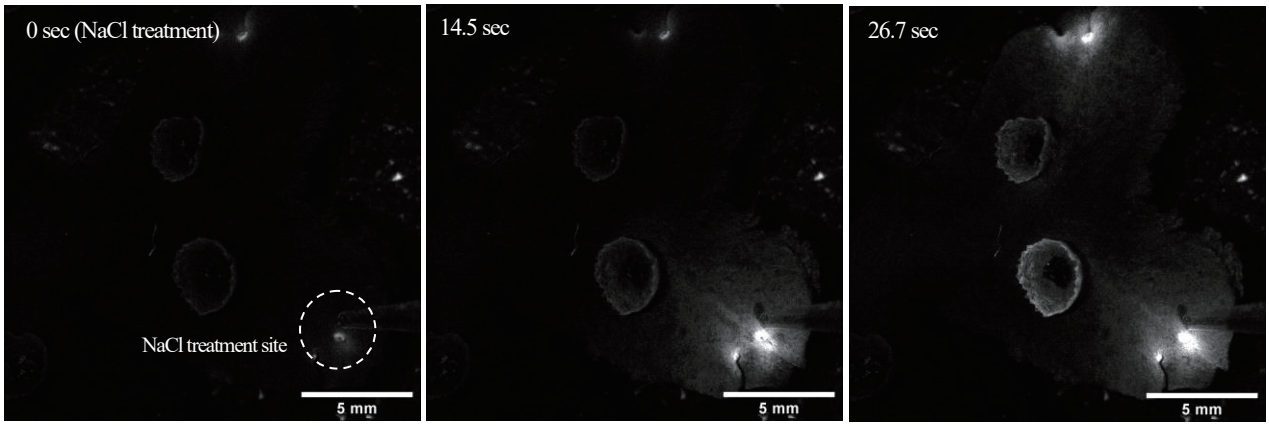

Fig. 1 Imaging the propagation of Ca^{2+} signal in response to NaCl treatment

P-21

Regulation of cell proliferation and differentiation by NADPH oxidase-mediated ROS production in the development of a model liverwort *Marchantia polymorpha*

Kazuyuki Kuchitsu[1,2], Yuki Hagiwara[1], Daisuke Miyamoto[1], Kenji Hashimoto[1,2]
[1]Dept. Appl. Biol. Sci. & [2]Imaging Frontier Center, Tokyo Univ. of Science, Noda, Japan

Reactive oxygen species (ROS) are highly toxic molecules generated during photosynthesis and aerobic respiration. However, tightly regulated ROS production by NADPH oxidases/respiratory burst oxidase homologs (Rbohs) integrate multiple signal transduction network in plants. Rbohs are synergistically activated by Ca^{2+} binding to the N-terminal EF-hand motifs and phosphorylation by several families of protein kinases [1-7]. Spatiotemporal pattern of Rboh-mediated ROS production and the ROS-Ca^{2+} signal network plays key roles in regulating a broad range of physiological processes, such as growth and development including tip growth of root hairs [2,7] and pollen tubes [4], defense responses against biotic and abiotic stresses [3], long-distance signaling as well as cell wall metabolism.

Unlike functional diversification of Rbohs in seed plants (for example, 10 Rbohs in *Arabidopsis thaliana* [7]), only two isozymes exist in a model basal liverwort *Marchantia polymorpha*. Genetic and imaging analyses revealed their distinct physiological roles in development, morphogenesis and environmental stress responses. *MpRbohA* is expressed in the cell-dividing apical meristematic zones and its knockout lines showed reduced cell proliferation at the apices as well as defects in gametophyte development. Moreover, the double mutant *mprbohA mprbohB* exhibited severe defects in cell differentiation. These results suggest that Rboh-mediated ROS production is involved in the maintenance of stem cells as well as the regulation cell proliferation and differentiation. We also performed computer simulation of the growth of the wild type and *mprbohA* mutant to understand possible roles of MpRbohA-mediated ROS production. Evolutionary aspects and molecular regulatory mechanisms of Rboh/ROS-mediated signaling will also be discussed.

1. Ogasawara *et al.* (2008) *J. Biol. Chem.* 283: 8885-8892.
2. Takeda *et al.* (2008) *Science* 319: 1241-1244.
3. Kurusu *et al.* (2013) *Trends in Plant Science* 18: 227-233.
4. Kaya *et al.* (2014) *Plant Cell* 26: 1069-1080.
5. Kärkönen and Kuchitsu (2015) *Phytochemistry* 112: 22-32.
6. Hyodo K *et al.* (2017) *PNAS* 114: E1282-E1290.
7. Kaya H *et al.* (2019) *Plant J.* 98: 291-300.

P-22

Imaging of ROS dynamics and roles of the ROS-producing NADPH oxidase in tapetal programmed cell death during pollen maturation in rice

Togo Fukunaga[1], Jumpei Sawada[1], Kazunori Ogawa[1], Bunki Toh[1], Kenji Hashimoto[1,2], Shigeru Hanamata[2,3], Seijiro Ono[4], Ken-ichi Nonomura[4], Takamitsu Kurusu[2,5], Kazuyuki Kuchitsu[1,2]

[1]Dept. Appl. Biol. Sci. & [2]Imaging Frontier Center, Tokyo University of Science, [3]Grad. Sch. Sci. & Tech., Niigata Univ., [4]Natl. Inst. Genetics, [5]Fac. Eng., Suwa Univ. of Science

In flowering plants, programmed cell death (PCD) of the tapetum, the innermost layer of the anther, is one of the most critical and sensitive steps for pollen maturation and fertility. It is severely affected by various environmental stresses, which cause serious problems in agriculture. Production of reactive oxygen species (ROS) has been shown to be required for post meiotic anther development including the tapetal PCD and pollen maturation in rice. However, these spatiotemporal dynamics had remained poorly understood.

We here established an *in vivo* imaging system to analyze the dynamics of ROS in rice anther including the tapetum cells by using several ROS-specific probes during pollen maturation. Imaging analyses showed that ROS accumulated in the tapetum cells transiently prior to the tapetal PCD. The present monitoring system for ROS accumulation offers a powerful tool for determining the relationship between ROS signaling and regulation of rice tapetal PCD during pollen maturation.

Furthermore, we identified a ROS producing-NADPH oxidase/respiratory burst oxidase homolog (Rboh) specifically expressed in rice anther and generated its knockout mutant by genome editing. We will report its phenotype and discuss possible involvement of NADPH oxidase-dependent ROS production as well as transcriptional network in the regulation of autophagy and the proper timing of tapetal PCD during pollen maturation.

P-23

Imaging autophagy in the anther tapetum cells during pollen maturation in rice

Kazunori Ogawa[1], Jumpei Sawada[1], Togo Fukunaga[1], Bunki Toh[1], Kenji Hashimoto[1,2], Shigeru Hanamata[2,3], Seijiro Ono[4], Kenichi Nonomura[4], Takamitsu Kurusu[2,5], Kazuyuki Kuchitsu[1,2]

[1]Dept. Appl. Biol. Sci. & [2]Imaging Frontier Center, Tokyo University of Science,
[3]Grad. Sch. Sci. & Tech., Niigata Univ., [4]Natl. Inst. Genetics, [5]Fac. Eng., Suwa Univ. of Science

Autophagy contributes to various cellular processes including maintenance of cellular homeostasis, innate immunity, development, and programmed cell death (PCD) in multicellular organisms. We showed that autophagy is required for post meiotic anther development including programmed cell death (PCD)-mediated degradation of the tapetum and pollen maturation in rice [1-5]. However, the spatiotemporal dynamics of autophagy in the tapetum remain poorly understood. We established an *in vivo* imaging technique to analyze the dynamics of autophagy in rice tapetum cells by expressing green fluorescent protein-tagged AtATG8, a marker for autophagosomes [6]. 3D-imaging analysis revealed that the number of autophagosomes/autophagy-related structures is extremely low at the tetrad stage, and autophagy is dramatically induced at the uninucleate stages throughout the tapetal cells during anther development. The present monitoring system for autophagy offers a powerful tool to analyze the regulation of autophagy in rice tapetal cells during pollen maturation. We will discuss possible mechanisms for the regulation of autophagy and its physiological significance in tapetal PCD during pollen maturation.

1. Kurusu *et al.* (2014) *Autophagy* 10: 860-870.
2. Hanamata *et al.* (2014) *Front. Plant Sci.* 5: 457.
3. Kurusu *et al.* (2016) *Bioimages* 24: 1-11
4. Kurusu & Kuchitsu (2017) *J. Plant Res.* 130: 491-499.
5. Kurusu *et al.* (2017) *Plant Signal. Behav.* 12: e1365211
6. Hanamata *et al.* (2019) *Plant Biotechnol.* in press

P-24

Dynamic Photocontrol of Biomachines During Cell Division

Kazuya Matsuo[1], Mafy Nusrat Noushaba[1], Shota Hiruma[2], Ryota Uehara[2], Nobuyuki Tamaoki[1]

[1]Research Institute for Electronic Science, Hokkaido university

[2]Graduate School of Life Science, Hokkaido University

OBJECTIVE

In eukaryotic cell division, chromosomes work as the key player to transfer the genetic information to the next generation of cells. After chromosome replication in S phase of cell division, the chromosomes migrate from spindle pole to the metaphase plate during metaphase. In this dynamic process, various biomachines including kinesin and dynein family proteins can concertedly work with high accuracy and precision for the successful cell division. However, the dysfunction of these biomachines can activate the spindle assembly checkpoint through the misalignment of chromosomes at the metaphase plate. The prolonged mitotic arrest delays the cell-cycle progression, which eventually leads to the apoptotic cell death. Thus, "chromosome migration" triggered by biomachines should be the attractive target for unveiling the mitotic cell division. Herein, we report the novel approach for optochemically controlling the chromosome migration driven by the specific biomachine that is centromere-associated protein E (Cenp-E), using the imaging technique equipped with the light illumination system.

METHODS

Reversibly photoswitchable Cenp-E inhibitor was designed and chemically synthesized by the coupling of the azobenzene derivative with the core structure of the authentic Cenp-E inhibitor, GSK923295. We explored the fundamental properties of the synthesized photoswitchable Cenp-E inhibitor through the photophysical and biochemical experiments including ATPase assays *in vitro* and cell-based assays. As the unique technique for controlling the mitotic cell division, we attempted to establish the light-controllable system of chromosome migration driven by Cenp-E by the alternative illumination of ultraviolet (UV) / visible (Vis) lights.

RESULTS

Our Cenp-E inhibitor exhibited the high photoswitchability based on the reversible *cis-trans* photoisomeization of the azobenzene moiety by illuminating UV/Vis lights. Before light illumination or upon Vis light illumination, *trans* isomer in the azobenzene moiety was majorly formed, which worked as the potent Cenp-E inhibitor ($IC_{50\ \text{for before light illumination}}$ = 5.9 μM, $IC_{50\ \text{for Vis light}}$ = 14 μM from *in vitro* ATPase assay). In sharp contrast, upon ultraviolet light illumination, the predominant *cis* isomer was found to be a non-inhibitor for Cenp-E ($IC_{50\ \text{for UV light}}$ = 120 μM from *in vitro* ATPase assay). Depending on this drastic affinity change of our Cenp-E inhibitor by light stimuli, not only chromosome alignment/misalignement on the metaphase plate but also chromosome migration/positioning in live mitotic cells were photocontrolled in real time.

CONCLUSIONS

We have successfully developed the photoswitchable Cenp-E inhibitor, which enabled to spatiotemporally regulate chromosome migration driven by Cenp-E on spindle microtubules using light illumination. The further details will be discussed in the poster.

P-25

Development of Ratiometric Oxygen Probes Based on Green Fluorophore and Red Phosphor for Visualization of Intracellular Oxygen Level

Mami Yasukagawa, Seiji Tobita, Toshitada Yoshihara*

Department of Chemistry and Chemical Biology, Graduate School of Science and Technology, Gunma University

OBJECTIVE

Intracellular oxygen is an important indicator for cell metabolism. To clarify the intracellular oxygen level, we have recently developed ratiometric oxygen probes consisting of an oxygen-sensitive phosphor and an oxygen-insensitive fluorophore as reference dye [1,2]. In this study, we synthesized new ratiometric oxygen probes NBD-PR_7-BTQphen (**1**) and NBD-PR_{11}-BTQphen (**2**) (Fig. 1) in which a green fluorescent nitrobenzoxadiazole derivative NBD excitable at 480 nm and a red phosphorescent iridium complex BTQphen are connected with an oligoarginine linker. We investigated the photophysical properties of **1** and **2** in solution and attempted to visualize the oxygen levels in living cells by using these probes.

METHODS

The emission spectra of **1** and **2** in acetonitrile were measured upon excitation at 480 nm. The emission images of HeLa cells loaded with the probes were observed with a fluorescence microscope equipped with a dual wavelength simultaneous-imaging system.

RESULTS

We first examined emission spectra of **1** and **2** in acetonitrile upon excitation at 480 nm (Fig. 2). The new ratiometric oxygen probes showed dual emission bands derived from fluorescence of NBD and phosphorescence of BTQphen. Under different O_2 partial pressures, the fluorescence intensities of the probes were almost constant, whereas the phosphorescence intensities greatly decreased with increasing the O_2 partial pressure, indicating that the probes in acetonitrile are sensitive to O_2 concentration.

We next carried out cell culture experiments using the ratiometric probes. The sufficient emission signal could be obtained after HeLa cells was incubated with these probes (2 μM, 2h). Then, we attempted to image the oxygen levels of HeLa cells using ratiometric probes. when the O_2 partial pressure was changed from 21% to 2.5% O_2 condition, the ratio between the phosphorescence and fluorescence intensities increased.

CONCLUSIONS

We designed and synthesized the new ratiometric O_2 probes **1** and **2**, in which a green fluorescent NBD molecule and a red phosphorescent BTQphen molecule are connected with arginine peptide linker. These ratiometric probes showed dual emission bands in solutions and living HeLa cells. The O_2 levels in living HeLa cells could be imaged by ratiometric measurements using developed probes.

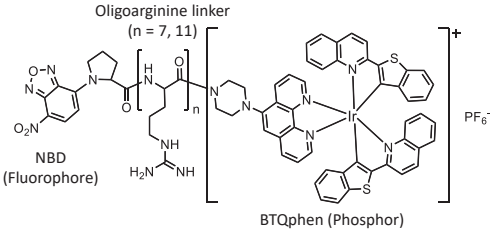

Fig. 1 Chemical structure of ratiometric oxygen probes NBD-PR_7-BTQphen (**1**) and NBD-PR_{11}-BTQphen (**2**).

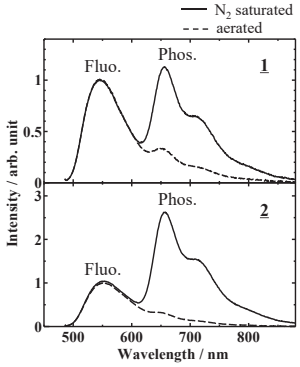

Fig. 2 Emission spectra of **1** and **2** in acetonitrile.

[1] Yoshihara, T.;Yamaguchi, Y.; Hosaka, M.; Takeuchi, T.; Tobita, S. *Angew. Chem. Int. Ed.*, **2012**, *124*, 4224-4227.
[2] Yoshihara, T.; Murayama, S.; Tobita, S. *Sensors*, **2015**, *15*, 13503-13521.

Cell cycle dependence of phototoxicity caused by irradiation of blue laser light

***Naohiro Kanamaru[1], Mikiya Yamaguchi[1], Tetsuya Matsuyama[1],**
Kenji Wada[1], Koichi Okamoto[1],
Ai Kawakita[2], Kaori Murata[2], Kenji Sugimoto[2]
[1] Graduate School of Engineering, Osaka Prefecture University
[2] Graduate School of Life and Environmental Sciences, Osaka Prefecture University

INTRODUCTION

Exposure to a large amount of short wavelength light is known to cause diseases such as age-related macular degeneration (AMD) and retinal photolesion. To prevent diseases, the generation mechanism of phototoxity due to short wavelength visible light irradiation should be elucidated. We have performed quantitative evaluation of phototoxity caused by short wavelength light irradiation on living cells by using live cell imaging method. As a result, the dependence of phototoxity on the intensity and wavelength of irradiated light has been partly clarified [1]. In this study, we investigate the cell cycle dependence of phototoxity caused by the irradiation of blue laser light.

EXPERIMENTAL

Figure 1 shows the experimental setup for live cell imaging using a light emitting diode (LED) and a laser diode (LD). Nucleus and proliferating cell nuclear antigen (PCNA) of the cell (human malignant melanoma-derived cell: MDA-MB-435S, culture condition: DMEM, 37℃, 5% CO_2) were labeled with fluorescent proteins of mPlum and EGFP, respectively. The light suitable for the excitation of fluorescent protein was extracted from white LED light by an excitation filter. Extracted light was reflected with a dichroic mirror and condensed through an objective lens (x60) to irradiate cells in the laboratory dish. The fluorescence from the cells was detected with an EMCCD camera after passing through the objective lens, the dichroic mirror and the fluorescence filter. After the laser light was adjusted to a low intensity with a variable-attenuator, it was guided to the microscope using the surface reflection of a cover glass to irradiate the specific site in the cell.

RESULTS

The center of nucleus of cells in M, G1, middle S and late S phase of cell cycle was irradiated with 405 nm laser light of 100 W/cm^2. Table 1 shows the irradiation energy dependence of the cell viability (viable cell number / observed cell number) within 24 hours after the laser irradiation to cells in each phase of the cell cycle. As shown in Table 1, the cell viability decreases with increasing the irradiation energy in all phases of the cell cycle. The viabilities of cells in M and G1 phases are relatively lower than those in middle S and late S phases where DNA is synthesized and repaired.

CONCLUSIONS

To investigate the cell cycle dependence of phototoxity caused by the irradiation of blue laser light, we measured the cell viability within 24 hours after the 405 nm laser irradiation to cells in M, G1, middle S and late S phase. The viabilities of cells in M and G1 phases were confirmed to be lower than those in middle S and late S phases, suggesting that the phototoxity of blue laser light on living cells depends on the phase of the cell cycle.

[1] K. Takahashi et. al., The 27th Annual Meeting of the Bioimaging Society of Japan, P-7

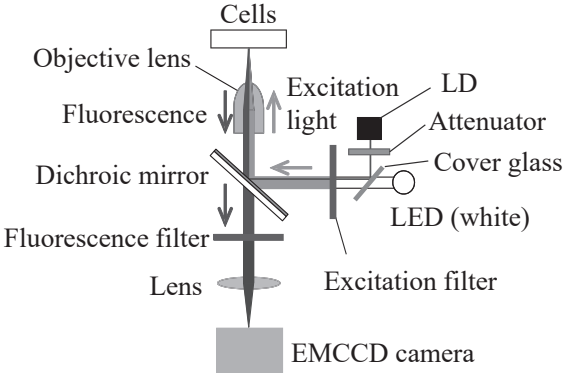

Fig. 1. Configuration of fluorescent microscope

Table 1. The dependence of the phase of the cell cycle and the irradiation energy on the cell viability

Irradiation energy (kJ/cm^2)	Cell viability (Viable cell number / Observed cell number)				
	M	G1	MidS	LateS	Total (%)
0	5 / 5	5 / 5	5 / 5	5 / 5	20 / 20 (100 %)
12	3 / 5	2 / 5	4 / 5	3 / 5	12 / 20 (60 %)
18	2 / 5	1 / 5	3 / 5	3 / 5	9 / 20 (45 %)
24	1 / 5	0 / 5	2 / 5	3 / 5	6 / 20 (30 %)

P-27

Development of novel microbubbles for ultrasound imaging

Tamotsu Maruyama[1], Daiki Omata[1], Lisa Munakata[1], Tadamitsu Shima[1], Saori Kageyama[1], Fumiko Hagiwara[1], Yuno Suzuki[1], Kazuo Maruyama[2], Ryo Suzuki[1,*]

[1]Laboratory of Drug and Gene Delivery Research, Faculty of Pharma Science, Teikyo University

[2]Laboratory of Theranostics, Faculty of Pharma Science, Teikyo University

OBJECTIVE

Ultrasound imaging is non-invasive and provide real-time imaging. However, it is difficult to observe a small blood flow such as a tumor tissue. In order to solve this problem, microbubbles (MBs) as ultrasound contrast agents are utilized. Sonazoid which is approved contrast agent is applied for detection of liver and breast cancer. Sonazoid is actively uptaken into Kupffer cells in liver due to be composed with phosphatidylserine. Therefore, it can negatively stain tumor region without Kupffer cells in liver. The blood flow imaging in breast cancer is performed at the vascular phase before liver accumulation of Sonazoid. Generally, the clearance of Sonazoid is fast. Thus, it is thought that the properties of MBs such as the blood clearance and their stability would be affected by the shell composition of MBs. In this study, we focused on the shell composition of the MBs and tried to develop MBs with long blood circulation.

METHODS

Liposomes composed of DSPC, DSPG and DSPE-PEG (2k) OMe were prepared using the lipid film hydration method. The liposome suspension was homogenized (15,000 rpm, 5 min) under the perfluoropropane (C_3F_8) atmosphere to make MBs (DSPG-MBs). The DSPG-MBs dispersion was mixed with sucrose solution and freeze-dried. To evaluate blood circulation of MBs, DSPG-MBs or Sonazoid were intravenously injected into the mice. After injection of MBs, blood flow in the kidney was observed with the contrast mode of ultrasonography. Next, to evaluate the hepatic accumulation of MBs, DSPG-MBs or Sonazoid were intravenously injected into mice. At 10 minutes after DSPG-MBs or Sonazoid injection, the mice were perfused to remove DSPG-MBs or Sonazoid in the blood. Then, the liver was extirpated and observed with contrast mode of ultrasonography. And to evaluate the biodistribution, DiR labeled DSPG-MBs or Sonazoid were intravenously injected into mice. The mice were observed with *in vivo* imaging system. The intensity of fluorescence in the liver was quantified.

RESULTS AND DISCUSSION

In liposome research, it was reported that addition of DSPG into the lipid membrane could enhance the liposome stability. Generally, MBs are necessary to escape the reticuloendothelial system (RES) and to be stable in blood flow for developing the long circulating MBs. Therefore, we assessed the effect of DSPG on circulating time. 60% DSPG containing-MBs (DSPG60-MBs) showed longer blood circulation than Sonazoid. And the signal intensity of the DSPG60-MBs in liver was lower than that of Sonazoid. In addition, we also examined the liver accumulation of MBs labeled with DiR. At 15 min after injection of DiR labeling Sonazoid or DSPG60-MBs, the accumulation of DSPG60-MBs into liver was lower than that of Sonazoid. These results suggested that DSPG60-MBs were stable in blood flow and long circulation microbubbles by escaping the RES.

CONCLUSION

We succeeded to develop the novel MBs (DSPG-MBs) with long circulation by adding DSPG to the shell composition of MBs. The hepatic accumulation of DSPG-MBs was lower than that of Sonazoid due to be less uptaken into kupffer cells. Therefore, DSPG-MBs would be an effective diagnosis agent for many cancers.

Contribution of cellular immune response in tumor growth suppression by the combination of microbubbles and ultrasound

Eri Chiba[1], Lisa Munakata[1], Daiki Omata[1], Tadamitsu Shima[1], Saori Kageyama[1]
Fumiko Hagiwara[1], Yuno Suzuki[1], Kazuo Maruyama[2], Ryo Suzuki[1,*]
[1]Laboratory of Drug and Gene Delivery Research, Faculty of Pharma Science, Teikyo University
[2]Laboratory of Theranostics, Faculty of Pharma Science, Teikyo University

OBJECTIVE

Microbubbles have various behaviors such as oscillation and cavitation under ultrasound field. The oscillation is utilized to ultrasound imaging of blood flow in microvascular. On the other hand, cavitation would be utilized to drug and gene delivery by opening the transient pore in cell membrane and enhancing the permeability of blood vessels. In addition, cavitation of microbubbles induces jet stream and/or heat generation. This phenomenon would be applied for direct killing of cancer cells. Moreover, direct cell damage may be induced the release of tumor associated antigens in tumor tissue. And this is expected that the combination therapy of microbubbles and ultrasound would activate the cellular immune response for cancer cells. In this study, we examined the anti-tumor effects by the combination of microbubbles and ultrasound. Moreover, in this combination therapy, we also assessed the contribution of cellular immune response for tumor growth suppression.

METHODS

Colon-26 cells (mouse colon carcinoma) were inoculated into the back of mice. After 8 days, our microbubbles were intratumorally injected and ultrasound (Frequency: 1 MHz, Intensity: 4 W/cm^2, Duty: 50%, Burst rate: 2 Hz, Time: 2 min) was transdermally exposed toward tumor tissue. The anti-tumor effect was evaluated by measuring tumor volume. To assess the effect of cellular immunity on tumor growth suppression, we also examined in CD8 positive T cells depleted mice by injection of anti-CD8 antibody.

RESULTS and DISCUSSION

In the combination of microbubbles and ultrasound, tumor growth was significantly suppressed (Fig. 1). And this tumor growth suppression was cancelled in the CD8 positive T cell depleted mice. This result suggested that the combination of microbubbles and ultrasound would be an effective cancer therapy based on priming the cellular immune response.

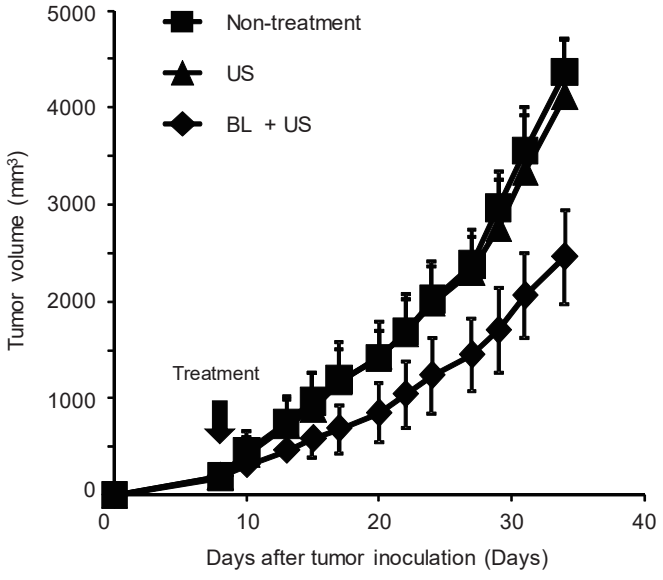

Fig. 1 Tumor growth suppression by the combination of microbubbles and ultrasound

CONCLUSION

The combination of microbubbles and ultrasound had anti-tumor effect cause of the direct damage of tumor tissue. This damage could prime the cellular immune response which can suppress the tumor growth. Therefore, this combination therapy would be a novel cancer immunotherapy based on changing the immunological microenvironment in tumor tissue.

P-29

Evaluation of Transporter Function in Brain Microvascular Endothelial Cells Derived from Human Induced Pluripotent Stem Cells

Toshiki Kurosawa,[1] Yuma Tega,[1] Tomoko Yamaguchi,[3] Tatsuki Mochizuki,[2] Yasuhiro Hayashi,[1] Atsushi Yamashita,[1] Hiroyuki Kusuhara,[2] Kenji Kawabata,[3] Yoshiharu Deguchi[1,*]

[1]Fac. Pharm-Sci., Teikyo Univ., [2] Grad.Sch. Pharma-Sci., Univ. Tokyo., [3]Nat. Instit. Biomed. Innov. Health Nut.

OBJECTIVE

Brain microvascular endothelial cells derived from human induced pluripotent stem cells (hiPS-BMECs) are thought to have the potential to become an innovative human blood-brain barrier (BBB) model. However, functional expression of various transporters in these cells has not yet been fully evaluated. This information is important for constructing a high-quality BBB model that mimics the *in vivo* human BBB. The objective of this study was to clarify the expression and function of nutrient and drug transporters in BMECs derived from hiPS.

METHODS

BMECs were differentiated from the hiPS cell line, IMR90-4. mRNA and protein expression levels of transporters were measured by the quantitative real-time polymerase chain reaction and immunohistochemical staining analyses, respectively. Transport function was evaluated by uptake and transcellular transport studies. Drugs were quantified by a LC-MS/MS system or liquid scintillation counter.

RESULTS

hiPS-BMECs expressed endothelial cell markers, such as platelet endothelial cell adhesion molecule -1, vascular endothelial-cadherin, and glucose transporter 1, and tight-junction proteins such as claudin-5, occludin, and zonula occludens-1. In addition, cultures of these cells on Transwell membranes showed high TEER values (> 2000 $\Omega \cdot cm^2$), and negligibly small transcellular transport rates of lucifer yellow (a paracellular marker). These results suggest that hiPS-BMECs are endothelial cells with strong tight junctions.

mRNAs encoding solute carrier transporters, such as high affinity cationic amino acid transporter 1 (CAT1), sodium-dependent glutamate/aspartate transporter 1 (GLAST), L-type amino acid transporter 1 (LAT1), and monocarboxylate transporter 1 (MCT1), were highly expressed in hiPS-BMECs. Transcellular transport studies showed that [^{3}H]L-arginine, [^{3}H]L-glutamate, gabapentin, and [^{14}C]L-lactate (substrates of CAT1, GLAST, LAT1, and MCT1, respectively) were transported symmetrically and/or asymmetrically across the hiPS-BMEC monolayer. Substrates of CAT1, GLAST, LAT1, MCT1, organic cation/carnitine transporter 2 (OCTN2), and the proton-coupled organic cation (H^+/OC) antiporter, were taken up by hiPS-BMECs time-, temperature-, and concentration-dependently. Furthermore, these uptakes were decreased markedly by inhibitors of the corresponding transporter.

Regarding ABC transporters, breast cancer resistant protein (BCRP), multidrug resistance associated protein (MRP) 1, MRP4, and MRP5 showed relatively high mRNA and protein expression levels. Dantrolene (a substrate for BCRP) showed superior asymmetrical transport in the abluminal-to-luminal direction. This asymmetric transport was abolished by knockdown of the BCRP gene using an electroporation gene transfer method.

CONCLUSIONS

The results of the present study indicate that hiPS-BMECs not only form strong tight junctions, but also express multiple functional nutrient and drug transporters, including CAT1, GLAST, LAT1, MCT1, the H^+/OC antiporter, and BCRP. Our findings contribute to the development of high-fidelity *in vitro* models of the BBB.

P-30

Development of new anticancer drug delivery system with ultrasound for cancer therapy

Yuno Suzuki[1], Daiki Omata[1], Lisa Munakata[1], Tadamitsu Shima[1], Saori Kageyama[1], Fumiko Hagiwara[1], Kazuo Maruyama[2], Ryo Suzuki [1,*]

[1]Laboratory of Drug and Gene Delivery Research, Faculty of Pharma-Science, Teikyo University
[2]Laboratory of Theranostics, Faculty of Pharma-Science, Teikyo University

OBJECTIVE

Currently, anticancer drug-encapsulated liposomes are approved for cancer therapy. These liposomal drugs accumulate to tumor tissue based on the Enhanced Permeability and Retention (EPR) effect. However, most of liposomal drugs have not provided enough therapeutic effects in many types of cancer. It was reported that a permeability of neo-vasculature in human tumor tissue would not be enhanced due to interstitial pressure in tumor tissue, and existence of pericytes. These obstacles would prevent nano-sized particles such as liposomes from passing across the blood-tumor barrier (BTB) in human. In addition, to obtain efficient antitumor effects, anticancer drugs should be transferred into tumor cells. Therefore, it is necessary to develop a novel active drug delivery system for tumor tissue.

Previously, we reported that the combination of microbubbles (MBs) and ultrasound (US) could open blood-brain barrier (BBB). In this BBB opening, the mechanical effect by the oscillation of MBs under ultrasound field loosen the tight-junction between endothelial cells. In tumor tissue, it is expected that this mechanical effect could induce BTB opening and enhance liposomal drugs accumulation into the tumor tissue. To achieve the efficient liposomal drugs delivery, it is important that liposomes are loaded on MBs. Because when liposomes-loaded MBs are exposed to US, the collapse of MB has two functions such as the release of the liposomes from MB and BTB opening. Finally, these functions would lead liposomal drugs to an active drug delivery for tumor tissue. In this study, we prepared doxorubicin-encapsulated liposomes (D-Lipo)-loaded microbubbles (D-Lipo-MBs) and assessed the feasibility of D-Lipo-MB as active drug delivery system.

METHODS

Preparation of liposomes loaded microbubbles

Lipid suspension (DSPC:PEG_{40}-monostearate:DSPE-PEG(2k)-biotin = 90:10:1 in molar ratio) was put into a vial. The air in head space of the vial was replaced with perfluorobutane (C_4F_{10}) gas, and the vial was capped. Then, the vial was vigorously shaken with VIALMIX® to form MBs. The MBs were incubated with avidins to make avidin modified MBs (avidin-MBs). To prepare D-Lipo-MB, avidin-MB and biotinylated D-Lipo (DPPC:Cholesterol:DSPE-PEG(2k)-biotin = 55:40:5 in molar ratio) were mixed. To confirm D-Lipo loading on MBs, the D-Lipo-MB was observed with a fluorescence microscope.

Assessment of cell viability by the treatment of D-Lipo-MB and US

D-Lipo-MBs were added to pancreatic cancer cells (PAN02). Immediately, US (Frequency; 1 MHz, Intensity; 0.5 W/cm^2, Exposure time; 10 sec, Duty; 50%) was exposed to the mixture of D-Lipo-MBs and the cells. After incubation for 1 day, the cell viability was assessed with MTT assay.

RESULTS and DISCUSSION

D-Lipo-MBs were observed with a fluorescence microscope to confirm whether D-Lipo was loaded on MBs. doxorubicin-derived fluorescence was detected on the MB surface. This result suggested that D-Lipo was loaded on MBs by avidin-biotin interaction. In addition, the combination of D-Lipo-MBs and US significantly reduced the cell viability compared with the treatment of D-Lipo-MBs only. From these results, it was thought that the US triggered release from MBs was induced and resulted in delivering doxorubicin into cancer cells. Thus, the combination of D-Lipo-MBs and US would be a useful active delivery system for cancer therapy.

P-31

Induction of the accelerated blood clearance (ABC) phenomenon by polyethyrene glycol (PEG) modified microbubbles

Tadamitsu Shima[1], Tamotsu Maruyama[1], Takumi Yamada[1], Daiki Omata[1], Lisa Munakata[1], Saori Kageyama[1], Fumiko Hagiwara[1], Yuno Suzuki[1], Ryo Suzuki[1,*]

[1]Laboratory of Drug and Gene Delivery Research, Faculty of Pharma-Science, Teikyo University

OBJECTIVE

Microbubbles (MBs) are clinically utilized as ultrasound contrast agents. In general, MBs have lower frequency of severe side effects compared with other contrast agents utilized as other diagnostic methods such as MRI and CT. Therefore, MBs would be able to apply for repeated use. This point is an advantage of ultrasound imaging with MBs. To enhance the MB stability and prolong the half-life of MB in blood stream, we have developed the novel type of MBs by optimization of shell components on MB surface. Our MBs are composed with DSPC, DSPG and PEGylated lipid as lipid shell. Recently, it has been reported that MB modified with PEG induced the accelerated blood clearance (ABC) phenomenon. The ABC phenomenon is normally caused by anti-PEG antibody induction after repeated injection of PEGylated particles. Therefore, it is thought that our MB might be cleared from blood flow with the repeated injection by the induction of the ABC phenomenon. The ABC phenomenon may affect the effectiveness of the diagnosis and therapeutics. Therefore, in this study, we examined whether our MBs induce anti-PEG antibody and the ABC phenomenon.

METHODS

Liposomes composed of DSPC, DSPG and DSPE-PEG (2k) OMe were prepared using the lipid film hydration method. The liposome suspension was homogenized (15,000 rpm, 5 min) under the perfluoropropane (C_3F_8) atmosphere to make MBs (DSPG-MBs). MBs were intravenously injected into mice, and blood was collected at each time point. The antibody titer of anti-PEG antibody was measured by ELISA. To measure the MB clearance from blood flow, we observed the renal blood flow after MBs injection with sonography. Seven days later, MBs were re-injected, and renal blood flow was observed with sonography, and the imaging signals in the contrast mode were measured. Furthermore, to consume anti-PEG antibody in the mice induced the ABC phenomenon, excess of free PEG was injected. Then, our MBs were intravenously injected and the cancellation of the ABC phenomenon was observed.

RESULTS and DISCUSSION

The injection of our MBs increased the antibody titer for PEGylated lipids which were the components of MB shell. In addition, in the re-injection of MBs to mice at 7 days after the first injection, the imaging signal quickly decreased compared with first injection of MBs. It was suggested that the repeated injection of our MB induced the ABC phenomenon for our MB. Thus, we assessed the contribution of anti-PEG antibodies on accelerated blood clearance of our MBs. In this experiment, excess of free PEG and our MBs were intravenously injected into the mice which was alleviated the ABC phenomenon for our MBs. The shortening of imaging signal was alleviated. This result showed that anti-PEG antibody was competitively inhibited by free PEG and could not bind to MB. Therefore, it was suggested that the ABC phenomenon was related to anti-PEG immune response.

Our PEGylated MBs have a property of long circulation after single injection. On the other hand, in the repeated injection, they induced anti-PEG immune response. In the liposome research, the induction of the ABC phenomenon was depending on injection dose and interval. In other MB study, it was reported that anti-PEG antibody was temporally induced. From these reports, it is thought that there would be some condition to avoid the induction of anti-PEG immune response and escape of the ABC phenomenon even in the repeated injection. Therefore, we will try to find out the conditions that can escape from the ABC phenomenon in the repeated injection of our MB.

P-32

Development and evaluation of antibody-modified nanobubbles using Fc binding polypeptides for tumor imaging

Nobuhito Hamano[1], Yusuke Yano[1], Yamato Kikkawa[2], Tomomi Kobayashi[1], Yoko Endo-Takahashi[1], Ryo Suzuki[3], Kazuo Maruyama[3], Motoyoshi Nomizu[2], and Yoichi Negishi[1*]

[1] Dept. of Drug Deliv. and Mol. Biopharm., School of Pharmacy, Tokyo Univ. of Pharmacy and Life Sci.,
[2] Dept. of Clin. Biochem., School of Pharmacy, Tokyo Univ. of Pharmacy and Life Sci.,
[3] Lab. of Drug and Gene Deliv. Res., Faculty of Pharma-Sci., Teikyo Univ.

OBJECTIVE

Ultrasound (US) imaging is a widely used imaging technique. The use of US contrast agents such as microbubbles, which consist of phospholipids and are filled with perfluorocarbon gases, has become an indispensable component of clinical US imaging, while molecular US imaging has recently attracted significant attention in combination with efficient diagnostics. Microbubbles aid in enhancing the specificity and sensitivity of US imaging and can be applied for various types of diseases, particularly tumors. For this purpose, targeting strategies for microbubbles have been demonstrated. Among these targeting strategies, antibodies have been used as a targeting moiety of microbubbles, and the avidin–biotin interaction has often been adopted to modify microbubbles with antibodies. However, avidin still has limitations in its usefulness because of the immunogenicity of streptavidin in humans. Therefore, in this study, as an alternative to the avidin–biotin interaction in antibody modification, we developed antibody-modified NBs using Fc-binding polypeptides for US imaging.

METHODS

We prepared polyethyleneglycol (PEG) -modified liposomes which were composed of DSPC and DSPE-PEG_{2000}. To modify the Fc-binding polypeptide in the liposomes, we used the post-insertion method. Antibody (anti-CD146 antibody) was added to the polypeptide-modified liposomes and incubated for 15 min at RT. Then, antibody-modified NBs was prepared by entrapping US imaging gas (C_3F_8) into antibody-modified liposomes. We examined specific adhesion of antibody-modified NBs to HUVECs by fluorescence microscopy. In US imaging, female KCN nu/nu mice (5–6 weeks old) were injected s.c. into the right flank region with SKOV3 cells (5×10^6 cells/mouse). We administered antibody-modified NBs via a tail vein when the tumors reached 100 mm^3. US imaging was performed using an Aplio80 US diagnostic machine (Toshiba Medical Systems, Tokyo, Japan) and a 12-MHz wideband transducer with contrast harmonic imaging at a mechanical index of 0.25.

RESULTS

First, we prepared anti-CD146 antibody-modified NBs (m146-NBs) using Fc-binding polypeptide. The mean particle diameter of the non-labeled and m146-NBs ranged from 500 to 700 nm, with a narrow distribution. To examine the specific attachment of m146-NBs to HUVECs, which are known to express high levels of CD146, the cell attachment of the NBs was observed by fluorescence microscopy. The m146-NBs exhibited a high level of attachment to the HUVECs, while attachment of non-modified NBs to the HUVECs was not observed. We next attempted US imaging in tumor-bearing mice. The m146-NBs showed strong signals at 1 min post-administration compared to the non-modified NBs. In addition, the contrast images for the m146-NB group were maintained for up to 20 min, in contrast to the observations for the non-modified group. This result suggests that m146-NBs may target tumor vessels, leading to longer US imaging.

CONCLUSIONS

In this study, as an alternative to the avidin–biotin interaction in antibody modification, we developed antibody-modified NBs using Fc-binding polypeptides for US imaging. m146-NBs displayed specific attachment to HUVECs. Moreover, US imaging analysis demonstrated that the contrast images for the group injected with m146-NBs had a longer duration compared with those of the non-modified group. Thus, the modification method using Fc-binding polypeptides is suitable for providing an antibody linker. Therefore, this antibody-modified method using an Fc-binding polypeptide may be useful for developing next-generation antibody-modified US imaging agents.

P-33

CpG oligodeoxynucleotide loaded lipid nanoparticles activate CD8$^+$ T cells and exert antitumor effect for murine colon carcinoma

Lisa Munakata[1], Daiki Omata[1], Yasunari Haseda[2], Shohei Koyama[3], Yoshiaki Okada[4], Yasuo Yoshioka[2, 4], Taiki Aoshi[2], Ryo Suzuki[1, *]

[1]Faculty of Pharma-Science, Teikyo University, [2] Research Institute for Microbial Diseases, Osaka University, [3] Graduate School of Medicine, Osaka University

[4] Graduate School of Pharmaceutical Sciences, Osaka University

OBJECTIVE

CpG oligodeoxynucleotide (ODN), a ligand of Toll-like receptor 9 (TLR9) is known as adjuvant expect for activating both of innate and adoptive immune system. Type-A CpG, a kind of CpG ODN has an ability to induce production of IFN-α from plasmacytoid dendritic cells (pDCs) via activation of TLR9. IFN-α can activate Th1-associated immunity. Accordingly, it is anticipated antitumor effect by CD8$^+$ T cells. Nevertheless, CpG ODN has few efficacy, because of its lower cellular interaction. In this study, we tried to develop novel lipid nanocarrier of CpG ODN (CpG lipid nanoparticles; CpG LNPs) to overcome this problem. Moreover, we attempted to evaluate antitumor effect of CpG LNPs and elucidate the contribution of CD8$^+$ T cells in this antitumor effect.

METHODS

Preparation of CpG LNPs; CpG LNPs were prepared with microfluidics (NanoAssemblr Benchtop, Precision NanoSystems Inc.). Briefly, the lipid solution in ethanol and CpG solution in acetate buffer were mixed in the microfluidic mixer. This mixture was dialyzed against 5% glucose solution to remove ethanol from CpG LNP suspension. Further, the CpG LNPs suspension was concentrated by ultrafiltration, then passed through 0.22 μm filter.

Evaluation of Antitumor Effect; C57BL/6 mice were inoculated MC38 cells (murine colon carcinoma) in their right flank. After 9 days from inoculation, CpG LNPs (4.5 μg CpG equivalents) were intratumorally administrated. The administration was repeated 5 times every 2 days. The antitumor effect was evaluated by the tumor volume.

Elucidation the contribution of CD8$^+$ T cells in antitumor effect; To deplete CD8$^+$ T lymphocytes, tumor inoculated mice were intraperitoneally administrated anti-CD8a antibody at 6 and 13 days after from tumor inoculation. Then they were treated with CpG LNPs. Finally, at day 21 after from tumor inoculation, tumors were collected and embedded in O.C.T. compound for making frozen slices. The frozen slices were observed with confocal fluorescence microscope after staininig with the following fluorescent dye and antibodies. The nuclei were stained with DAPI, the blood vessels were stained with anti-mouse CD31-Alexa Fluor 647 and the CD8$^+$ T cells were stained with anti-mouse CD8b-PE.

RESULTS AND CONCLUSION

The average size of CpG LNPs were 54.0 nm and the size distribution was narrow. In the evaluation of antitumor effect, any tumor growth suppression was not observed in the CpG treated mice. On the other hand, the tumor growth in the mice treated with CpG LNPs was significantly suppressed. Thus, it was suggested that CpG LNPs could enhance the antitumor effect but CpG could not its own. Further, we elucidated the contribution of CD8$^+$ T cells to this antitumor effect. In consequence, the antitumor effect by CpG LNPs were completely canceled in CD8$^+$ T cells depleted mice. Histological examination of tumor at day 21 from inoculation supported that anti-CD8a antibody administration depleted CD8$^+$ T cells completely in the tumor tissue. Although MC38 tumor contains many CD8$^+$ T cell infiltrations without treatment, CD8$^+$ T cell infiltration in the tumor would be more aggressive with CpG LNPs treatment. Therefore, CpG LNPs would be an immunostimulatory formulation to have an ability to exert antitumor effect via activating cell-mediated immunity.

ACKNOWLEDGEMENTS

This research was supported by AMED under Grant Number JP19cm0106310.

P-34

Development of fluorescence / NanoSIMS bioimaging coupled with immunostaining using novel hybrid probe

Naoya Iwano,[1] Wataru Haya,[1] Yasuhiko Fujita,[1] Kohji Shimoda,[2] Yasushi Miyauchi,[3] Takuo Onizuka[1]
[1] Toray Research Center, Inc., [2] Toray Industries, Inc., [3] Kamakura Techno-Science, Inc.

OBJECTIVE

The distribute evaluation of a specific target in a biological sample is one of the most important subject in life sciences. Recently, there are extensive studies using super-resolution microscope or electron microscope technique which has a spatial resolution beyond the diffraction limit of light, while only few studies have been reported with the high lateral resolution MS (Mass Spectrometry) imaging. Here, we synthesized a novel probe tag which is compatible both with fluorescence and NanoSIMS (Nano-scale Secondary Ion Mass Spectrometry) analysis, and the probe tag was labelled with an antibody. We developed the MS imaging method by combining NanoSIMS and an immunostaining method using the probe-labelled antibody. Our developed MS imaging method has a high lateral resolution (< 50 nm), and we will show the results obtained by our imaging method.

METHODS

A probe tag detectable by fluorescence (Cy5) and NanoSIMS was synthesized and conjugated to the antibody by a maleimide hinge method. We chose β-Actin in mouse nerve fibers as a model target of the imaging method, and prepared a paraffin-fixed tissue stained by the probe-labelled antibody as a measurement sample. Fluorescence images with excitation light at 633 nm were observed using a confocal laser microscopy. Subsequently, the surface of the sample was subjected to NanoSIMS imaging by the Cs^+ primary ion beam. The detectors of NanoSIMS were set to various elements including one derived from the probe tag.

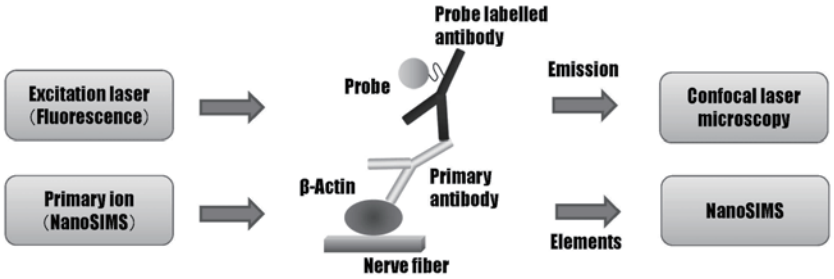

RESULTS

The results of β-Actin imaging in the mouse nerve fiber are shown in Fig. 1 (fluorescence) and Fig. 2 (NanoSIMS). β-Actin was distributed in periphery of each nerve fiber both in NanoSIMS and fluorescence imaging.

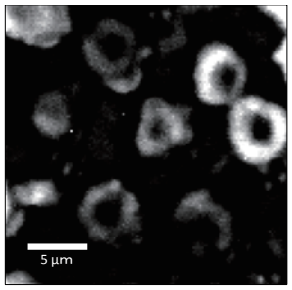

Fig. 1 Fluorescence imaging

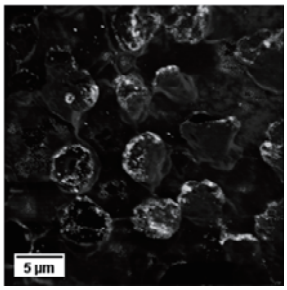

Fig. 2 NanoSIMS imaging

CONCLUSIONS

The new synthesized probe tag can be applicable to fluorescence and NanoSIMS analysis. The NanoSIMS imaging enables elemental imaging of the sample surface with high lateral resolution (<50 nm), and the result is similar to fluorescence imaging. The developed method combining immunostaining and NanoSIMS has the highest lateral resolution of MS imaging and can be a powerful tool for bioimaging.

P-35

Promotion of α2,3-Sialylation of Glycoproteins by a Passport Sequence Tag Recognized by Cargo Receptor

Rino Yamada[1], Hirokazu Yagi[1], Rena Honda[2,3,5], Maho Yagi-Utsumi[1,2,3,5], Kazuhiro Aoki[2,4], and Koichi Kato[1,2,3,5,*]

[1] Graduate School of Pharmaceutical Sciences, Nagoya City University, [2] Exploratory Research Center on Life and Living Systems (ExCELLS), [3] Institute for Molecular Science, and [4] National Institute for Basic Biology, National Institutes of Natural Sciences, [5] School of Physical Science, SOKENDAI (The Graduate University for Advanced Studies)

OBJECTIVE

The 53-kDa ERGIC marker protein, ERGIC-53, and its binding partner, multiple coagulation factor deficiency 2 (MCFD2), mediate the secretion of blood coagulation factor V (FV) and factor VIII (FVIII) in the early secretory pathway. These two proteins are known to be the causative gene products of combined deficiency of FV and FVIII, an autosomal recessive bleeding disorder in which the plasma levels of these coagulation factors are diminished. Cumulative evidence has revealed that ERGIC-53 possesses a luminal carbohydrate recognition domain that binds the high-mannose-type glycans displayed on cargo glycoproteins in a pH-dependent manner. Recently, we have identified a 10-aminoacid segment in factor VIII that is recognized by MCFD2 in the cargo receptor complex. Interestingly, we found that, in addition to secretion level, α2,3-sialylation level of recombinant erythropoietin was significantly elevated by C-terminal tagging it with the 10-aminoacid segment. This raises the possibility that interactions of the secretory glycoproteins with the cargo receptor complex not only facilitate their vesicular transport from the ER to the ERGIC but also have impacts on the subsequent glycosylation pathways in the Golgi apparatus. Herein we address the enhancement mechanisms of α2,3-sialylation owing to the 10-aminoacid segment tagging through investigations of localization of glycosyltransferase and secretary routes of tagged glycoproteins.

METHODS

Erythropoietin, a model glycoprotein, with or without the 10-aminoacid segment and α2,3-/α2,6-sialyltransferases fused with fluorescence proteins were expressed in a human colon cancer cell line, HCT116, or a human embryonic kidney cell line, Expi293 cells. For analyzing the localization of the fluorescence-labeled proteins, cell images were recorded using a fluorescence microscope BZ-X700 and BZ-H3XF / Sectioning Module (Keyence).

RESULTS

We found that several trans-Golgi resident α2,3-/α2,6-sialyltransferases were located in distinct subcellular zones. In addition, the erythropoietin tagged with the 10-aminoacid segment visited the α2,3-sialyltransferase zones on its secretory route.

CONCLUSIONS

Based on these results, we propose that distinct localizations of sialyltransferases in the trans-Golgi can be determining factors of specific sialylation of glycoproteins on their secretory pathways. Our findings also suggest that the secretory routes of glycoproteins can be switched just by tagging them with the specific aminoacid segment, offering a novel strategy for controlling glycoforms of recombinant glycoproteins of biopharmaceutical interest.

P-36

Quantitative analysis of cell cycle progression within heterogeneous cell population using information theory

Ryu Yamanaka,[1,2] Kotaro Oka[1,3,4,*]

*[1]Dep. of Biosci. and Info., Fac. of Sci. and Tech., Keio Univ., Japan, [2]Faculty of Pharm. Sci., Sanyo-Onoda City Univ., Japan, [3]Grad. Inst. of Med., Col. of Med., Kaohsiung Med. Univ., Taiwan, [4]Waseda Res. Inst. for Sci. and Eng., Waseda Univ., Japan. *Corr. Auth.*

OBJECTIVE

Biological systems utilize even variability and heterogeneity within population for their efficient sustainability and survival at all levels from cells to ecosystems. The properties of individual cells and collective features of cell population influence each other, and the interaction between the part and whole across levels of organization orchestrates the dynamical changes of cellular states including differentiation and cell cycle progression. Each cell continuously replicates identical copies with the allowance of some fluctuations, and it enables the process of the evolution in cell population. Thus, cell proliferation is a fundamental process for not only survival of organism but also evolution of living system. However, it has been little known what to extent cells adjust to proliferation and what type of sub-populations proliferates quickly in multi-cellular populations.

METHODS

Massive-scale data of signal dynamics from cell-cycle reporter Fucci2 at a single-cell level in HeLa cells were obtained by the combination of fluorescence live cell imaging and image-processing-based cell tracking algorithm. Shannon's information theory was applied for quantification of the properties of individual cells within heterogeneous population during cell cycle progression, which has temporally different probabilistic distributions, *i.e.* time-variant system.

RESULTS

Our analysis revealed that cells proliferate with keeping the characteristic levels of variation at each stage of cell cycle, and cells with the high rate of proliferation likely to belong to the minority population. This suggests that cells are not completely adjusted to the proliferation. Furthermore, cells growing fast during cell cycle progression are likely to pass the major transition at each step, and change into the cell states with more choice at the next step. Together, cells growing fast are likely to progress through cell cycle with more frequent changes at short-term transition and with less frequent trajectory in long-term vicissitude.

CONCLUSIONS

Our approach on the basis of information theory revealed that the progression of cell cycle is not globally but locally optimized in HeLa cells. These findings possibly show the rules that individual cancer cells within heterogeneous population are subjected to in the process of tumor occurrence and development. Thus, our observation about the part-whole interaction cross the levels of organization gives the novel insights to both biology and medicine.

P-37

Simultaneous visualization of intracellular energy substrates by using dual FRET imaging

Yutaka Shindo,[1] Mitsuru Iizumi,[1] Ryu Yamanaka,[2] Kohji Hotta,[1] Kotaro Oka[1,3,4,*]

[1] Biosci Info., Keio Univ., [2] Pharmac. Sci. Sanyo-Onoda City Univ., [3] Inst. Med., Kaohsiung Med. Univ., [4] Waseda Res Inst. Sci., Waseda Univ.

OBJECTIVE

Mammalian cells consume glucose and produce ATP in two pathways. One is glycolysis, which yields ATP and pyruvate. The other is oxidative phosphorylation in mitochondria. A portion of pyruvate is utilized in mitochondria as an energy substrate. And the other portion of it is converted to lactate, which is also utilized energy substrate or released to extracellular fluid. Balance between glycolysis and oxidative phosphorylation is varied in different cell types. For example, astrocytes dominantly use glycolysis and yield and release lactate, while neurons mainly use oxidative phosphorylation by using pyruvate and received lactate from astrocyte as substrates. Therefore, to understand energy metabolism in cells, measuring these two energy substrates is important. In this study, we aimed to develop different color version of genetically encoded lactate or pyruvate sensor and to achieve simultaneous visualization of lactate and pyruvate by using dual FRET imaging technique.

METHODS

Different color version of lactate or pyruvate sensor were developed from genetically encoded FRET based lactate sensor, Laconic (Martin et al., 201), or pyruvate sensor, Pyronic (Martin et al., 2014), by changing fluorescent proteins from mTFP and Venus pair to the other colored pairs. The developed sensors were induced in HeLa cells, cultured rat hippocampal neurons and cultured rat astrocytes, and dual FRET imaging was performed on confocal microscope.

RESULTS

In the developed color-converted sensors, only red-colored Pyronic (LSSmOrange and mKate2 pair) responded to its substrate. LSSmOrange is a long stokes shift orange fluorescent protein, and we can simultaneously excite it and mTFP at 440 nm. Therefore, by using original Laconic (mTFP and Venus pair) and red-shifted Pyronic, one-excitation and four-emission type dual FRET imaging was achieved. Upon an application of pyruvate (1 mM), cytosolic pyruvate concentration increased steeply followed by a gradual increase in lactate concentration. On the other hand, an application of lactate (1 mM) increased only cytosolic lactate concentration and had no effect on pyruvate concentration. Glutamate (100 μM), an excitatory neurotransmitter, increased both lactate and pyruvate concentration in cultured neurons, which suggesting an upregulation of glycolysis. It also induced decrease in cytosolic ATP concentration measured by using genetically encoded ATP sensor, ATeam (Imamura et al., 2009). The glutamate-induced decrease in cytosolic ATP concentration was attenuated in lactate (5 mM) containing medium. It indicates that lactate was taken into neurons and utilized as energy substrate in exciting neurons.

CONCLUSIONS

Simultaneous imaging of intracellular lactate and pyruvate by using dual FRET imaging was achieved by developing red version of pyruvate sensor, pyronic (LSSmOrange and mKate2 pair). It enabled us to compare the difference in energy metabolism in various cell types.

P-38

Intra-vital fluorescence imaging of interaction between transplanted stem cells and immune cells by quantum nano-materials and tissue clearing (CUBIC) technology

Toshiki Mizumaki,[1,*] Hiroshi Yukawa,[1,2,3] Kodai Kitamura,[1] Daisuke Onoshima,[1,2] Etsuo A. Susaki,[4,5] Hiroki R. Ueda,[4,5] Yoshinobu Baba,[1,2,3,6]

[1]Dept. Biomolecular Eng., Grad. Sch. Eng., Nagoya Univ., [2] Inst. Nano-Life-Systems, Inst. Innovation for Future Society, Nagoya Univ., [3]National Institute of Radiological Science (NIRS), National Institute for Quantum and Radiological Science and Technology (QST), [4]Dept. Systems Pharmacology, Grad. Sch. Med., Tokyo Univ., [5]Laboratory for Synthetic Biology, Center for Biosystems Dynamics Research, RIKEN, [6]Health Research Institute, AIST

OBJECTIVE

In regenerative medicine, cell transplantation therapy plays an extremely important role in the diseases that are still difficult to treat by tissue and organ reconstruction. It is absolutely essential to elucidate the interaction between transplanted cells and immune cells for the realization and further development of cell transplantation therapy. In this study, we worked on establishing an *intra-vital* imaging technique using two-photon excitation microscope to observe the real-time behavior of immune cells against stem cells transplanted to acute liver failure model mice. Furthermore, we tried to elucidate the comprehensive interaction between transplanted stem cells and immune cells in the liver by applying tissue clearing technology.

METHODS

Adipose tissue-derived stem cells (ASCs) were labeled with quantum dots (QDs), a fluorescent nanoparticle which has optical properties of high definition, high sensitivity and long fluorescence lifetime, by introducing QDs into ASCs using cell membrane penetrating peptide. After labeling with QDs, ASCs were transplanted to acute liver failure model mice from the tail vein. At first, time points at which transplanted ASCs began to be eliminated were examined by observing fixed tissues at some time points of 1 to 72 hours after ASCs transplantation. Then, *intra-vital* fluorescence imaging of interaction between ASCs and immune cells was performed at appropriate time point by incising abdomen of mouse under anesthesia administration and pressing the lens of two-photon excitation microscope against liver that transplanted ASCs were accumulated. Next, the liver was cleared by tissue clearing technology called CUBIC (Clear, Unobstructed Brain/Body Imaging Cocktails and Computational analysis), and comprehensive imaging of cell-to-cell interaction was examined using Light sheet fluorescence microscopy.

RESULTS

As a result of *intra-vital* fluorescence imaging of interaction between transplanted stem cells and immune cells by two-photon excitation microscope, we succeeded in capturing the moment at which immune cell approaches to transplanted stem cell for phagocytosis. Furthermore, we succeeded in comprehensively visualizing the function of immune cells against transplanted stem cells in the inflamed tissue by clearing liver of acute liver failure model mice.

CONCLUSIONS

The present study enabled us to establish an *intra-vital* fluorescence imaging technique to observe the real-time interaction between transplanted stem cells and immune cells in inflamed liver. Tissue clearing is expected to be a very effective method for comprehensive visualization of the function of immune cells against transplanted stem cells.

P-39

Brain-targeted Gene Delivery using Microbubbles and Ultrasound

Daiki Omata[1], Fumiko Hagiwara[1], Lisa Munakata[1], Tadamitsu Shima[1], Saori Kageyama[1], Yuno Suzuki[1], Kazuo Maruyama[2], Ryo Suzuki[1,*]

[1]Laboratory of Drug and Gene Delivery Research, Faculty of Pharma-Science, Teikyo University

[2] Laboratory of Theranostics, Faculty of Pharma-Science, Teikyo University

OBJECTIVE

The blood brain barrier (BBB) restricts transportation of molecules between the blood and the brain parenchyma. The BBB is a major obstacle to development of effective medicine for treatment of brain diseases, as many drugs including macromolecules cannot pass the BBB and reach the brain parenchyma. Recently, it has been noted that gene therapy could be useful to treat brain diseases, such as Alzheimer's disease, Perkinson's diseases and Huntington's disease. To achieve successful therapy, a development of gene delivery systems which are safe and efficiently can deliver genes are desired. A combination of ultrasound (US) and microbubbles (MBs), which is US contrast agent, has attracted attention as promising technology for brain-targeted drug delivery. We previously reported that the combination of MBs and US could be useful for delivering genes *in vitro* and *in vivo*. In this study, we examined the feasibility of MBs and US for brain-targeted gene delivery.

METHODS

Mixture of MBs (500 μg of lipid) and pcDNA3-Luc (100 μg), which is a plasmid DNA (pDNA) encoding the firefly luciferase gene under the control of cytomegalovirus promoter, was injected into tail vein of ddY mice. Immediately, brain was exposed to transcranial non-focused US (Frequency: 1 MHz, Intensity: 1.2 W/cm^2, Duty: 10%, Time: 1 min). After 1 day, luciferase activities in the brain and several tissues were measured by a luciferase assay system. To determine in which cells gene expression was induced, immunofluorescence analysis was performed. Briefly, Venus/pCS2, which is an expression vector encoding mutant GFP gene, was delivered to the brain using MBs and US. After 2 days, the brain was collected and cryosections were prepared. The sections were stained with antibody against GFP, followed by treatment of tyramide signal amplification system. In addition, the sections were stained with antibody against CD31, which is a marker of endothelial cells, and fluorescent secondary antibody. The cells expressing GFP was observed using confocal laser scanning microscopy.

RESULTS

The treatment of MBs and US showed about 1000-hold higher luciferase activity in the brain than that of treatment with only pDNA, pDNA with US, or pDNA with MBs. To assess the brain selective gene delivery, we examined gene expression in several tissues after treatment of MBs and US. As a result, luciferase activity of the brain treated with MBs and US is higher than that of other tissues such as liver, kidney, heart, lung and spleen. For evaluation of the damage to brain, we observed the appearance of brain treated with MBs and US. Neither hemorrhage or degeneration of brain was observed. These results suggested that MBs and US could selectively deliver genes into brain without notable damage. As a result of immunostaining, GFP expression was observed in not only endothelial cells but also parenchyma cells. This result suggested that MBs and US could deliver genes to parenchyma cells through the BBB.

CONCLUSION

MBs and US selectively delivered genes into brain without notable damage and gene expression in parenchymal cells was observed. In conclusion, it is expected that the combination of MBs and US would be a useful tool to establish minimally invasive brain-targeted gene delivery system.

P-40

Blood-brain barrier opening using 220-kHz transcranial MRI-guided focused ultrasound and microbubbles in mouse and rat

[1]Michiharu Yoshida, [2]*Kazuo Maruyama, [3]Yasutaka Kato, [4]Rachmilevitch Itay, [4]Shuji Suzuki, [4]Omer Brockman, [4]Yeruham Shapira, [5]Kenji Moriyama, [2]Daiki Omata, [2]Ryo Suzuki, [1]Hajime Kamada

[1]Department of Neurosurgery, Hokuto Hospital, [2]Faculty of Pharma-Sci., Teikyo Univ., [3]Laboratory of Cancer Med-Sci., Hokuto Hospital, [4]InSightec Ltd., [5]Department of Radiology, Hokuto Hospital

OBJECTIVE

In neuro-oncology, it is believed that one major obstacle to effective chemotherapy is the high vascularity and heterogenous permeability of brain tumors. Focused ultrasound (FUS) exposure with the microbubbles has been shown to transiently open the blood-brain barrier (BBB) without depositing thermal energy, and thus may enhance the delivery of various therapeutic drugs into brain tumors. The aim of this study was to evaluate the BBB opening using 220-kHz transcranial MRI-guided FUS (TcMRgFUS) device and microbubbles in mouse and rat.

METHODS

The experiments were performed with the 220-kHz ExAblate Neuro TcMRgFUS system (InSightec) and novel lipid bubbles (LB, Teikyo Univ.). Normal mouse and rat brains were irradiated with TcMRgFUS (output power, 5W; duration of irradiation, 30 s; duty cycle 100%) following intravenous injection of 6×10^7 LB per mouse and rat, respectively. On irradiation, target temperature rise was monitored by MR thermometry. Immediately after irradiation, BBB opening and complications were detected based on T1, T2, T2*, and Gadolinium (Gd) enhanced T1-weighted images.

RESULTS

The maximum temperature of brain tissue was under 42 ℃. The FUS-LB exposure induced successful BBB opening effect in both mouse and rat, confirmed by Gd enhancement in the target region, lateral ventricles, and sulcus (Figure). In addition, there were no complications such as edema, coagulation, and hemorrhage.

CONCLUSIONS

Although there remain many conditions to be optimized, BBB opening using a 220-kHz TcMRgFUS device and LB can offer a non-invasive and feasible drug delivery for brain malignancies.

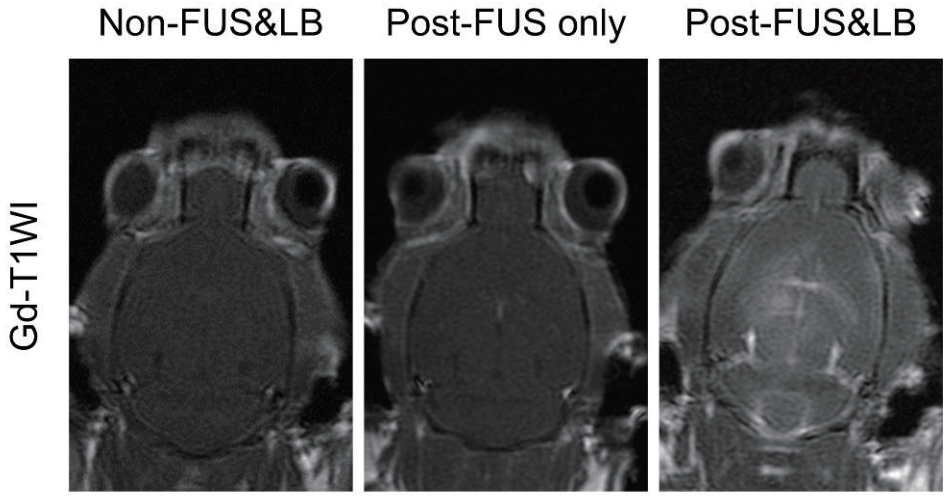

P-41

Enhanced chemotherapy effects on gynecological cancers by using the combination of lipid bubble and ultrasound

Kohei Yamaguchi[1], Yoko Matsumoto[1] *, Haruka Nishida[1], Daiki Omata[2], Michihiro Tanikawa[1], Kenbun Sone[1], Katsutoshi Oda[1], Yutaka Osuga[1], Ryo Suzuki[2], Kazuo Maruyama[2], Tomoyuki Fujii[1]

[1]*The Department of Obstetrics and Gynecology, The University of Tokyo*

[2]*Laboratory of Drug and Gene Delivery System, Faculty of Pharma-Science , Teikyo University*

OBJECTIVE

Delivering anticancer drugs effectively to tumor cells with less side effects, is a key strategy in cancer treatment. Lipid bubble (LB) is a compound which increases vascular permeability of the tumor under diagnostic ultrasound (US) exposure and enables drugs to be carried effectively to the tumor cells. The aim of our study is to establish a novel drug delivery strategy for chemotherapy, by using LB and the US exposure, in gynecological cancers.

METHODS

All studies were approved by our institutional animal care and use committee. We developed endometrial cancer and cervical cancer cell lines *in vitro*. Then we administrated cisplatin or doxorubicin with or without LB under the ultrasound. The anticancer effects were evaluated by MTT assay.

We made xenograft models with nude mice. LB with chemotherapy was injected intravenously and the US was applied onto the tumor. The anticancer effect was evaluated by the tumor size and TUNEL staining. Drug penetration and accumulation were analyzed by laser-scanning microscope.

RESULTS

When administrated with LB and US exposure to cancer cells in vitro, the viability of both cervical and endometrial cancer was not reduced, compared with chemotherapy alone. But in vivo models, Tumor volume reduction by either cisplatin or doxorubicin was enhanced by the administration of LB and US exposure. Drug accumulation by this drug delivery strategy was confirmed in laser-scanning microscope.

CONCLUSIONS

The combination of LB with US enhanced the effect of anticancer drugs. This technology may be a promising drug delivery system in the clinical settings.

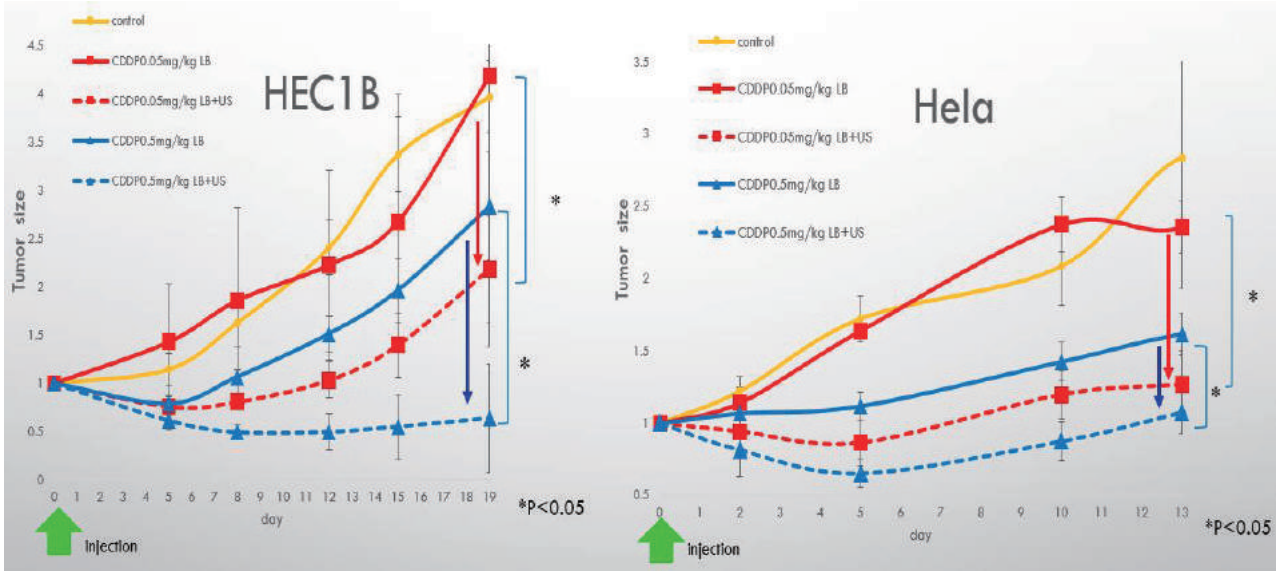

P-42

Bioimaging of inhalable nanocarriers with aggregation-caused quenching dye to visualize retention in the respiratory system

Kohei Yamada,[1] Tetsuya Matsushita,[1] Kurt D. Ristroph,[2] Hoang D. Lu,[2] Yoshiki Seto,[1] Wei Wu,[3] Hak-Kim Chan,[4] Robert K. Prud'homme,[4] Hideyuki Sato,[1] Satomi Onoue[1,*]

[1]Laboratory of Biopharmacy, School of Pharmaceutical Sciences, University of Shizuoka, Japan,
[2] Department of Chemical & Biological Engineering, Princeton University, USA,
[3] Key Laboratory of Smart Drug Delivery of MOE & PLA, Fudan University, China
[4] Advanced Drug Delivery Group, The University of Sydney, Australia

OBJECTIVE

Retention of inhaled drugs in the respiratory system is desirable for effective treatment of lung and respiratory diseases. However, inhaled drugs are rapidly cleared toward the pharynx by mucociliary clearance (MCC), an innate clearance mechanism of the respiratory tract. To develop inhalable nanocarriers (NCs) with excellent pulmonary retention, controlling the diffusiveness of NCs in airway mucus upon mucosal drug delivery system could be a promising strategy. This study was undertaken to evaluate retention of mucopenetrating and mucoadhesive NCs upon fluorescence imaging with P2 probe, a self-developed environment-responsive aza-BODIPY dye quenching in water.

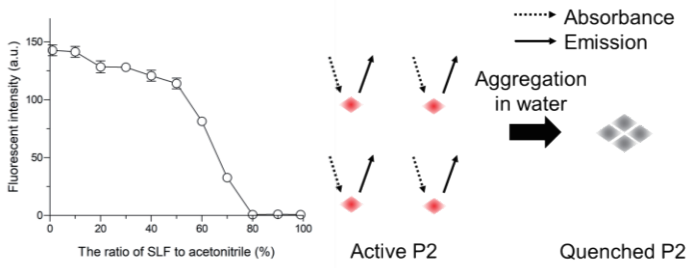

METHODS

Aggregation-caused quenching effect and rekindling of P2 probe were evaluated in simulated lung fluid (SLF). NCs containing P2 probe were prepared by flash nanoprecipitation and coated with neutral polymer (NCs/N) for mucopenetration and with cationic polymer (NCs/C) for mucoadhesion. Physicochemical properties of prepared NCs were characterized. After intratracheal administration of NCs to rats, the lungs were removed and subjected to imaging by *in vivo* imaging system (IVIS). Sectioned lungs were observed with confocal laser scanning microscope (CLSM).

RESULTS

The fluorescent intensity of P2 in acetonitrile solution abruptly decreased when the ratio of SLF to acetonitrile reached 50%. While quenched P2 exhibited rekindling in acetonitrile and 1%-Tween 80 solution, marked rekindling was not observed in SLF. These properties of P2 suggest its applicability as an environment-responsive dye for reliable fluorescence imaging of insufflated NCs. P2-loaded NCs/N and NCs/C had a mean diameter of approximately 150 nm and high dispersion stability in SLF up to 6 h. NCs/N and NCs/C possessed ζ-potentials of approximately 4 and 40 mV, respectively. Although the fluorescent intensity of both NCs in aqueous solvent slightly decreased in 4 h, the leakage of P2 from NCs was limited. Quartz crystal microbalance analysis showed that NCs/C strongly interacted with mucin, a major component in mucus, compared with NCs/N. NCs/N, which had limited interactions with mucin, exhibited high mucodiffusiveness compared with NCs/C in a diffusion test using artificial mucus. CLSM images of the lungs excised at 30 min after intratracheal administration in rats showed that NCs/C were present in clumps away from the epithelium. On the other hand, NCs/N displayed homogenious distribution across the respiratory surfaces in close proximity to the epithelial cells, suggesting rapid mucus penetration. Intratracheal NCs/C were cleared from lower RT to the pharynx, possibly due to MCC. In contrast, intratracheal NCs/N exhibited better pulmonary retention, which may be due to their avoiding MCC because of their high mucodiffusiveness in the respiratory system.

CONCLUSIONS

Mucopenetrating nanoparticulate drug delivery would be a promising approach to offer prolonged drug exposure to the respiratory system, possibly resulting in better clinical outcomes.

P-43

Development of Caged Gene Regulators for Application to Control of Genetic Recombination in vivo

Kurumi Yoshida,[1,*] Masafumi Minoshima,[1] Kazuya Kikuchi [1,2]

[1]Graduate School of Engineering, Osaka University. [2] Immunology Frontier Research Center, Osaka Univ.

OBJECTIVE

Gene targeting through site-specific homologous recombination is a powerful tool for generating predetermined changes in genomes and controlling gene expression in vivo. Cre-ER^{T2}/loxP system, a modified Cre/loxP system, allows homologous recombination induced by exogenous chemical ligands. Cre-ER^{T2}, a fusion protein of Cre recombinase with mutated ligand-binding domain of human estrogen receptor (ER-LBD), does not bind endogenous 17β-estradiol (E2) but binds synthetic ER ligands such as 4-hydroxycyclofen (4-OHC). While this system enables ligand-dependent genetic recombination, the precise spatiotemporal control is limited due to the diffusion of the ER ligands after administration.

Thus, we focused on photoresponsive caged ER ligands for spatiotemporal control of gene expression using Cre-ER^{T2}/loxP system. Moreover, two-photon illumination enables three-dimensional control of cells within complex and deeper tissue. However, current caged ER ligands have small two-photon uncaging action cross section, which limits to applications in deeper tissues using two-photon irradiation. In this study, we aimed to develop caged ER ligands with large two-photon uncaging action cross sections to control gene expression in vivo.

METHODS

We designed and synthesized caged 4-OHC incorporating nitrobiphenyl groups as photoremovable protecting groups (PPGs) with large two-photon uncaging action cross sections. Photocleavage reaction was initially performed by one-photon excitation using UV light. We analyzed the reaction of the caged 4-OHC by high-performance liquid chromatography and mass spectrometry. Moreover, we investigated whether light irradiation would induce genetic recombination through Cre-ER^{T2}/loxP system in caged 4-OHC-treated cells.

RESULTS

We developed caged 4-OHC (ANBPC1 and ANBPC2) incorporating 2-(4'-(bis(methyl)amino)-4-nitro-[1,1'-biphenyl]-3)yl)propan-1-ol and 2-(4'-(bis((2-methoxyethoxy)ethyl)amino)-4-nitro-[1,1'-biphenyl]-3)yl)propan-1-ol, respectively. HPLC analysis indicated that 4-OHC was released in a time-dependent manner after light irradiation. Furthermore, using reporter genes, we observed robust genetic recombination in ANBPC2-treated cells after light irradiation.

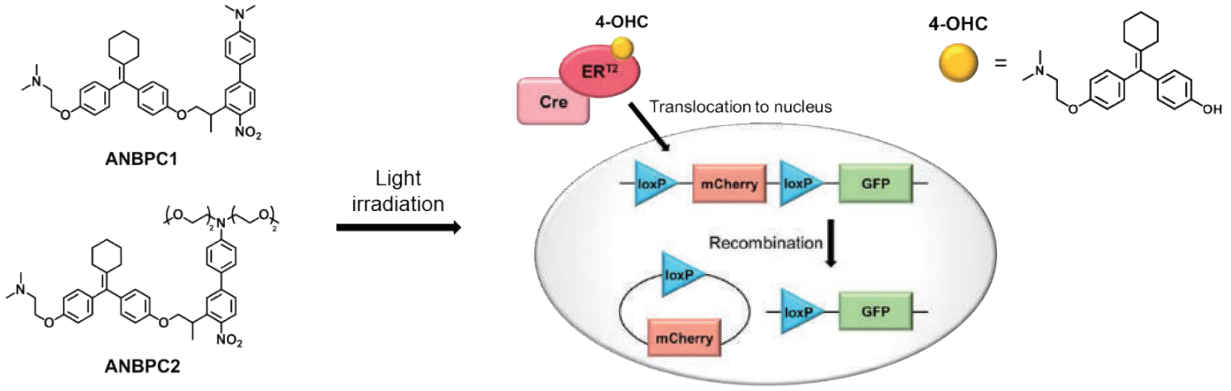

CONCLUSIONS

In summary, we developed caged 4-OHC to photocontrol genetic recombination by incorporating nitrobiphenyl groups with large two-photon uncaging action cross sections. We found induction of reporter gene expression with ANBPC2 and light, which demonstrates light-controlled homologous recombination through Cre-ER^{T2}/loxP system in living cells. Our future effort will focus on precise spatiotempotal control genetic recombination in vivo using caged 4-OHC and two-photon illumination.

Image evaluation of biological tissue using Bio-LSI

Ryoma Kumagai,[1] Ankush Prasad,[2] Teruya Sato,[1] Kosuke Ino,[3] Hitoshi Shiku,[3] Shigenobu Kasai[1]

([1]Graduate Department of Electronic, Tohoku Institute of Technology, Sendai, Japan, [2]Department of Biophysics, Centre of the Region Haná for Biotechnological and Agricultural Research, Faculty of Science, Palacký University, Olomouc, Czech Republic [3]Graduate School Department of Applied chemical – electrochemical science and technology, Tohoku University, Sendai, Japan)

1. OBJECTIVE

Scanning electrochemical microscopy (SECM) is a method that can be employed for imaging tissues using amperometry. There is a problem which limit is wide usage that it takes longer scanning time. Therefore, Bio-LSI, which is an electrochemical device capable of measuring 400 electrodes simultaneously, was developed. We have evaluated the distribution of POD activity in plant tissues using SECM[1)] and the photosynthetic activity of spinach young leaves using Bio-LSI[2)]. In this study, we focused on the evaluation of biological tissue and carried out real-time imaging evaluation of peroxidase (POD), a growth factor of plant tissue using Bio-LSI, and respiratory activity in human epidermal cells.

2. METHODS

1) Real-time imaging of plant tissue POD activity

We used ferrocene methanol (F_CCH_2OH) as an electron transfer mediator and evaluated POD activity by the reduction current of $F_C{}^+CH_2OH$. We made a cruciform cut on the celery leaves. We added 0.5 mM FCCH2OH and 0.05 mM H2O2 mixed solution to Bio-LSI, added Ag/AgCl reference electrode, counter electrode (Pt wire (2.4 mm^2)), and applied +0.05 Vvs.Ag/AgCl. We fixed celery leaves on a Bio-LSI sensor and grasped real-time images.

2) Respiratory burst imaging in epithelial cell sheet

We performed simultaneous measurement of respiratory activity of a cell sheet in UV-irradiated area and non-irradiated area by irradiating UV after covering the cell sheet with a mask which has a cruciform light transmittable area. We put 2 mL of 11.4 mM glucose-containing phosphate buffer solution for measurement into the Bio-LSI and placed an Ag/AgCl reference electrode and a counter electrode (Pt wire). We filled the chamber with oxygen gas and applied -0.5 Vvs.Ag/AgCl. We then excised a cell sheet and put a mask, irradiated UVB to irradiation energy of 1.5 J/cm^2, introduced the cell sheet at a distance of 100 um between the electrode and the cell sheet and performed the measurement.

3. RESULTS AND DISCUSSION

1) Real-time imaging of plant tissue POD activity

Fig.1(A) shows a photograph of damaged celery leaves. Figs.1(B and C) show the POD activity in real-time of celery leaves. These images reflect the cruciform scratches of celery leaves.

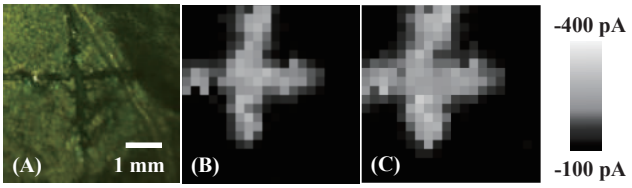

Fig.1 The celery leaf photography and real time image
(A) Injured celery leaf photograph
(B), (C) Real-time image after 90 seconds after 120 seconds from the start of POD activity measurement

2) Respiratory burst imaging in epithelial cell sheet

Fig.2(D) shows a photograph of a cell sheet irradiated with UV and Fig.2(E) shows a bio-LSI image of the cell sheet. Fig.2(E) shows that the oxygen reduction current value in the irradiated area is the lowest. This result shows that this area is causing a respiratory burst. We also obtained respiratory activity images in areas with the other cell sheet.

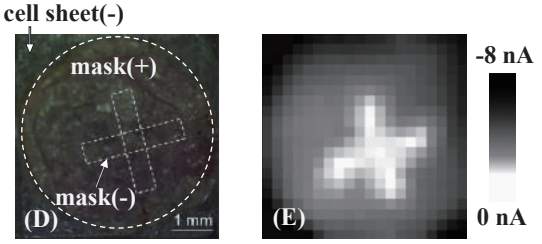

Fig.2 Picture of cell sheet and respiratory activity of cell sheet by UV stimulation
(D) Picture of cell sheet
(E) Image from the installation after 5 minutes

4. CONCLUSIONS

In this study, we have captured real-time images of celery's POD activity and image of a cell sheet normal respiration and respiratory bursts caused by UV stimulation. In the future, we plan to focus on the simultaneous imaging of POD activity and the production of Reactive Oxygen Species (ROS) in plant tissue.

REFERENCES

(1)H. Zhou, et al., *Bioelectrochemistry, 2001, 54, 151-156*., (2) S. Kasai, et al., *231st ECS MEETING, 2017, MA2017-01 1732.*

P-45

Study on Photodynamic diagnosis for micrometastases using photosensitizer Talaporfin sodium

[1]Saito Takuma[1] , [2]Furuya Kazunari[1] , Li Liming[1]

[1]Graduate School of Chitose Institute of Science and Technology

OBJECTIVE

The first cause of death in Japanese is cancer and the first ranking of females is colon cancer. In Japanese after colorectal cancer treatment, the site of resection where the cancer cells first occur and lymph node dissection are important to prevent metastasis and prolong the patient's life. In the current medical field, it takes time to investigate the metastasis of dissected lymph nodes. Therefore, the method of photodynamic diagnosis (PDD) real time diagnosis was examined. PDD is a diagnostic method that accumulates a photosensitizer having affinity for cancer cells at the cancer site of a patient and observes fluorescence obtained by excitation of light of a specific wavelength. In this study, we are aimed to detect colon cancer lymph nodes and evaluate metastasis, based on the fluorescence spectra and images derived from photosensitizers.

METHODS

Human colon adenocarcinoma cell line HT29 was incubated with Talaporfin for 1 hour. Thereafter, the medium was replaced with fresh medium, cultured for 8 hours or 12 hours, and measured by FACS. HT29 was used to create mouse lymph node metastasis model. Talaporfin was administered to the tail vein at the dose of 10 mg / kg after 6 or 12 hours before the experiment and Indocyanine Green (ICG) was administered at the dose of 5 mg / kg near the anus to the mouse model. Three samples were used for each mouse under each condition. After sacrificing the mouse, visual images, fluorescence images and fluorescence spectra were measured using a laparoscopic system for lymph node metastasis. Lasers with wavelengths of 405 nm and 664 nm to excite Talaporfin and 785 nm to excite ICG were used as the excitation light sources.

RESULTS

As a results of in vitro, HT29 retained Talaporfin even after culture for 8 or 12 hours. Fig.1 is a fluorescence image and an HE-stained tissue image in a lymph node. Fluorescence of Talaporfin accumulating in cancer at the lymph node and fluorescence of ICG capable of detecting lymph nodes were obtained from the same position. Therefore, colon cancer is thought to have spread to lymph nodes. Metastasis of cancer was confirmed from HE stained tissue image. Fig.1 (F) is the fluorescence spectrum in the lymph node. In cancer metastatic lymph nodes, Talaporfin fluorescence was obtained in the vicinity of 670 nm for 12 hours after.

CONCLUSIONS

Based on the above results, Talaporfin was accumulated in cancer metastatic lymph nodes. We demonstrated the possibility of diagnosis of colon cancer lymph node metastasis by using Talaporfin.

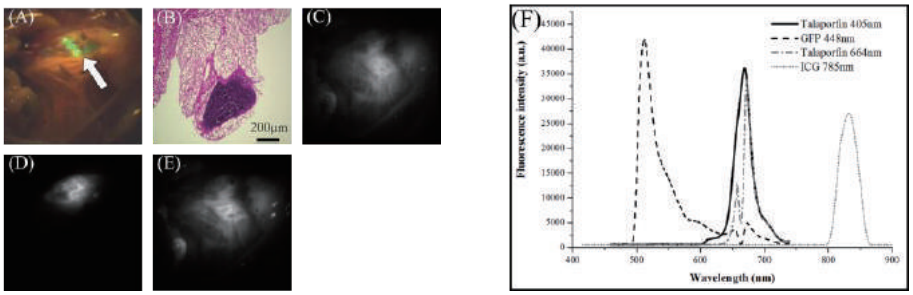

Fig.1 mouse model imaging & fluorescence spectrum: (A) White light + visible image (white arrow is tumor GFP), (B) HE-stained tissue image, (C) 785nm laser + fluorescence image, (D) 405nm laser + fluorescence image, (E) 664nm laser + fluorescence image, (F) Fluorescence spectrum in the lymph node

P-46

In vivo imaging of exosomes derived from stem cells by using quantum nano-optics for regenerative medicine

Yuka Kumon,[1] Hiroshi Yukawa,[1,2,3] Onoshima Daisuke [1,2], Yoshinobu Baba[1,2,3,4]

[1] Grad. Sch. of Engineering, Nagoya Univ., [2] Institutes of Innovation for Future Society, Nagoya Univ.
[3]National Institutes for Quantum and Radiological Sci. and Tech. (QST), [4]Health Research Institute, AIST

OBJECTIVE

In regenerative medicine, it is known that transplantation of stem cells into the whole body or the affected area promotes regenerative therapeutic effect on the affected area by the grow factor produced by stem cells. In recent years, it has been clarified that exosomes released from stem cells have a regenerative function, and administration treatment of stem cells derived exosomes are attracting attention as a new therapeutic tool for regenerative medicine. However, the regeneration mechanism of stem cells derived exosomes remains unclear. The main cause is appears to be due to a lack of *in vivo* imaging and detecting technology of exosomes. In this study, we established a method of *in vivo* imaging of exosomes with high sensitivity by using quantum dots (QDs). QDs have higher luminance than the conventional fluorescent dyes and have wavelengths in the near infrared region (NIR). Furthermore, we established a more stable labeling method by spontaneously incorporating them using glucose transporters expressed by exosomes.

METHODS

Glucose modification was performed on QD655 and the shape, particle size and zeta potential of Glucose-modified QDs were measured using TEM and dynamic-light-scattering (DLS). For the introduction of glucose-modified QDs into mouse adipose tissue-derived stem cells (mASCs), glucose-modified QDs containing medium were added into mASCs and incubated at 37 °C for 3 hours. Then, the mASCs were washed by PBS in order to remove the remaining QDs, and QDs labeled mASC were evaluated by fluorescence observation, and flow cytometry. Exosomes were purified from mASCs, and collected by ultracentrifugation. After suspending in PBS, exosomes were incubated with glucose-modified QDs, at 37 °C for 3 hours and recollected by Exo-Quick for *in vivo* imaging of exosomes.

RESULTS

The particle diameter and zeta potential of QDs with and without glucose modification were 29.9 nm, 33.4 nm, and -29.5 mV, -19.0 mV, respectively. The diameter size of QDs were increased and zeta potential of QDs were decreased by glucose modification. In addition, white contrast was confirmed around the QDs from the TEM image. These data suggest that QDs were covered with glucose. Next, after the addition of glucose-modified QDs into mASCs, the red fluorescence of QD655 was confirmed in mASCs by a confocal microscopy. In cytotoxicity test, the cell viability of mASCs labeled with QDs remained almost 100% even at 24 nM of QDs. No significant differences in cell proliferation rates between labeled and non-labeled mASCs was confirmed, therefore confirming that the glucose-modified QDs had no effect the cell proliferation ability of mASCs. Moreover, the introduction efficiency of QDs to mASCs was 85.6% at 8 nM of QDs by a flowcytometry analysis. Similarly, the introduction efficiency of QDs to exosomes derived from mASCs was showed 95.6% at the same concentration. On the other hand, the membrane of the QDs labeled exosome was stained with a cell membrane staining reagent in order to perform double labeling, and observed with a super resolution microscope. The yellow fluorescence of exosomes labeled with glucose-modified QDs were observed by the merging of the red fluorescence of QD655 and the green fluorescence of cell membrane staining reagent (PKH67).

CONCLUSIONS

We succeeded in the establishment of a new introduction method of QDs into mASCs and mASC-derived exosomes *via* glucose transporters. Glucose-modified QDs have no effect on cytotoxicity and self-proliferative ability, suggesting that they are excellent quantum nano-imaging materials with high biocompatibility. The introduction-technology of QDs inside exosomes by using glucose transporters is expected to be an extremely stable and highly sensitive imaging technique in comparison to the conventional methods such as labeling of exosome membrane using fluorescence dyes.

P-47

Ex vivo fluorescent imaging of macromolecule kinetics by nose-to-brain delivery with functional arginine-rich peptides

Takumi Kurano,[1,2] Takanori Kanazawa,[1,2,*] Mami Kaneko,[2] Hisako Ibaraki,[2] Yuuki Takashima,[2] Toyofumi Suzuki,[1] Yasuo Seta,[2]

[1]Sch. Pharm., Nihon Univ., [2]Tokyo Univ. Pharm. & Life Sci.

OBJECTIVE

Nose-to-brain delivery is a highly versatile route, which, in combination with novel macromolecule drugs being developed for treating intractable CNS diseases, is a promising approach for the treatment of disorders. Furthermore, basic peptide carriers may improve nose-to-brain drug delivery by their capability to increase the stability of the encapsulated nucleic acids against chemical and biological degradation. In this study, to investigate the nose-to-brain pathway using basic peptide carriers, the distribution kinetics of macromolecule in whole brain, nasal mucosa, and trigeminal nerve after intranasal administration with arginine-rich peptide carriers modified with hydrophobic or hydrophilic moiety.

METHODS

We used CHHRRRRHHC peptide ($CH_2R_4H_2C$) as arginine-rich peptide carriers, and modified with polyethylene grycol-based block-copolymer (PEG-PCL) as hydrophilic moiety or stearic acid (STR) as a hydrophobic moiety. To examine their utility as nose-to-brain drug delivery carrier, we compared the transmissibility of the model macromolecules to the brain, we observed extracted each tissues following intranasal administration of model fluorescein-macromolecule drugs (Alexa Fluor®647-dextran, Mw: 10,000) alone, or Alexa-dextran complexed with PEG-PCL- $CH_2R_4H_2C$ or STR- $CH_2R_4H_2C$ to rats by fluorescent imaging system.

RESULTS

Significantly stronger fluorescence was observed in the whole brain, nasal mucosa and trigeminal nerve following intranasal administration of Alexa-dextran with both peptide carriers than that of Alexa-dextran alone. In the rats receiving the Alexa-dextran/PEG-PCL- $CH_2R_4H_2C$ complexes, strong fluorescence was observed in the not only nasal mucosa and olfactory bulb but also trigeminal nerve. Furthermore, spreading of the fluorescence was observed after 30 min and 1 h in whole brain. Whereas, in the rats receiving the Alexa-dextran/STR- $CH_2R_4H_2C$ complex, although the fluorescence intensity was weaker in the trigeminal nerves, very strong fluorescence of Alexa-dextran was observed in the nasal mucosa. In addition, strong fluorescence was observed in the olfactory bulb in the forebrain.

CONCLUSIONS

Both $CH_2R_4H_2C$ peptide-based carriers have also demonstrated the ability to improve the delivery of model drugs from the nose to the brain. In addition, PEG-PCL-$CH_2R_4H_2C$ can improve drug distribution throughout brain tissues after movement from the nose to the brain compared with STR-CH2R4H2C. These results suggest that the enhancement of drug-delivery achieved via the nose-to-brain route may depend on the properties of the carriers.

Grant & Foundation Acknowledgements

JSPS KAKENHI Grant Number 19HP0304

The NAGAI FOUNDATION TOKYO

TERUMO LIFE SCIENCE FOUNDATION

Kato Memorial Bioscience Foundation

Sponsor Acknowledgements

Sponsors with Exhibition and Advertisement

BizCom Japan, Inc.

CYBERDYNE, Inc.

Hamamatsu Photonics K.K.

HIGH-TECH CORPORATION

LightStone Corp.

NANOSEED

Nepa Gene Co., Ltd.

Summit Pharmaceutics International Corporation

Sysmex corporation

Yokogawa Electric Corporation

Sponsors with Advertisement

Bruker Japan K.K.

Olympus Corporation

Olympus Medical Science Sales Corporation

Ozakirika, Inc.

Thorlabs Japan Inc.

Author Index

T

U

W

Y

Z

総会資料）

2019 年度　日本バイオイメージング学会

総会資料

2019 年 9 月 23 日
日本バイオイメージング学会
会長　船津　高志

会場:　帝京大学板橋キャンパス（大学棟本館３F）

議題：　2018 年度事業報告、2019 年度事業経過報告および 2020 年度事業計画

総会議案

各委員会より報告

１．庶務報告
２．財務報告
３．会計監査
４．企画委員会
５．バイオイメージング誌委員会
６．bioimages 誌編集委員会
７．ホームページ編集委員会
８．集会委員会
９．賞選考委員会
１０．β研究助成選考委員会
１１．β講習会委員会
１２．β国際交流委員会
１３．β新技術情報委員会
１４．β男女共同参画委員会
１５．β人事
１６．βその他

各委員会資料

１．庶務報告(岡)

18 年度事業報告

1) 会報などを各委員会と協力して発送
2) 会員情報の管理・更新
3) その他

19 年度事業経過報告

1) 会報などを各委員会と協力して発送
2) 会員情報の管理・更新
3) その他

20 年度事業計画

1) 会報などを各委員会と協力して発送
2) 講習会への協力
3) 公開講座、科学研究費補助金（研究成果公開促進費）20 年度申請(予定)
4) 会員情報の管理・更新
5) その他

２．財務報告（太田）（添付資料　参照）

18 年度財務報告

1) 収支のまとめ
2) 会員への会費振込依頼、入金確認等
3) 学術集会会場での会費徴収

19 年度財務経過報告

1) 収支のまとめ
2) 会員への会費振込依頼、入金確認等
3) 学術集会会場での会費徴収

20 年度財務計画

1) 収支のまとめ
2) 会員への会費振込依頼、入金確認等
3) 学術集会会場での会費徴収

３．監査（木原、高松）

1) 監査結果の報告

４．企画委員会（加藤（晃））

18 度事業報告

1) 賛助会員への勧誘
2) 会報「バイオイメージング」への広告勧誘（エーイー企画との連携）
3) エーイー企画(広告代理店)と連携し集会の展示、広告を担当

19 年度事業経過報告

1) 賛助会員への勧誘
2) 会報「バイオイメージング」への広告勧誘（エーイー企画との連携）
3) エーイー企画(広告代理店)と連携し集会の展示、広告を担当

20 年度事業計画

1) 賛助会員への勧誘
2) 会報「バイオイメージング」への広告勧誘（エーイー企画との連携）
3) エーイー企画(広告代理店)と連携し集会の展示、広告を担当

５．バイオイメージング誌委員会(朽津)

18 年度事業報告

1) 会報発行　和文誌「バイオイメージング」第 27 巻 2 号まで発行
2) 和文誌「バイオイメージング」の Web-site での公開
3) 和文誌「バイオイメージング」と英文誌「Bioimages」の編集方針の見直し（和文の総説･解説、原著論文は、「Bioimages」に掲載の方向）に基づく、投稿規定の改定準備
4) 投稿(研究室紹介等)呼びかけ、特集記事の充実

19 年度事業経過報告

1) 会報発行　和文誌「バイオイメージング」第 28 巻 2 号まで発行
2) 和文誌「バイオイメージング」の Web-site での公開
3) 和文誌「バイオイメージング」と英文誌「Bioimages」の編集方針の見直し（和文の総説･解説、原著論文は、「Bioimages」に掲載の方向）に基づく、投稿規定の改定準備
4) 投稿(研究室紹介等)呼びかけ、特集記事の充実

20 年度事業計画

1) 和文誌「バイオイメージング」第 29 巻発行
2) 和文誌「バイオイメージング」の Web-site での公開、和文誌ホームページの充実
3) 投稿(研究室紹介等)呼びかけ、特集記事の充実

６．bioimages 誌編集委員会(小島)

18 年度事業報告

1) Bioimages Vol26 の論文のアップロード準備中
2) Bioimages の ESCI 収載の可能性について検討

19 年度事業経過報告

1) Bioimages Vol27 の論文のアップロード準備中
2) Bioimages の ESCI 収載の可能性について検討

20 年度事業計画

1) Bioimages Vol28 の論文のアップロード
2) Vol.6(1998)以前のバックナンバーのオンライン化を継続
3) 投稿規定の改訂

７．ホームページ編集委員会（曽我）

18 年度事業報告

1) 運用体制の確立

19 年度事業経過報告

1) 特になし

20 年度事業計画

1) 特になし

９．集会委員会（永井）

18 年度事業報告

第 27 回学術集会

日程： 2018 年 9 月 3 日（日）～4 日（火）
会場： 産業技術総合研究所 つくばセンター共用講堂
大会長： 加藤 薫 （産業技術総合研究所 バイオメディカル研究部門）
参加費： 一般（正会員：6,000 円、非会員：8,000 円）
学生（学部学生無料、会員大学院生 2,000 円、非会員大学院生：3,000 円）
公開講座： 「顕微鏡イメージングを学ぶ」
共催： 日本バイオイメージング学会、産業技術総合研究所
参加費： （無料）
会期：2017 年 9 月 2 日（月） 12:00～18:30
会場：産業技術総合研究所 つくばセンター共用講堂

19 年度事業経過報告

第 28 回学術集会（第 6 回国際バイオイメージングシンポジウム同時開催）

日程： 2019 年 9 月 21 日（土）～23 日（月）
会場： 帝京大学板橋キャンパス（東京都板橋区加賀２－１１－１）
大会長： 鈴木 亮 （帝京大学 薬学部 薬物送達学研究室）
参加費： 一般（正会員：8,000 円、非会員：10,000 円）
学生（学部学生（4 年生以下）無料、会員大学院生（学部 5 年生以上）3,000 円、非会員（学部 5 年生以上）大学院生：5,000 円）
※参加費：第 5 回国際バイオイメージングシンポジウムとの同時開催のため、前回の国際シンポジウムと同額に設定（会員大学院生以外）。
また、薬学部は 6 年制であるため、学部学生を 4 年生以下、大学院

生を 5 年生以上と併記。

公開講座：開催なし

20 年度事業計画

第 29 回学術集会

日程：　2020 年 9 月 24 日（木）～25 日（金）

会場：　自然科学研究機構岡崎コンファレンスセンター

大会長：　根本　知己　（北海道大学電子科学研究所）

参加費：　一般（正会員：6000 円、非会員：8000 円）

学生（学部学生（4 年生以下）無料、会員大学院生（学部 5 年生以上）3,000 円、非会員（学部 5 年生以上）大学院生：5,000 円）

後援：　自然科学研究機生命創成探求センター

公開講座：　「けんびきょう」（仮）

主催：　日本バイオイメージング学会

後援：　自然科学研究機生命創成探求センター（仮）

参加費：　（無料）

会期：2020 年 9 月 26 日（土）

会場：自然科学研究機構岡崎コンファレンスセンター

８．賞選考委員会(高松)

18 年度事業報告

1）奨励賞：飯塚 怜 氏（東京大学大学院薬学研究科）を推薦

19 年度事業経過報告

1）奨励賞：小和田 俊行 氏（東北大学多元物質科学研究所）を推薦

2）文部大臣表彰：１名を研究支援賞に推薦

20 年度事業計画

1）奨励賞について、学会ホームページと和文誌「バイオイメージング」に、推薦のお願いを掲載予定。

９．研究助成選考委員会（菊地）

18 年度事業報告

1）特になし

19 年度事業経過報告

1）特になし

20 年度事業計画

1）特になし

１０．講習会委員会（加藤（薫））

18 度事業報告

1） 特になし

19 年度事業経過報告

1） 特になし

20 年度事業計画

1） 計画中

１１．国際交流委員会（鈴木）

18 年度事業報告

1） 第 6 回国際バイオイメージングシンポジウムに向けての準備

会期：Sep 21-23, 2019

開催場所：帝京大学板橋キャンパス（東京都板橋区加賀２－１１－１）

大会長：鈴木亮 （帝京大学薬学部）

共催：帝京大学、National University of Singapore, Mechanobiology Institute (MBI)

19 年度事業経過報告

1)第 6 回国際バイオイメージングシンポジウムの開催

会期：Sep 21-23, 2019

開催場所：帝京大学板橋キャンパス（東京都板橋区加賀２－１１－１）

大会長：鈴木亮 （帝京大学薬学部）

共催：帝京大学、National University of Singapore, Mechanobiology Institute (MBI)

20 年度事業計画

1）次回国際シンポジウム開催に向けての準備

１２．新技術情報委員会（根本）

18 年度事業報告

1）特になし

19 年度事業経過報告

1）特になし

20 年度事業計画

1）特になし

１３．男女共同参画委員会（洲崎）

18 年度事業報告

1) 男女共同参画学協会連絡会 16 期運営委員会に出席

2) 内閣府理工チャレンジ～女子学生・生徒の理工系分野への選択～　リコチャレ応援団体として参加、理工系女子応援ネットワークに参加

3) 女子中高校生夏の学校(8 月 9 日～11 日)、協賛及びポスター参加

19 年度事業経過報告

1) 男女共同参画学協会連絡会 17 期運営委員会に出席

2) 内閣府理工チャレンジ～女子学生・生徒の理工系分野への選択～　リコチャレ応援団体として参加、理工系女子応援ネットワークに参加

3) 女子中高校生夏の学校(8 月 9 日～11 日)、協賛及びポスター参加

4) 第 28 回学術集会、第 6 回国際シンポジウムにおいて NUS MBI との共同セッションとして Women in Science を実施

20 年度事業計画

同様の活動を継続予定

１４．その他

審議事項：

１）第 29 回学術集会の準備について

２）和文誌と欧文誌の統合について

３）その他

2018年度決算書（2018年1月1日～2018年12月31日）

日本バイオイメージング学会

会長　　船津　高志　印

理事(財務担当)　太田　善浩　印

一般会計

収入	
2017年より繰越	4,675,321
利息	11
会費	917,000
学術集会余剰金	852,989
懇親会費	65,000
収入計	6,510,321

支出	
バイオイメージング印刷費	141,102
ジャパンメディカル英文校正	40,919
通信・郵送費	83,252
謝金・人件費	130,000
男女共同参画	80,712
奨励賞	100,000
会議費	129,707
振込手数料	5,184
学術集会準備金	300,000
HP作成維持費	70,200
雑費	56,757
小計	1,137,833
2019年度への繰越	5,372,488
支出計	6,510,321

特別会計(国際学会準備金等)

収入	
2017年度より繰越	4,290,669
収入計	4,290,669

支出	
2019年度への繰越	4,290,669
支出計	4,290,669

監査　　2019年　　月　　日

監事　木原　裕　　印

監事　高松　哲郎　印

2020年度予算案(2020年1月1日～2020年12月31日)

一般会計

収入		支出		
繰り越し	4,749,488	バイオイメージング印刷費	150,000	広報
会費	917,000	Bioimages アップロード費	100,000	広報
		ホームページ管理費	70,200	広報
		謝金・人件費	50,000	庶務、会計
		英文校閲費	80,000	編集
収入計	5,666,488	会議費	130,000	庶務
		通信・郵送費	110,000	庶務、会計
		奨励賞･研究助成	100,000	賞選考
		男女共同参画（分担金 他）	99,000	男女共同･国際
		学術集会準備金	300,000	集会
		雑費	60,000	庶務･会計
		予備費	4,417,288	
		支出計	5,666,488	

特別会計（国際学会準備金等）

収入		支出	
繰り越し	3,290,669	2021年度への繰越	3,290,669
収入計	3,290,669	**支出計**	3,290,669

２０１９年度の各委員会：名簿

〇：委員長

１．会　　長　：船津 高志
２．副 会 長　：岡 浩太郎、洲崎 悦子
３．庶　　務　：〇岡 浩太郎
４．財　　務　：〇太田 善浩
５．企　　画　：〇加藤 晃一、竹本 邦子、橋本 香保子、長谷川 明洋、
＊公開講座の企画を含む（学術集会付設の公開講座は大会長が企画）
６．バイオイメージング誌編集　：加藤 有介、菊地 和也、〇朽津 和幸、曽我 公平、桧垣 匠、樋口 ゆり子、宮川 拓也
７．bioimages 誌編集　：大幡 久之、朽津 和幸、小島 清嗣、〇小島 正樹、斎野 朝幸、洲崎 悦子、寺川 進、宮川 拓也
８．ホームページ編集　：岡 浩太郎、小島 正樹、朽津 和幸、〇曽我 公平、桧垣 匠
９．集　　会　：太田 善浩、加藤 薫、立野 玲子、〇永井 健治
10. 賞 選 考　：大塩 力、高松 哲郎、◯田中 直子、田之倉 優、寺川 進、浜口 幸久
11. 研究助成選考：〇菊地 和也、鈴木 和男、中山 俊憲、根本 知己
12. 講 習 会　：岡部 弘基、〇加藤 薫、櫻井 孝司、佐々木 章、中村 岳史、企業から（オリンパス、カールツァイス、ニコン、浜松ホトニクス）
13. 国 際 交 流　：木原 裕、〇鈴木 和男、鈴木 亮、永井 健治
アドバイザー：A. Wheatley, J. Girkin, F. Maxfield, R. Hoffmann, N. Demaurex, Lowrel Bolin, D. Ehrhardt, M. E. P. Murphy, W. Dawson, M. Jaconi
＊国際バイオイメージング学会の対応を含む
14. 新技術情報　：荒井 祐仁、加藤 薫、後藤 英一、鶴旨 篤司、◯根本 知己、晝馬 亨
15. 男女共同参画：加藤 有介、朽津 和幸、〇洲崎 悦子、田中 直子、橋本 香保子、樋口 ゆり子

[付属資料]

１．役員

１）評議員（２０２２．１２．３１まで）（現員３９名）

荒井 祐仁、池水 信二、大塩 力、太田 善浩、大幡 久之、岡 浩太郎、加藤 薫、加藤 晃一、加藤 有介、川西 徹、菊地 和也、朽津 和幸、小島 正樹、後藤 英一、齋野 朝幸、洲崎 悦子、鈴木 和男、鈴木 亮、曽我 公平、竹本 邦子、立野 玲子、田中 直子、田之倉 優、鶴旨 篤司、寺川 進、冨田 光子、永井 健治、中村 岳史、中山 俊憲、根本 知己、橋本 香保子、長谷川 明洋、浜口 幸久、桧垣 匠、樋口 ゆり子、晝馬 亨、船津 高志、古野 忠秀、宮川 拓也

２）監　事（２名：２０２０．１２．３１まで）

木原 裕、高松 哲郎

３）理　事（１６名：４年任期、２年毎半数改選、評議員により互選）（現員１５名）

２０２０．１２．３１まで

太田 善浩、岡 浩太郎、加藤 薫、加藤晃一、小島 正樹、曽我 公平、永井 健治、船津高志

２０２２．１２．３１まで

菊地 和也、朽津 和幸、洲崎 悦子、鈴木 和男、鈴木 亮、田中 直子、根本 知己

４）特任理事（２年任期）（６名まで）

２０２０．１２．３１まで

大塩 力、田之倉 優、寺川 進、浜口 幸久

５）会長、副会長、庶務担当、財務担当（理事により互選：２年任期）

会　　長：２０２０．１２．３１まで：　船津 高志

副　会　長：２０２０．１２．３１まで：　岡 浩太郎、洲崎 悦子

庶務担当理事：２０２０．１２．３１まで：　岡 浩太郎

財務担当理事：２０２０．１２．３１まで：　太田 善浩

２．名誉会員（非役員）

新井 孝夫、荒田 洋治、石村 巽、大木 和夫、柏木 浩、関塚 永一、脊山 洋右、中西 守、南谷晴之、安岡 則武

日本バイオイメージング学会入会のお願い

日本バイオイメージング学会では会員の募集を致しております。会員の方の周囲に画像に関心のある方がおられましたら入会されるようご勧誘をお願い致します。入会される方は、本誌末の入会申込書をご利用ください。

正会員:　　5，000円
学生会員:　　2，000円
団体会員:　　10，000円（図書館対象）
賛助会員:一口　100，000円
評議員会費:　　8，000円

申込先
学会事務局
〒223-8522　神奈川県港北区日吉 3-14-1
慶應義塾大学理工学部生命情報学科　生物物理・神経情報学研究室内
日本バイオイメージング学会事務局
TEL:　045-566-1728
FAX:　045-566-1789
E-mail:　office@j-bioimaging.org
郵便振替:00130－3－73565
名　　義:日本バイオイメージング学会事務局

日本バイオイメージング学会賛助会員入会のお願い

本学会は、画像解析技術を基に生命原理を解明し、人類の福祉に貢献することを目的としております。つきましてはこの趣旨に御賛同いただき御機関に賛助会員として参加いただければありがたく思います。日本における基礎生命科学と応用開発研究との有機的結合実現のためぜひ御協力ください。
賛助会員入会御承諾の場合は下記口座への会費の振込とともに、本誌末の入会申込書（学会入会申込書と同じ）に必要事項を御記入の上、返送をお願い致します。

賛助会員　会費:一口　年10万円
会費振込先:　郵便振替:00130－3－73565
日本バイオイメージング学会事務局

特　典:展示会での優先展示、学会誌、広報誌、学会要旨集への広告優先権

問合せ先　〒223-8522　神奈川県港北区日吉 3-14-1
慶應義塾大学理工学部生命情報学科　生物物理・神経情報学研究室内
日本バイオイメージング学会事務局
TEL:　045-566-1728　FAX:　045-566-1789
E-mail:　office@j-bioimaging.org

会費納入のお願い

日本バイオイメージング学会学会費の納入をお願いいたします。
すみやかな納入をお願いいたします。
正会員:　　5，000円
学生会員:　　2，000円
団体会員:　　10，000円（図書館対象）
賛助会員:一口100，000円
評議員会費　　8，000円

会費振込先:　郵便振替:00130－3－73565
　　日本バイオイメージング学会事務局

学会のホームページは以下の通りです。ご利用ください。

http://j-bioimaging.org

日本バイオイメージング学会定款℃

℃　　℃℃℃℃℃℃℃℃第１章　　総　　則

第１条　この学会は、日本バイオイメージング学会という。

第２条℃　この学会は、事務所を庶務担当理事の勤務先におく。

第３条　この学会は、評議員会の議決を経て必要の地に支部をおくことが出来る。

第２章　　目的および事業

第４条　この学会は、会員の研究発表、知識の交換ならびに会員相互および関連学（協）会との連絡提携の場となり、バイオイメージング学の進歩普及をはかり、もって学術、文化の発展に寄与することを目的とする。

第５条　この学会は、前条の目的を達成するために次の事業を行う。

１　研究発表会および講演会の開催

２　会誌、研究報告および資料の刊行

３　内外の関連学（協）会との連絡および協力

４　研究の奨励および研究業績の表彰

５　研究および調査

６　その他目的を達成するために必要な事業

第３章　　会　　員

第６条　この学会の会員は、次のとおりとする。

１　正会員　　バイオイメージング学に関する学識または経験を有する個人であって、この学会の目的に賛同し、別に定められた年会費を納める者

２　学生会員　大学またはこれに準ずる学校に在籍し、バイオイメージング学に関係のある学科を納める学生であって、この学会の目的に賛同し、別に定められた年会費を納める者

３　団体会員　この学会の目的に賛同し、別に定められた年会費を納める団体

４　賛助会員　この学会の事業を後援し、別に定められた年会費１口以上を納める者または法人

５　名誉会員　バイオイメージング学と本学会の発展に大いに貢献した個人で、評議員会の認めた者

第７条　会員になろうとする者は、会費を添えて入会申込書を提出し、理事会の承認を受けなければならない。

第８条　会員は、この学会が刊行する機関誌および図書の優先的配布を受けることができる。

第９条℃　会員は、次の事由によって資格を喪失する。

１　退会

２　禁治産および準禁治産の宣告

３　死亡、失踪宣告

４　除名

第１０条　会員で退会しようとする者は、理由を付して退会届を提出しなければならない。

第１１条　会員が次の各号の一に該当するときは、評議員会の議決を経て、会長がこれを除名することができる。

１　会費を滞納したとき

２　この学会の会員としての義務に違反したとき

３　この学会の名誉を傷つけ、あるいはこの学会の目的に反する行為をしたとき

第１２条　既納の会費は、いかなる理由があってもこれを返還しない。

第４章　役員、評議員および職員

第１３条　この学会には、次の役員をおく。

理　事　１２名以上１６名以内（うち会長１名、副会長２名）

特任理事　６名以内

監　事　２名

評議員　全会員の１０％程度

第１４条　１　評議員と監事は、正会員より総会で選出し、理事および特任理事は、評議員より評議員会で選出する。

２　理事は、互選で会長１名、副会長２名、庶務担当理事１名、財務担当理事１名、国際交流委員長１名を定め、常務理事とする。

第１５条　１　会長はこの学会の業務を総理し、この学会を代表する。

２　副会長は会長を補佐し、会長に事故ある時は会長業務を代行する。

３　庶務担当理事、財務担当理事は、会長を補佐し、理事会の決定事項に基づき事務を行う。

４　国際交流委員長は、理事会の決定事項に基づき、諸外国とのバイオイメージング研究の学術的交流と連携を図り、国際バイオイメージング会議を推進する。

第１６条　１　理事は、理事会を組織し、この学会の運営上重要な事項について決定し、執行する。

２　常務理事は常務理事会を組織し、必要な事項について協議し、理事会に諮る。

３　特任理事は、理事会の決定事項に基づき、特定の重要事項を担当する。

第１７条　監事は民法第 59 条の職務を行う。

第１８条　評議員は評議員会を組織して、この学会の運営上の重要事項にかかわる理事会の決定事項に関し、議事を開き議決する。

第１９条　１　会長、副会長、庶務担当理事、財務担当理事、監事の任期は２年とする。

２　理事の任期は４年とし、２年毎に半数を改選する。

３　特任理事の任期は２年とする。但し、再任を妨げない。

４　評議員の任期は４年とする。但し、再任を妨げない。

５　補欠または増員による役員の任期は、前任者の残任期間とする。

６　役員は、その任期満了後でも後任者が就任するまでは、なお、その職務を行う。

７　役員は、この学会の役員としてふさわしくない行為のあった場合、または特別の事情のある場合には、その任期中であっても評議員会の議決により、会長が任を解くことができる。

第２０条　役員は交通費、連絡費、日当の支給を受けることができる。

第２１条　１　この学会の事務を処理するため、書記等の職員をおくことができる。

２　職員は、会長が任免する。

３　職員は、有給とする。

第５章　会　　議

第２２条　１　通常総会は、毎年１回議長が召集する。

２　臨時総会は、理事会または監事が必要と認めたとき、いつでも召集することができる。

第２３条　会長は、会員現在数の５分の１以上から会議に付議すべき事項を示して総会の召集を請求された場合には、その請求のあった日から２０日以内に臨時総会を召集しなければならない。

第２４条　通常総会の議長は、会長とし、臨時総会の議長は会議のつど会員の互選で定める。

第２５条　総会の召集は、少なくとも１０日以前に、その会議に付議すべき事項、日時および場所を記載した書面または会誌の公告をもって通知する。

第２６条　次の事項は、通常総会に提出してその承認を受けなければならない。

１　事業計画および収支予算についての事項

２　事業報告および収支決算についての事項

３　財産目録

４　その他理事会において必要と認めた事項

第２７条　総会は、会員現在数の５分の１以上出席しなければ、その議事を開き議決をすることができない。ただし、当該議事につき書面をもってあらかじめ意志表示した者は、出席者とみなす。

第２８条　総会の議事はこの定款に別段の定めがある場合を除くほか、出席者の過半数をもって決し、可否同数の時は、議長の決するところによる。

第２９条　総会の議事の要項および議決した事項は、会員に通知する。

第３０条　１　評議員会は随時会長が召集する。

２　評議員会の議長は、会長がこれに当たる。

第３１条　評議員会は評議員数現在数の５分の１以上出席しなければ議事を議決することができない。

第３２条　評議員会は、この定款に別段の定めがある場合を除くほか、出席者の過半数をもって決し、可否同数のときは議長の決するところによる。

第３３条　理事会は、毎年２回会長が召集する。ただし、会長が必要と認めた場合、または、理事現在数の３分の１以上から会議の目的たる事情を示して請求のあったときには、会長は臨時理事会を召集しなければならない。

第３４条　１　理事会は理事現在数の３分の２以上出席しなければ議事を開き議決することができない。ただし、当該議事につき書面をもってあらかじめ意志を表示したものは、出席者とみなす。

２　理事会の議事は、この定款に別段の定めがある場合を除くほか、出席理事の過半数をもって決し、可否同数のときは、議長の決するところによる。

３　特任理事は理事会には参考人として出席できる。

第３５条　総会、評議員会および理事会の議事録は、議長が作成し、議長および出席者代表２名以上が署名押印の上、これを保存する。

第６章　資産および会計

第３６条　この学会の資産は、次のとおりとする。

１　この学会設立当初画像解析シンポジウムから継承した別紙財産目記載の財産

２　会費
３　事業に伴う収入
４　資産から生じる果実
５　寄付金品
６　その他の収入

第３７条　１　この学会の資産を分けて、基本財産および運用財産の２種とする。
２　基本財産は、別紙財産目録のうち、基本財産の部に記載する資産および将来基本財産に編入される資産で構成する。
３　運用財産は、基本財産以外の資産とする。
４　寄付金品であって、寄付者の指定のあるものは、その指定にしたがう。

第３８条　この学会の基本財産のうち現金は、理事会の決定によって定期郵便貯金とするか、もしくは定期預金として、会長が保管する。

第３９条　基本財産は、処分し、または担保に供してはならない。ただし、この学会の事業遂行上やむを得ない理由があるときは、評議員会および総会の議決を経、その一部に限り処分し、または担保の供することができる。

第４０条　この学会の事業遂行に要する費用は、会費、事業に伴う収入および資産から生ずる果実等の運用をもって支弁する。

第４１条　学会の事業計画およびこれに伴う収支予算は、評議員会で議決しなければならない。

第４２条　１　この学会の収支決算は、毎回、財産目録、事業報告書および会員の移動状況書とともに監事の意見をつけ、評議員会および総会の承認を受けなければならない。
２　この学会の収支決算に剰余金があるときには、評議員会の議決および総会の承認をうけて、その一部もしくは全部を基本財産に編入し、または翌年度に繰り越すものとする。

第４３条　収支予算で定めるものを除くほか、新たに義務の負担をし、または権利の放棄をしようとするときは、評議員会および総会の議決を受けなければならない。借入金（その会計年度内の収入をもって償還する一時借入金を除く）についても同様とする。

第４４条　この学会の会計年度は、毎年１月１日に始まり１２月３１日に終る。

第７章　定款の変更ならびに解散

第４５条　この定款は、評議員会および総会においておのおのの４分の３以上の議決を経なければ変更することができない。

第４６条　この学会の解散は、評議員会および総会においておのおのの４分の３以上の議決を経なければならない。

第４７条　この学会の解散に伴う残余財産は、評議員会および総会においておのおのの４分の３以上の議決を経て、この学会の目的に類似の目的を有する公益事業に寄付するものとする。

第８章　補　　則

第４８条　１．この定款施行についての細則は、評議員会の議決を経て別に定める。
２．本定款は１９９１年１０月１８日より実施する
３．事業年度の初年度は本会設立の日をもってはじまる

４．初年度は半期役員は互選で決定する

付　　則

本定款は、２０１１年１月１日より実施する。

℃℃℃℃℃℃℃℃

細　　則

１．この細則は、日本バイオイメージング学会定款４８条の１により、定めたものである。

２．本学会の事務所を、庶務担当理事の勤務先（〒223-8522 神奈川県横浜市港北区日吉 3 丁目 14 番 1 号　慶應義塾大学理工学部生命情報学科生物物理・神経情報学研究室）におく。

３．年会費は正会員５，０００円、学生会員２，０００円、団体会員１０，０００円、賛助会員１口１００，０００円とする。ただし、評議員の年会費は８，０００円とする。また、賛助会員の企業は、若干名を会員として登録することができる（これを登録会員という）。登録会員は、評議員会の議決をもって承認される。

４．第１４条で定める評議員（評議員という）のほかに、任期２年（再任を妨げない）の企業評議員をおくことができる。企業評議員は、本学会の活動に協力的な企業に属する正会員および賛助会員企業の登録会員より選出し、評議員会で承認する。ただし、企業評議員の人数は評議員の２０%以内とし、評議員の年会費を納める必要はない。

５．定款第１６条２の常務理事会は、常務理事とバイオイメージング誌編集委員会委員長、bioimages 誌編集委員会委員長より構成する。

６．副会長は、会長以外の常務理事と併任することができる。

７．定款第５条に定めた事業を行うため、企画、バイオイメージング誌編集、bioimages 誌編集、ホームページ編集、集会、賞選考、研究助成選考、講習会、国際交流、新技術情報、男女共同参画の各委員会を置く。各委員会には、必ず理事が属し、委員長は原則として理事がつとめる。ただし、特別の事情があるときは、評議員が委員長をつとめることができる。また、必要に応じて、これらの委員会のほかに、特別委員会を設けることができる。

特別委員会には、必ず理事が複数名加わるとともに、理事が委員長をつとめる。

８．本細則の変更については、評議員会の議決と総会の承認を必要とする。

付　　則

本細則は、２０１９年１月１日より実施する。

年会費

会員は次の会費年額を支払うこととする。

１．評議員　　年額８，０００円
２．正会員　　年額５，０００円
３．学生会員　　年額２，０００円
４．団体会員　　年額１０，０００円
５．賛助会員　年額１口１００，０００円

附則

１．㈱企業評議員は、個人正会員については会費年額５，０００円、賛助会員を代表して評議員となる場合には賛助会費のみとする。

バイオイメージング　第 28 巻第 2 号
2019 年 9 月 5 日発行

発行所：日本バイオイメージング学会
〒223-8522　神奈川県横浜市港北区日吉 3-14-1
慶應義塾大学理工学部生命情報学科　生物物理・神経情報学研究室内
電話　：　042-676-5498　；　FAX　：　042-676-5863
E-mail：office@j-bioimaging.org
URL：http://j-bioimaging.org/

株式会社ビジコムジャパンでご提供可能なサービス・製品

in vitro & in vivo イメージング用製品

Flamma™ シリーズ

▶ **優れた蛍光強度**と**水中での安定性**を兼ね備えた蛍光試薬

▶ ラベリングのための**各種官能基 (NHS, Amine, Vinyl Sulfone etc.)** を有するものをご用意

Flamma® Fluorophore

Flamma® Fluor	λ_{Ex} (nm)	λ_{Em} (nm)	励起レーザー波長	対応する既存試薬
Flamma® 406	401	434	UV	A 405, Cascade Blue®, D 405, C 405, Pacific Blue®
Flamma® 496	496	516	488 nm Laser	FAM, FITC, Fluorescein
Flamma® 488	495	519	488 nm Laser	A 488, C 2, D 488, C 488, A 488
Flamma® 552	550	565	532, 543, 546, 555 or 568 nm Laser	A 555, C 3, D 549, C 488, A 488
Flamma® 553	554	584	532, 543, 546, 555 or 568 nm Laser	A 546, TRITC
Flamma® 560	560	589	532, 543, 546, 555 or 568 nm Laser	A 568, C 568, A 565, TRITC
Flamma® 648	648	663	663, 635, or 640 nm Laser	A 647, C 5, D 649, C 647, A 647N
Flamma® 675	675	691	680 or 685 nm Laser	A 680, C 5.5, D 680, C 680, I 680LT
Flamma® 749	749	774	680, 685, or 750 nm Laser	A 750, C 7, D 750, C 750, I 750
Flamma® 774	774	806	785 nm Laser	C 7.5, C 770
Flamma® 800	775	795	785 nm Laser	A 790, D 800, C 790, 1800CW

BBB Flamma™ シリーズ

▶ **2018 年上市の新製品**

▶ BBB(Blood Brain Barrier) を通過して脳組織のイメージングが可能

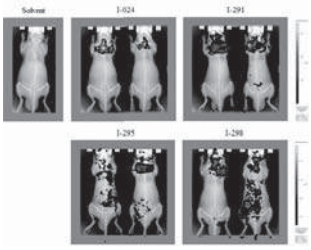

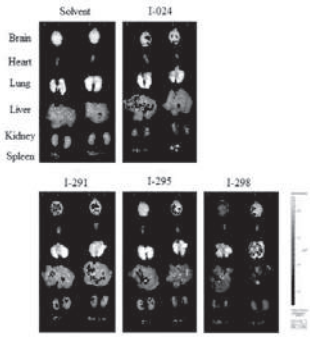

ポリグルタミン酸を利用したナノキャリア

ポリグルタミン酸 - 治療からイメージングまで

▶ **生体適合性と生分解性**

▶ リビング重合による**低い分子量分散度**

▶ **高分子量にも対応可能**

▶ 多くの種類の化合物を導入できるよう、**様々な官能基に対応可能**

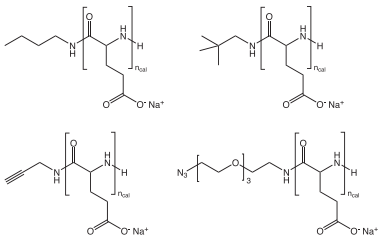

モノマー数 n	10	20	50	100	150	200	300
分子量 (Da)	1.500	3.000	7.500	15.000	22.000	30.000	45.000
分子量分散度 Đ	1.1-1.2	1.1-1.2	1.1-1.2	1.1-1.2	1.1-1.2	1.1-1.2	1.1-1.2

- 日本国内のお問い合わせは -

株式会社ビジコムジャパン

〒141-0022　東京都品川区東五反田 5-28-1 K2 ビル 7 階　　TEL. 03-6277-3233 FAX. 03-6277-3265

e-mail: sales@bizcomjapan.co.jp　　HP: bizcomjapan.co.jp

Acoustic X

CYBERDYNE LED

Photoacoustic Imaging System Using LED Light Source

Wide range of selectable light wavelengths, multi-wave length analysis, portable, and no protective eyewear needed!

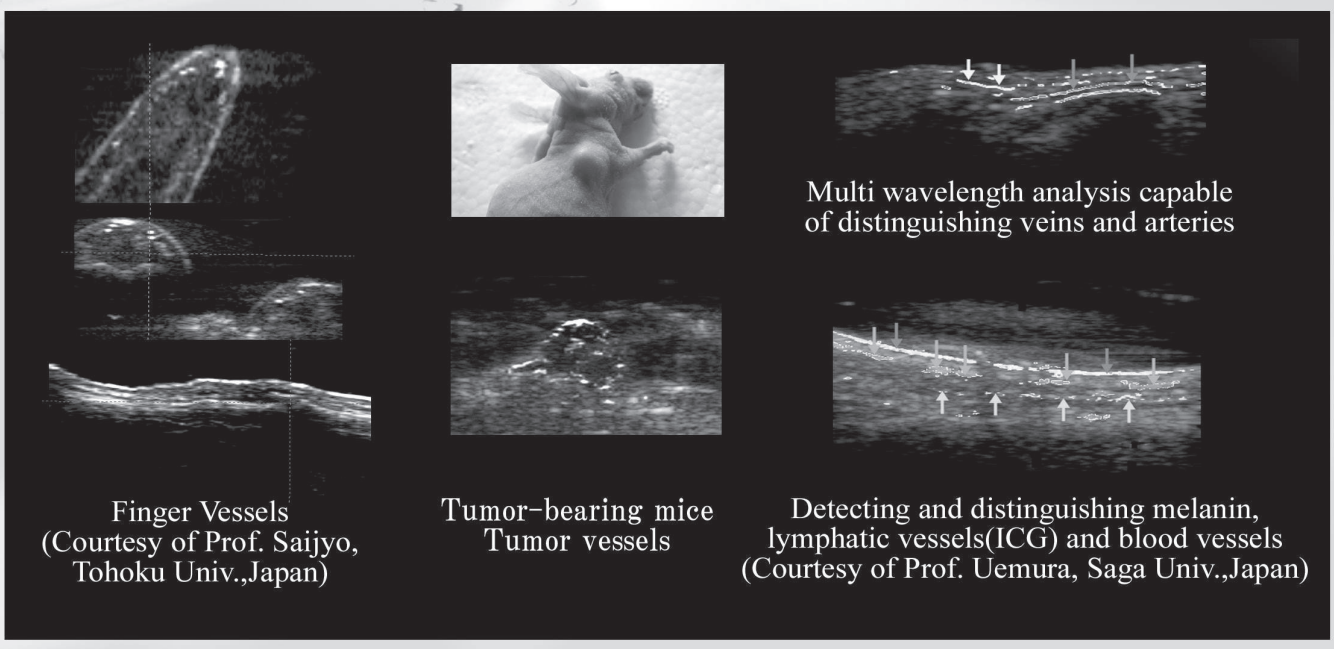

Finger Vessels
(Courtesy of Prof. Saijyo, Tohoku Univ.,Japan)

Tumor-bearing mice
Tumor vessels

Multi wavelength analysis capable of distinguishing veins and arteries

Detecting and distinguishing melanin, lymphatic vessels(ICG) and blood vessels
(Courtesy of Prof. Uemura, Saga Univ.,Japan)

HAMAMATSU
PHOTON IS OUR BUSINESS

ORCA®-Fusion

Digital CMOS camera C14440-20UP

New information updated as needed

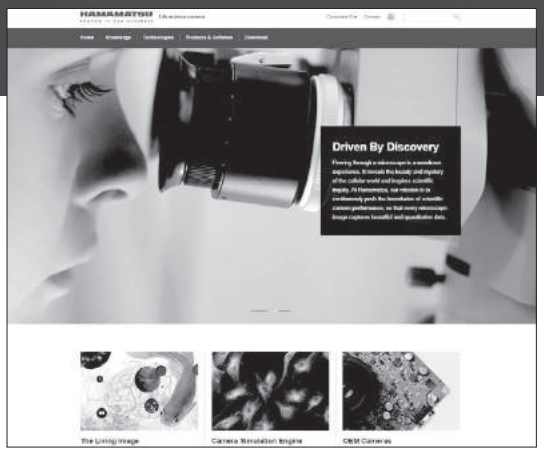

Hamamatsu Photonics, a leading life science camera company, has developed high-performance microscope cameras in the life science field. This time, ORCA-Fusion has been lined up, which has greatly improved S / N, which was a challenge for weak light imaging. Product information in the life science field of Hamamatsu Photonics, such as ORCA-Fusion, is introduced on our microscope imaging website.

HAMAMATSU PHOTONICS K.K. www.hamamatsu.com

HAMAMATSU PHOTONICS K.K., Systems Division
812 Joko-cho, Higashi-ku, Hamamatsu City, 431-3196, Japan, Telephone: (81)53-431-0124, Fax: (81)53-433-8031, E-mail: export@sys.hpk.co.jp

"Please refer to the Web page for the details" Life science camera Search

The latest catalog are updated in PDF data
Please feel free to access and download it

光源でお困りの方へ

フィルターのクロマがご提案します

CHROMA

高出力レーザー蛍光光源 LDi

安定で安全な画像取得を実現

こんな方にお勧めします

- 蛍光顕微鏡や蛍光実体でサンプルが暗いと感じている方
- ディスク共焦点顕微鏡でもっと多くの色素を使いたいと思っている方
- 光刺激やオプトジェネティックをやりたい方

５つの特長

７波長（標準）、高輝度、安定、長寿命、低価格

NEW!

寿命2年保証

■PtK2 細胞（ラットカンガルーの腎細胞）

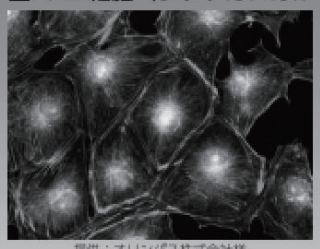

提供：オリンパス株式会社様

核
DAPI

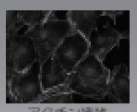

アクチン繊維
Alexa Fluor 488 phallidin

ミトコンドリア
Mito Tracker Red CMXRos

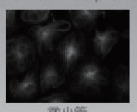

微小管
CY5

■主な仕様

光源	マルチモードレーザーダイオード						
寿命	平均 20,000 時間（2 年間保証）						
波長（nm）	405	445	470	520	528	555	640
出力（mW）	250	1,000	1,000	500	500	1,000	450
安定性（変動）rms	＜1%						
立ち上がり	＜10usec					＜1msec	＜10usec
ファイバー	液体ライトガイド（コア径 3mm）						
制御	TTL（＞2.3V）アナログ（0-5V）USB-CDP（virtual COM port）						
ソフトウェア	Windows 操作用、SDK						
レーザー安全	インターロック（ハウジング、ケーブル、キー）						
外形	318×234×146 mm						
重量	4Kg						
動作温度	5～30℃						
保存温度	−18～50℃						
湿度	＜85%						
電源	90～220VAC、50～60Hz						

クロマテクノロジジャパン合同会社

☎045-285-1583　✉japan@chroma.com　https://jp.chroma.com

超解像顕微鏡　解像度評価ツール

ナノルーラー

DNA折り紙技術により製造された「ナノルーラー」は
2点の蛍光色素が一定の幅（6～350nm）で発光します。
ナノルーラーは、ドイツGATTAquant社が開発しました。

◎超解像顕微鏡の性能確認
◎均一サンプルによる顕微鏡の性能比較
◎トラブルシューティング

対象顕微鏡

- SIM/STED／共焦点顕微鏡
- STORM／DNA-PAINT

画像例

DNA-Paint ナノルーラー
3つのスポットを持つタイプです。

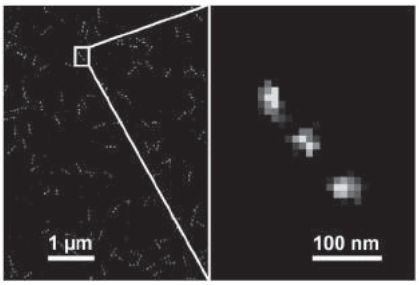

（幅：40nm、ATTO655）

GATTA-STED 90R ナノルーラー

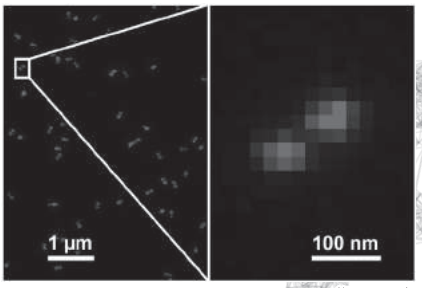

（幅：90nm）

各種ラインナップあり、カスタム対応も可能です。（幅、蛍光色素）

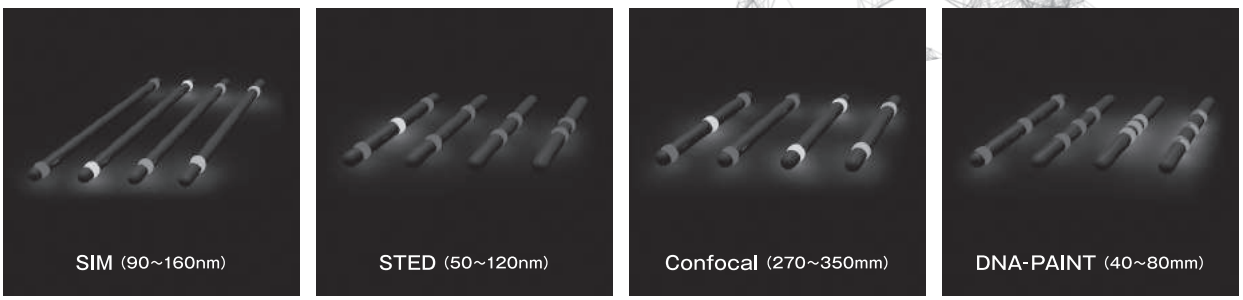

製品の詳しい情報はホームページ、又はお気軽にご連絡ください。 ナノシード 検索

NANOXEED
https://nanoxeed.co.jp/

株式会社 ナノシード
〒182-0022 東京都調布市国領町2-5-15 コクティー3F スモールオフィス
https://nanoxeed.co.jp/　info@nanoxeed.co.jp　03-4405-3913

小動物用超音波イメージング装置

Prospect T1

高分解能 in vivo 画像

Prospect は、最小 30μm の空間分解能を備えた小動物用超音波イメージングシステムです。20-30g 程度のマウスの解剖学的構造や血流機能も鮮明に観察することができます。リアルタイムで非侵襲的に in vivo 画像を得ることができ、3D イメージングで腫瘍のサイズを定量化することも可能です。

アプリケーション

心血管研究

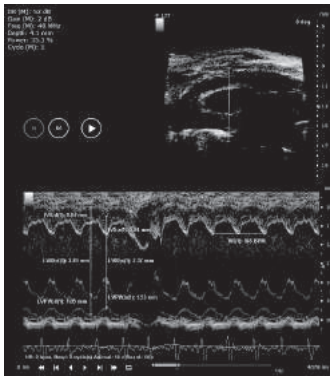

左心室の境界検出（M モード）

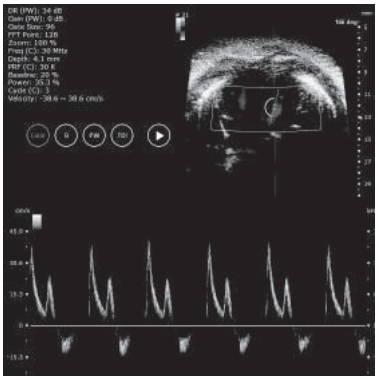

僧帽弁の血流測定（PW ドップラーモード）

眼科研究

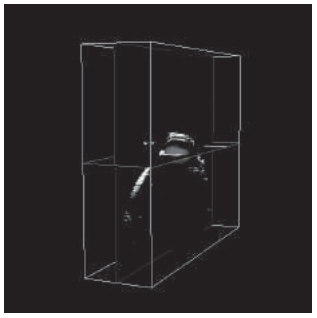

XYZ 面でのマウス眼の 3D 再構成
（3D イメージングモード）

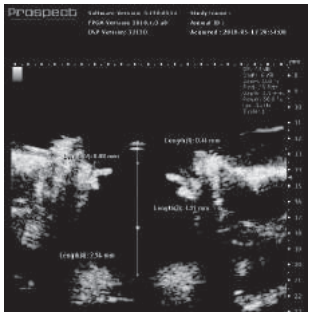

モルモットの眼のイメージング
角膜の厚さ、前房深度、
レンズの厚さ、硝子体腔
（B モード）

癌研究

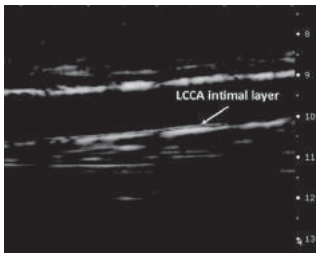

ラット左総頸動脈（LCCA）内膜層

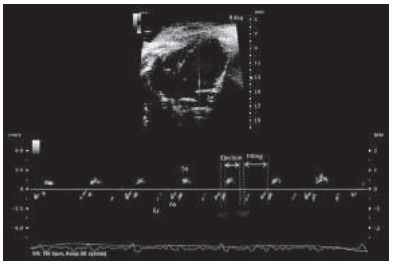

マウス血管組織のドップラー画像

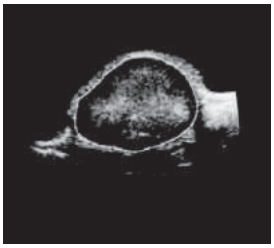

皮下腫瘍（ B モード）
測定ツールで腫瘍の体積を算出可能

造影剤を使ったマウスの
皮下腫瘍の分子イメージング
（コントラストモード）

NEPAGENE ネッパジーン株式会社

〒272-0114 千葉県市川市塩焼3-1-6
TEL：047-306-7222　FAX：047-306-7333
E-mail：info@nepagene.jp
URL：http://www.nepagene.jp

Next Generation In vivo Imaging

In vivo 2D/3D 発光・蛍光・チェレンコフ・X線・CTイメージング

IVIS Imaging System

In vivo光イメージングの世界最高峰

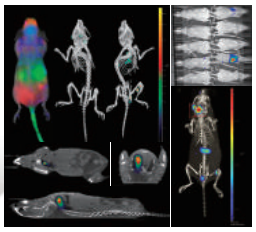

PerkinElmer For the Better

In vivo 3D 蛍光トモグラフィーイメージング

FMT Imaging System

深部の蛍光検出に優れた *in vivo*
3D 蛍光トモグラフィーイメージング

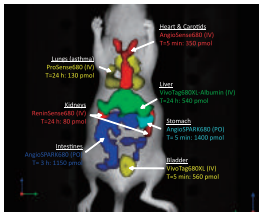

PerkinElmer For the Better

In vivo 可搬型蛍光イメージング

SAI-1000

SHIMADZU Excellence in Science

1000nm以上の波長域を用いた
革新の高精細蛍光イメージング

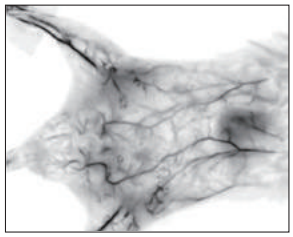

オープンエア蛍光イメージング

Solaris

中・大動物対象のガイデッドサージェリー
が可能なオープンエア蛍光イメージング

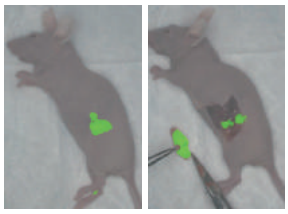

PerkinElmer For the Better

小型実験動物用 3DマイクロX線CTイメージング

CosmoScan GX Ⅱ

高速(3.9秒)、高解像(2.3μm)
広視野(86mm)撮影が可能な
進化版次世代CT

Rigaku

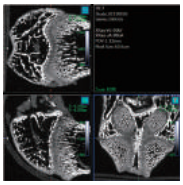

マウス摘出骨サンプル

小・中型実験動物用 3DマイクロX線CTイメージング

CosmoScan AX

約15kgの中型動物対応。
高速(18秒)・高解像(60μm)・
広視野(220mm)撮影が
可能なX線自己遮蔽型CT

Rigaku

卓上型・超高感度・高分解能 PET/CTイメージング

G8 PET/CT

コンパクト・高感度(15%以上)・
高分解能(1.4mm)を兼ね備えた
PETにCT機能も搭載

PerkinElmer For the Better

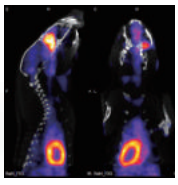

無冷媒超伝導マグネット 高磁場MRIイメージング

FlexiScan PET/SPECT-MRI

MR SOLUTIONS

超伝導マグネットによる小型・
高性能MRI。9.4T・7T・4.7T・
3Tの4種をラインナップ

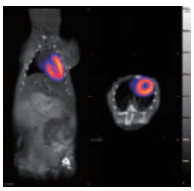

光音響3次元断層イメージング

MSOT Imaging System

組織深部のリアルタイム3次元断層撮影が
可能な光音響イメージング

iThera Medical

Multispectral
MSOT image

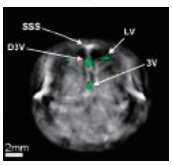

Reference cryoslice

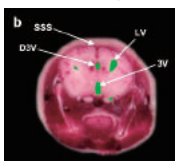

ハンドヘルド型光音響3次元断層イメージング

MSOT Acuity

iThera Medical

手持ち検出器で光音響イメージングが可能。
臨床研究にも対応するクリニカルユースの
操作性を実現※

※日本国内では研究
用途においてのみ
ご使用可能です。

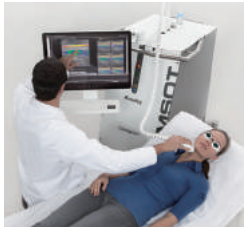

総販売元 SPI Summit Pharmaceuticals International
住商ファーマインターナショナル株式会社　バイオサイエンス事業部
〒100-0003 東京都千代田区一ツ橋一丁目2番2号　住友商事竹橋ビル12階
http://www.summitpharma.co.jp/
TEL：03-5220-1520　FAX：03-5220-1521　E-Mail：bioinfo@summitpharma.co.jp

sysmex | Lighting the way with diagnostics

ご存知でしたか？
超解像の新しい世界

- ☑ 最高23nmの高空間分解画像を提供します。
- ☑ 光軸調整等の面倒な作業が要りません。
- ☑ 電源ONしてサンプルをのせるだけ。すぐ撮像できます。

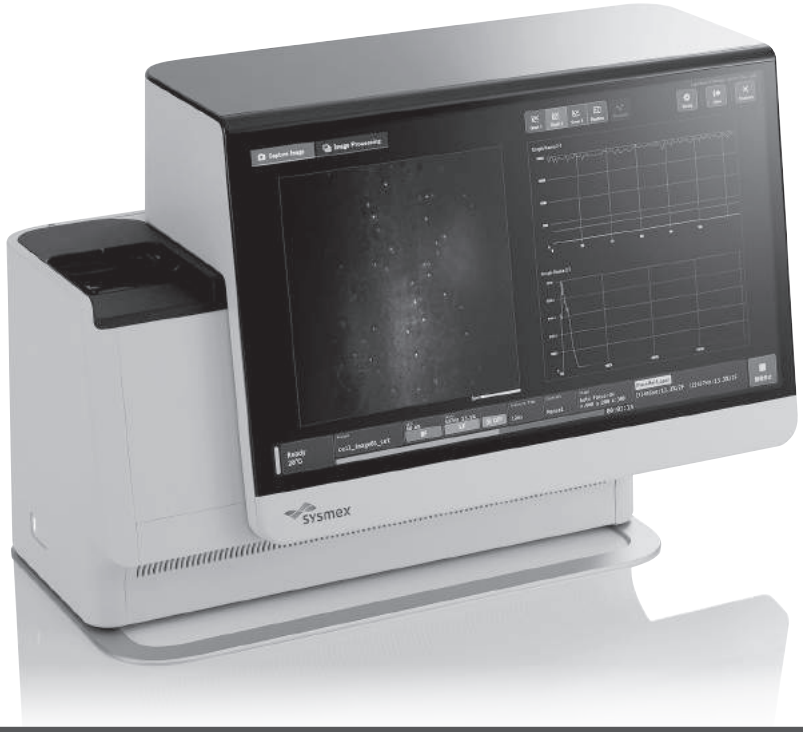

あなたの想像以上の使いやすさで、登場！

研究用1分子蛍光顕微鏡

HM-1000

主な仕様	
水平解像度	40 nm以下（最高到達分解能23 nm ※）
レーザー	405 nm、488 nm、561 nm、637 nm
寸法	幅 690 mm×奥行 420 mm×高さ 570 mm
構成	本体、制御用PC、電源ボックス

※SaraFluor650B(HMSiR)蛍光色素を用いた1分子計測の結果。
最高到達分解能は、用いるサンプルや蛍光色素により異なります。

お問合せ先
シスメックス株式会社 日本・東アジア地域本部 R&I事業推進部
ｿﾘｭｰｼｮﾝｾﾝﾀｰ 神戸市西区室谷1-3-2 〒651-2241 Tel 078-991-2091 Fax 078-997-9976
東京支社 東京都品川区大崎1-2-2 〒141-0032 Tel 03-5434-8556 Fax 03-5434-8557

sysmex-fcm.jp

YOKOGAWA

XY resolution of approx. 120nm ※

XY resolution has been improved by approximately 1.4x the optical limit based on spinning-disk confocal technology. Furthermore, a final resolution approximately twice the optical limit is realized through deconvolution.
* : For reference

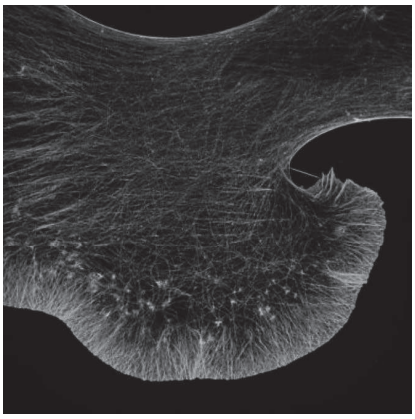

NG108 cell
Image provided by Dr. Kaoru Kato, Biomedical Research Institute, National Institute of Advanced Industrial Science and Technology (AIST)

Ideal for super-resolution live cell imaging

Just like the CSU, high-speed real time imaging can be performed with super-resolution.
In addition, live cell imaging is possible, reducing bleaching and phototoxicity.

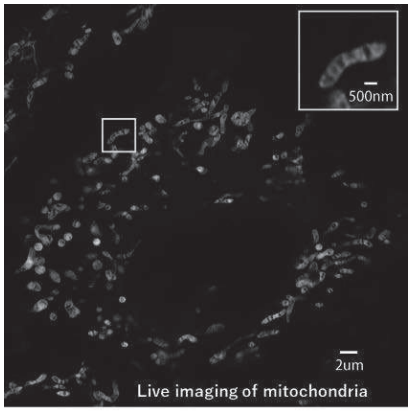

Real time live cell imaging of mitochondria (10FPS)
Image provided by Dr. Kaoru Kato, Biomedical Research Institute, National Institute of Advanced Industrial Science and Technology (AIST)

SoRa super-resolution principle

The image formation in regular confocal microscopes is shown as the product of the illumination PSF (point spread function) and detection PSF. If we consider the image formation on the pinhole at a position D from the optical axis, it is the product of the illumination PSF and detection PSF (as shown), and we can see that information at the position D/2 from the optical axis at the light source is transmitted. That is to say, information at the D/2 position at the light source is magnified to D on the pinhole. In order to correct this, a microlens is fitted and the individual focal points projected onto the pinhole are optically reduced by half, creating an ideal image formation.
By doing so, the resolution is made approximately equal to an ideal confocal microscope, in which the pinhole has been reduced to an infinitesimal size, producing an estimated 1.4x improvement upon regular confocal microscopes.

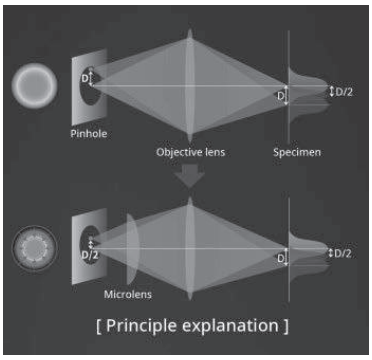

High-speed Super-resolution Confocal Scanner

CSU-W1 SoRa

Confocal Scanner Unit
Super resolution via **o**ptical **r**e-**a**ssignment

CSU-W1 SoRa
Product site

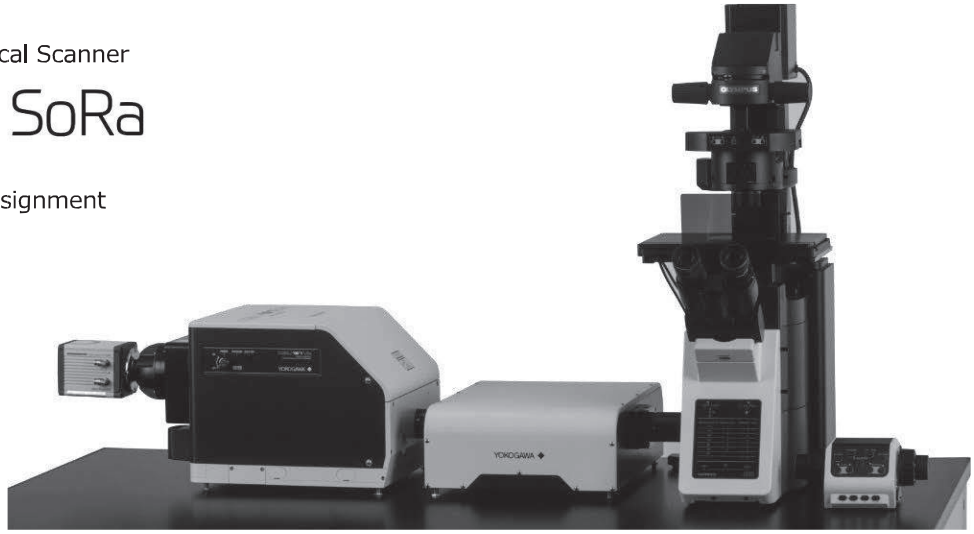

YOKOGAWA ELECTRIC CORPORATION
Bio Solution Center, Life Innovation Business HQ
2-3 Hokuyoudai, Kanazawa-shi, Ishikawa 920-0177, Japan
Phone : +81-76-258-7028
E-mail : csu_livecell_imaging@cs.jp.yokogawa.com
Website : https://www.yokogawa.com/solutions/products-platforms/life-science/

Website

OLYMPUS®

次世代型 共焦点レーザー走査型顕微鏡
FV3000シリーズ

新型分光システムTruSpectralと冷却GaAsP PMTによる圧倒的な明るさ

高感度・高精度のTruSpectral分光システム

2nmの高分解能と優れた透過率を実現する透過型回折格子を検出系に採用。
従来と比べ蛍光の検出効率が大幅に向上。

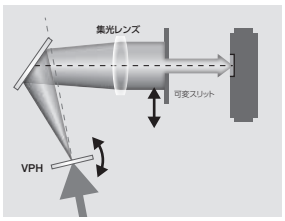

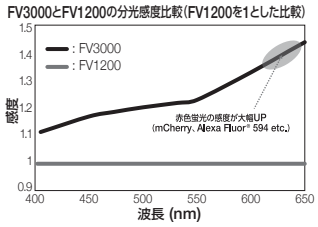

高感度冷却GaAsP PMT

高い量子効率とペルチェ冷却によるノイズ低減、
高S/N実現するGaAsP PMTを標準2Chで搭載。

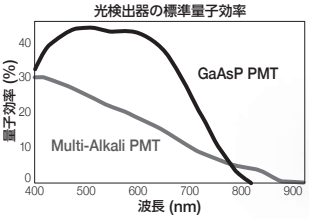

共焦点レーザー走査型顕微鏡 FV3000RS

超高速イメージング[*1]や広視野数18の高速イメージング[*2]を実現するレゾナントスキャナー

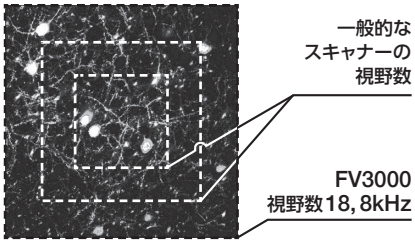

[*1] 最速438fps、512×32ピクセル　[*2] 30fps、512×512ピクセル

マクロ1.25倍からミクロ150倍、分解能約120nmの超解像まで広い倍率レンジでのシームレスなイメージング

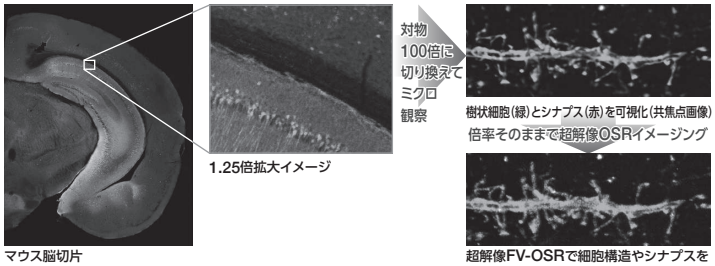

マウス脳切片
(1.25倍、ワンショットイメージ)

超解像FV-OSRで細胞構造やシナプスをさらに高精細に可視化

オリンパス株式会社　〒163-0914　東京都新宿区西新宿2-3-1　新宿モノリス
[お問い合わせ] お客様相談センター 0120-58-0414 受付時間 平日8:45～17:30
www.olympus-lifescience.com

September 21-23, 2019

Venue:
Teikyo University
Itabashi Campus Tokyo Japan

The 6th International Symposium on Bioimaging & The 28th Annual Meeting of the Bioimaging Society

Chair:
Ryo SUZUKI, PhD.
Teikyo University

Main Organizer
The Bioimaging Society

Co-organizers
Teikyo University
National University of Singapore
Mechanobiology Institute (MBI)

Leading to the Future with Bioimaging

Plenary lectures

- Prof. Paul MATSUDAIRA, PhD.
  National University of Singapore, MBI
  " Imaging the Mechanics of Early Zebrafish Development "
- Prof. Kazuo MARUYAMA, PhD.
  Teikyo University, Faculty of Pharma-Science
  " Ultrasound Theranostics (Imaging and Therapy) "

The Secretariat
Ryo SUZUKI, PhD., Daiki OMATA, PhD.
Teikyo University, Itabashi Campus
Faculty of Pharma- Science
Laboratory of Drug and Gene Delivery
2-11-1 Kaga, Itabashi, Tokyo 173-8605 Japan
int-symp-bioimaging2019@pharm.teikyo-u.ac.jp
URL : https://www.int-symp-bioimaging2019.org/

Image by Dr. Daiki OMATA and Dr. Yoshiharu DEGUCHI (Teikyo Univ.), Designed by Ms. Eri CHIBA (Teikyo Univ.)

ASTM
規格準拠

粒子や細胞の
高度検出・測定に最適!

NEW! DEEP LEARNING オプション

適用例

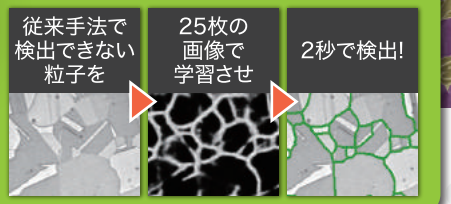

画像解析ソフトウェア

MIPAR
Image Analysis Software

Windows ／ Mac

(開発元／米国：MIPAR 社)

MIPAR(マイパー)はマウスで簡単に操作できるプログラムいらずの画像解析ソフトウェアです。
比類なき検出能力と測定機能を有しており、粒子解析(粒径分布、粒子数、粒子面積)をはじめ生命科学、医薬、金属材料、鉱物などの様々な分野にご利用頂けます。

MIPAR の主な機能

1. メニュー操作だけで、セグメント分割、パターン認識、エッジ抽出、セルのカウントなど、様々な検出が行えます。
2. レシピ(画像検出設定、測定設定)を自由に作成・保存・編集でき、複数の画像処理に利用できます。
3. バッチ機能にて、同じレシピで多数の画像を一括処理できます。
4. 検出した細胞や粒子の各種測定(面積など)を行い、CSV／TXTファイルで出力します。

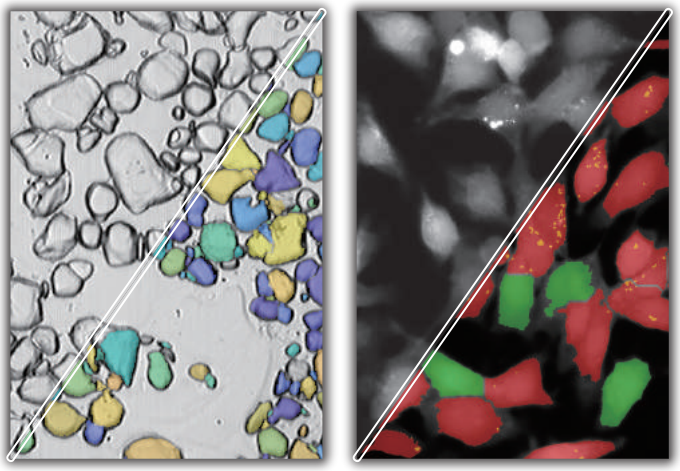

TIF、JPG、BMP、PNG、GIFの他、**150以上の画像フォーマットに対応!**

無料体験版のお申込みや見積もりのご依頼はこちらまで!

正規国内代理店
LightStone®
株式会社ライトストーン

〒101-0031
東京都千代田区東神田2−5−12 龍角散ビル7F
TEL 03−3864−5211　FAX 03−3865−0050
e-Mail ： sales@lightstone.co.jp
https://www.lightstone.co.jp/mipar/